JUNB regulatory functions in lymphangiogenesis: from mESCs to zebrafish

Dissertation
submitted to the
Combined Faculty of Natural Sciences and Mathematics
of the Ruperto Carola University Heidelberg, Germany
for the degree of
Doctor of Natural Sciences

Presented by
Laura Adriana Gutiérrez Miranda, M.Sc
13th December 2018

Dissertation
submitted to the
Combined Faculty of Natural Sciences and Mathematics
of the Ruperto Carola University Heidelberg, Germany
for the degree of
Doctor of Natural Sciences

Presented by
Laura Adriana Gutiérrez Miranda, M.Sc
born in: Valladolid, Spain
Oral examination:13th December 2018

JUNB regulatory functions in lymphangiogenesis: from mESCs to zebrafish

Referees: Prof.Dr.Peter Angel
PD.Dr.Karin Müller-Decker

Summary

In higher vertebrates, the development of a functional circulatory system based on blood and lymphatic vessels is a basic step in order to generate a full organism. The formation of the vasculature involves the generation of mesodermal-derived angioblasts and their subsequent differentiation into blood endothelial or lymphatic endothelial cell lineages. The switch between the undifferentiated and cell-specific genetic programs during cell differentiation requires an orchestrated spatiotemporal coordination of gene expression.

JUNB, a member of the AP-1 family, is a context-dependent transcription factor that exerts both positive and negative functions. Loss of function studies in mice revealed that JUNB is a key regulator of vascular development in embryos. Hence, JUNB transactivates pro-angiogenic molecules such as *Vegfa, Cbfβ* and *Hmox1*. Recently, Junb was described to regulate the development of lymphatic vessels in zebrafish via its target miR182. However, it remained unclear whether activator functions of JUNB are relevant for lymphangiogenesis. Therefore, I aimed to investigate whether JUNB is necessary for the formation of lymphatics and if so, to unravel in which specific step of the lymphatic vascular development JUNB is implicated. For this purpose, I used a dual approach of *in vitro* differentiation of mouse embryonic stem cells into lymphatic endothelial cells and an *in vivo* approach by generating *junb* mutant zebrafish in the background of the transgenic reporter line *Tg(fli:EGFP)^{y1}* to evaluate the development of the vasculature.

The study of the JUNB kinetics during the LEC differentiation process revealed that JUNB is strongly induced at the RNA and protein level during the angioblast formation until the formation of the LEC-like cells. Strikingly, *Junb$^{-/-}$* mESCs failed to form proper LECs due to considerable cell death during the angioblast formation. This increased apoptosis could be associated to a failure to initiate the induction of VEGFR1 and VEGFR2 expression. In the parallel *in vivo* approach, novel zebrafish mutants with ablated *junba* and *junbb* expression were generated using CRISPR-Cas9 technology. Successful mutations resulted in a premature end of the reading frame. Homozygous *junba$^{-/-}$* embryos could not be identified and the Mendelian ration of wildtype and heterozygous offspring suggests a recessive lethal phenotype. By contrast, *junbb* mutants were detected according to expected Mendelian ratio, reached adulthood and were fertile. Albeit the mutant embryos exhibited an allele-dependent decrease in the number of parachordal cells present at 3 days post fertilization; almost all the analyzed embryos displayed a complete thoracic duct at 5 dpf. Surprisingly, the mutants developed ectopic sprouts at the dorsal side of the trunk from 3 dpf until 5 dpf recapitulating the phenotype previously observed upon neuronal loss of soluble *vegfr1* in zebrafish. In summary, these data underscore the role of JUNB not only in lymphangiogenesis but also at an earlier developmental stage, namely the angioblast formation and suggest a JUNB-dependent regulation of vascular endothelial growth factor receptors during development.

Zusammenfassung

In höheren Wirbeltieren ist die Entwicklung eines funktionellen Kreislaufsystems, bestehend aus Blut- und Lymphgefäßsystem, ein grundlegender Schritt um einen vollständigen Organismus zu bilden. Für die Ausbildung der Blutgefäße ist die Entstehung von Angioblasten aus dem Mesoderm und deren anschließender Differenzierung in Blut- oder Lymphendothelzellen notwendig. Das Umschalten zwischen den undifferenzierten und zell-spezifischen genetischen Programmen während der Differenzierung erfordert eine abgestimmte räumliche und zeitliche Koordination der Genexpression.

JUNB, ein Mitglied der AP-1 Familie, ist ein Kontext-abhängiger Transkriptionsfaktor, der positive und negative Funktionen ausübt. Studien an Mäusen mit einem Junb Funktionsverlust zeigten dass JUNB ein Schlüsselregulator der vaskulären Entwicklung ist, indem JUNB pro-angiogene Moleküle wie *Vegfa, Cbfβ* und *Hmox1* transaktiviert. Vor kurzem wurde beschrieben, dass Junb die Entwicklung lymphatischer Gefäße in Zebrafischen über das Zielgen miR182 reguliert. Jedoch ist noch unklar, ob zusätzlich auch aktivierende Funktionen von JUNB relevant für die Lymphangiogenese sind. Ziel der Disseration war daher zu untersuchen, ob JUNB für die Entstehung der Lymphgefäße notwendig ist, und aufzuklären in welche spezifischen Schritte der Lmyphgefäßentwicklung JunB involviert ist. Aus diesem Grund habe ich einen dualen Ansatz gewählt bei dem *in vitro* die Differenzierung von murinen embryonalen Stammzellen (mESC) zu lymphatischen Endothelzellen untersucht wurde und *in vivo* Zebrafische mit mutiertem Junb im Hintergrund der Reporterlinie *Tg(fli:EGFP)*^{y1} generiert wurden um die Gefäßbildung zu erforschen.

Die Untersuchung der Expressionskinetik von JUNB während Differenzierungsprozesses zu Lymphendothelzellen (LEC) hat gezeigt, dass JUNB auf RNA und Protein Ebene während der Angioblast Entstehung bis hin zur Bildung der LEC-ähnlichen Zellen induziert wird. Interessanterweise können *Junb*$^{-/-}$ mESC aufgrund von erheblichem Zelltod während der Angioblast Entstehung keine richtigen LEC ausbilden. Diese erhöhte Apoptose war mit einem Defekt in der Induktion von VEGFR1 und VEGFR2 verbunden.
In einem parallelen *in vivo* Ansatz wurden mit Hilfe der CRISPR-Cas9 Technologie neuartige Zebrafischmutanten mit defekter *junba* und *junbb* Expression generiert. Gelungene Mutationen resultierten in einem frühzeitigen Ende des Leserasters. Homozygote *junba*$^{-/-}$ Embryonen konnten nicht detektiert werden, wobei die Mendelsche Rate der Wildtyp und Hetreozygoten Nachkommen auf eine rezessive letale Phänotyp hinweist. Im Gegensatz traten *junbb* Mutanten im erwarteten Mendelschen Verhältnis auf erreichten das Erwachsenenalter und waren fertil. Obwohl, die Mutanten eine Allel-abhängige Verringerung der Anzahl an parachordalen Gefäßen zum Zeitpunkt 3 dpf aufwiesen, zeigten fast alle untersuchten Embryonen einen kompletten Ductus thoracicus zum Zeitpunkt 5 dpf. Interessanterweise, entwickelten die Mutanten

ektopische Gefäßaussprossungen an der dorsalen Seite des Gefäßstrangs zwischen dem Zeitpunkten 3 dpf und 5 dpf und rekapitulieren damit einem Phäenotyp, der nach neuronalem Verlust von löslichem Vegfr1 im Zebrafisch beobachtet wurde. Zusammenfassend unterstreichen diese Daten die Rolle von JUNB nicht nur während der Lymphangiogenese sondern auch bei vorausgehenden Entwicklungsschritten, wie der Angioblast Entstehung, und deuten darauf hin, dass die Regulierung der Rezeptoren für vaskuläre endotheliale Wachstumsfaktoren, 1 und 2 während der Entwicklung vom JUNB abhängig ist.

Acknowledgements

This thesis was conducted between the Division of Signal Transduction and Growth Control at the German Cancer Research Center (DKFZ) in Heidelberg (Germany) and the Department of Biological Regulation of the Weizmann Institute of Science in Rehovot (Israel). I am very grateful to everyone who helped me during my PhD journey.
First of all, I would like to thank all my supervisors:

- Prof.Dr. Peter Angel for giving me the opportunity of joining his lab first as a trainee and later on as a PhD student and for being my first referee.
- PD.Dr. Marina Schorpp-Kistner, my mentor, for her supervision and support during these years and for giving me the freedom to develop my own ideas.
- Prof.Dr. Karina Yaniv who welcomed me with open arms in her lab and for countless encouraging discussions.

I would like to thank PD.Dr. Karin Müller-Decker for accepting to be my second referee and Prof.Dr. Kroll and Prof.Dr. Hecker for being examiners in my dissertation.
I would like to thank Prof.Dr. Wiemann and Prof.Dr. Kroll for being part of my Thesis Advisory Committee and for their helpful feedback during these years. Thanks to Prof.Dr.Kopp-Schneider and Shifra Ben-Dor for statistical and bioinformatics support. Thanks to the German Israeli Helmholtz Research School of Cancer Biology for the funding and to Lindsay Murrels and Evelyn Müller for all the help during my stays abroad.

During these five years, I had the honour of sharing bench and coffee breaks with two great teams: one at the DKFZ and one at the Weizmann Institute of Science.
I would like to first thank the DKFZ crew and especially the JUNB subgroup for accompanying me through the ups and downs of this journey. Thanks Melanie for being the best translator of german bureaucracy, for always offering to get the buffers in the upper shelfs for me and for being my extra pair of hands during the uncountable transfections and luciferase experiments. Promega will regret not awarding us with Luci and Reni. Thanks to Betty and Jule, renamed *Wutssschka* during these years, for being awesome booth partners.
Thanks to the Podoplaninis (Barbara, Meli, Tanja), the Liver booth (Doris, Te, Macrina and Thomas) and Lena for creating such a great working atmosphere, for the fun coffee breaks and the random baking. Thank you Sybille for your contagious laugh and always checking if I was doing alright.
Very special thanks to my friends and colleagues: Barbara Costa, Doris Schneller (the best translator ever), Maria Llamazares, Aurora de Ponti and Christine Bauer for all the laughs. It would have not been the “saaaaaaame” without you girls.

I would also like to thank the Weizmann team for teaching me that there are no bad projects if you ask the correct questions and to always think outside the box. Thanks for sharing all your knowledge, your hummus and bambas with me.
Special thanks to the Argentinean team,Yona and Julian, for making me feel at home since day one. Thanks to Hanoch, AKA *Kapara,* for being a great lab partner and a good friend although probably the worst Hebrew teacher ever. Thanks to the staff of the Fish Facility for taking care of my babies and placing them in the lower racks so I don't need to jump (a lot).

Since not everything during these years has been about science and I would like to thank:

- my best friends and expats: Sara, Marta, Guille, Blanca and David. Special thanks to Borja and Brandan and María for proofreading and for creating a tiny home here in Heidelberg. I can't believe how lucky I am to have you around .
- my beer friends Alicia, Sonia and Saray for always being there to share terror stories about our PhD journey. I am so proud we somehow survived and made it work.
- my Weizmann roomies and brunch team: Amal, Thea and Deborah and my DKFZ friends Mahak and crazy Anca for all the laughs together.
- my GIHRSCB friends for sharing all the Germany-Israel experience together. Special thanks to my dear Chiara for being such a good friend and a wonderful swimming pal and Moritz for all the laughs through these years.
- my non-scientist friends in Heidelberg for not complaining too much when I had to work on weekends. Special thanks to Iñaki for being a good friend and providing ice cream when needed. It has been a pleasure to start the journey towards diabetes with you.

A mi familia, por todas las llamadas por skype y los wassaps de ánimo. A mi madre por escucharme y apoyarme y siempre acabar la conversación con un "cariño,ya saldrá mañana". A mi hermana Bea por ser simplemente la mejor, por todas las conversaciones frikis y las risas mientras escribíamos en paralelo nuestras tesis. Has sido el mejor apoyo que he podido tener. A mi padre, que vió empezar esta tesis pero no llegó a verla terminada. Gracias por apoyarme siempre y motivarme a hacer lo que me gusta aunque significase estar lejos de casa. Estoy segura de que esta tesis te hubiese encantado porque aunque está en inglés, la he puesto muchos colorines y me ha quedado muy "chungi".

Anything of this would not have been possible without your enduring support and love. Thanks a lot from the bottom of my heart.

"Es de bien nacido, ser agradecido", Refrán castellano

Table of Contents

SUMMARY I

ZUSAMMENFASSUNG III

ACKNOWLEDGEMENTS V

LIST OF FIGURES X

LIST OF TABLES XII

ABBREVIATIONS XIII

1.INTRODUCTION 3

1.1 JUNB, an AP-1 transcription factor 3
1.1.1 AP-1 signaling 3
1.1.2 Context-dependent JUNB function 4
1.1.3 Role of JUNB in vascular biology 5
1.2 Lymphatic vascular system 7
1.2.1 Functions and network structure 7
1.2.2 Lymphangiogenesis 8
1.3 Experimental models 11
1.3.1 Stem cells 11
1.3.2 *Danio rerio* 13
1.4 Aim of the study 15

2.MATERIALS 17

2.1 Equipment 19
2.2 Consumables 20
2.3 Chemicals 21
2.4 Software 22
2.5 Molecular Biology reagents 23
2.6 Buffers and Solutions 25
2.7 Oligonucleotides 26
2.8 Plasmids 28
2.9 Antibodies 28
2.10 Cell lines and cell culture media 29
2.11 Zebrafish lines 30

3.METHODS **31**

3.1 Molecular Biology 33
3.1.1 DNA extraction 33
3.1.2 RNA isolation 33
3.1.3 DNA/RNA quantification 33
3.1.4 Reverse transcription 34
3.1.5 Polymerase Chain Reaction 34
3.1.6 Design and validation of quantitative Real Time PCR primers 35
3.1.7 Quantitative Real Time-PCR 36
3.1.8 Gel agarose electrophoresis 37
3.1.9 Nucleic acids purification 37
3.1.10 Sequencing 37
3.2 Protein methods 37
3.2.1 Whole cell protein isolation 37
3.2.2 Protein quantification 38
3.2.3 SDS-PAGE electrophoresis 38
3.2.4 Western Blot 38
3.2.5 Western blot quantification 39
3.3 Flow Cytometry 39
3.4 Cloning methods 40
3.4.1 pGEM®-T cloning 40
3.4.2 Generation of dre-flt1 800bp-pGL3 construct 41
3.4.3 Site-directed mutagenesis 42
3.4.4 Bacterial transformation 43
3.4.5 DNA isolation from plasmids: minipreps and maxipreps 43
3.5 Cell culture methods 43
3.5.1 Culture conditions and maintenance 43
3.5.2 Differentiation of stem cells 43
3.5.3 Freezing and thawing of cells 44
3.5.4 Mycoplasma check 44
3.5.5 Transient transfection of cells 45
3.6 Luciferase Reporter Assay 45
3.7 Animal experiments 46
3.7.1 Maintenance and breeding 46
3.7.2 Preparation of injection needles and plates 46
3.7.3 Injections 47
3.7.4 Wholemount In situ Hybridization 47
3.7.5 CRISPR design and mutant generation 49
3.7.6 *junb*-kalt4 reporter mutant 49
3.7.7 Generation of overexpression vector 50
3.7.8 Scoring and Morphological analyses of the embryos 50
3.8 Imaging and imaging processing 51
3.9 Statistical analysis 51

4.RESULTS **53**

4.1 Role of JUNB in an *in vitro* LEC differentiation model 55
4.1.1 Optimization of a mESC differentiation protocol into LECs 55
4.1.2 JUNB activity is increased during *in vitro* LEC differentiation 55
4.1.3 *Junb*$^{-/-}$ mESC fail to form LEC-like cells 60
4.1.4 *Junb*$^{-/-}$ mESC fail to upregulate VEGFR2 during LEC differentiation 62
4.1.5 Surviving *Junb*$^{-/-}$ mESCs form immature LEC-like cells 66
4.2 Impact of Junb in lymphangiogenesis in Zebrafish 68
4.2.1 *junba* and *junbb* are differently expressed in zebrafish development 68
4.2.2 CRISPR-Cas-mediated generation of *junb* mutants 72
4.2.3 *junb* mutants are fertile and reach adulthood 75
4.2.4 *junb* mutants partially phenocopy the morphants 78
4.2.4.1 *junb* mutants display an allele-dependent loss of PACs 78
4.2.4.2 *junb* mutants develop a normal thoracic duct 81
4.2.5 *junb* mutants generate ectopic sprouts from 3 dfp until 5 dpf 84
4.3 Outlook 88
4.3.1 *dre-flt1* is a JUNB-direct target 88
4.3.2 Generation of a gain of function mutant 90

5.DISCUSSION **93**

5.1 JUNB is induced during *in vitro* differentiation of mESCs into LECs 95
5.2.JUNB-dependent control of VEGFRs during LEC differentiation and its effect on survival and differentiation potential 98
5.3 *Junb* loss does not affect LEC specification 102
5.4 *junb* mutants partially phenocopy the morphants 102
5.4.1 Loss of *junb* provokes a defect on the formation of the lymphatic system 102
5.4.2 Unlike morphants, *junb* mutants do not display any cardiovascular defects 106
5.4.3 Development of ectopic sprouts in *junba* and *junbb* mutant zebrafishes 107
5.4.4 Differences between the murine *Junb*$^{-/-}$ and the zebrafish mutant embryos 110

6.REFERENCES **115**

DECLARATION OF AUTHORSHIP **127**

List of Figures

INTRODUCTION

Figure 1-1: Vascular processes affected upon *Junb* loss. 6
Figure 1-2: Lymphangiogenenesis in mammals. 10
Figure 1-3: Vascular development in zebrafish. 14

RESULTS

Figure 4-1: Feeder-free mESC differentiation protocol into LECs. 56
Figure 4-2: Validation of a feeder-free three-step mESCs differentiation protocol into Lymphatic Endothelial Cells 57
Figure 4-3: Expression switch from stem cells to lymphatic markers during the *in vitro* LEC differentiation. 58
Figure 4-4: JUNB is induced during *in vitro* LEC differentiation at the transcript and protein level. 59
Figure 4-5: $Junb^{+/+}$ and $Junb^{-/-}$ mESCs behaved similarly during the first steps of LEC differentiation. 60
Figure 4-6: $Junb^{-/-}$ mESCs exhibited increased apoptosis rate during LEC differentiation. 61
Figure 4-7: Expression of both VEGFR1 and VEGFR2 is affected in $Junb^{-/-}$ mESCs during spontaneous differentiation. 63
Figure 4-8: Transformed murine endothelioma cells lacking one or two Junb alleles display similar expression of endothelial markers CD105 and CD31. 64
Figure 4-9: Diminished VEGFR1 and VEGFR2 expression in $Junb^{-/-}$ endothelioma cells. 65
Figure 4-10: $Junb^{+/+}$ and $Junb^{-/-}$ LEC-like cells express comparable levels of lymphatic markers transcripts. 66
Figure 4-11: Surviving $Junb^{-/-}$ cells generate immature LEC-like cells in the presence of endothelial stimuli. 67

Figure 4-12: *junba* and *junbb* paralogues share sequence homology with their murine and human orthologues. 69
Figure 4-13: Differential expression of *junba* and *junbb* in time and space during zebrafish development. 71
Figure 4-14: Model of the two different approaches followed to generate *junb* mutant zebrafish. 72

Figure 4-15: Generation of *junb* mutant zebrafish applying the CRISPR-Cas9 technology. 74
Figure 4-16: Differential Mendelian ratio between *junba* and *junbb* mutants. 75
Figure 4-17: Generation of *Tg (UAS:Kaede, junba-Kalt4)* reporter line. 77
Figure 4-18: *junb* mutants display an allele-dependent decrease in PACs formation at 72 hpf. 80
Figure 4-19: *junb* mutants are able to form a complete thoracic duct by 5 dpf. 82
Figure 4-20: *junb* mutants display no signs of edema or lymphatic malfunction at 6 dpf. 83
Figure 4-21: *junba* and *junbb* mutants exhibit dorsal vessel branching at 72 hpf until 5 dpf. 85
Figure 4-22: Retraction and sprout growth was traced in the *junb* mutants. 86
Figure 4-23: *dre-flt1* transactivation is TRE-dependent. 89
Figure 4-24: Overexpressing vectors drive zebrafish *junb* expression in F9 cells. 90
Figure 4-25: Generation of a tissue-specific overexpression *junb* line. 92

DISCUSSION

Figure 5-1: Schematic model of the *in vitro* LEC differentiation. 100
Figure 5-2: Schematic model of the lymphangiogenesis steps that are affected upon *Junb* loss. 113

List of Tables

Table 1-1.	Summary of endothelial cell differentiation methods	12
Table 2-1.	Buffers and buffer composition.	25
Table 2-2.	Primers used for genotyping.	26
Table 2-3.	Primers used for qRT-PCR.	26
Table 2-4.	Primers used for zebrafish line generation.	27
Table 2-5.	Primers used for promoter cloning.	27
Table 2-6.	Primers used for sequencing.	27
Table 2-7.	Plasmids used for cloning.	28
Table 2-8.	Antibodies used for Western Blot.	28
Table 2-9.	Antibodies used for Flow cytometry.	29
Table 2-10.	Cell lines used for experiments.	29
Table 2-11.	Culture media for the different cell types.	29
Table 2-12.	Transgenic lines used for experiments.	30
Table 4-1.	Collection of all the mutants sequenced during the study.	72
Table 4-2.	Origin and development of the ectopic sprouts at 5 dpf.	86
Table 5-1.	Comparison of morphants and mutants phenotypes of lymphatic regulators	104

List of Equations

Equation 1.	Calculation of real time PCR primers efficiency.	35
Equation 2.	Mathematical model used for relative quantification.	36
Equation 3.	Quantification of western blot signals.	39
Equation 4.	Calculation of the insertion volume for pGEM-T ligation	40

Abbreviations

A	Ampere
A, C, G, T	Adenosine, cytidine, guanosine, thymidine
aISVs	Arterial Intersegmental vessel
AP-1	Activating Protein 1
APS	Ammonium Peroxodisulfate
BCIP	X-Phosphate/5-Bromo-4-Chloro-3-indolyl-phosphate
bp	base pairs
BSA	Bovine Serum Albumin
Cas9	CRISPR-associated protein 9 nuclease
cDNA	Complementary DNA
CO_2	Carbon dioxide
COUP-TFII	COUP Transcription Factor II
CRE	cAMP Responsive Elements
CRISPR	Clustered Regularly Interspaced Short Palindromic Repeats
Ct	Cycle of threshold
DA	Dorsal Aorta
DMEM	Dulbecco's Modified Eagles Medium
DIG	Digoxigenin
DLAV	Dorsal Longitudinal Anastomotic Vessel
DLLV	Dorsal Longitudinal Lymphatic Vessel
DMSO	Dimethyl sulfoxide
DNA	Deoxyribonucleic Acid
DNAse	Desoxyribonuclease
dNTPs	deoxynucleotide triphosphate
dpf	days post fertilization
dre	*Danio rerio*
DTT	Dithiothreitol
E	Embryonic day
EC	Endothelial Cell
ECGS	Endothelial cell growth supplement
ECL	Enhanced chemoluminescence
EGFP	Enhanced Green Fluorescent Protein
END	Endothelioma cells
EXP	Expansion step
FACS	Fluorescence-Activated Cell Sorting
FBS	Fetal Bovine serum
FGFR	Fibroblast Growth Factor Receptor
for	forward primer
GOI	Gene of Interest
gRNAs	guide RNAs
HDR	Homology-Directed Repair
HM	Horizontal myoseptum
hpf	hours post fertilization
HRP	Horseradish peroxidase
IPTG	Isopropyl β-D-1-thiogalactopyranoside
ISLV	Intersegmental Lymphatic Vessel
ISV	Intersegmental Vessels
KDa	KiloDalton
LECs	Lymphatic Endothelial Cells
LIF	Leukemia Inhibiting Factor
LRU	Luciferase Relative Units
MCS	Multiple Clonal Site
MEFs	Mouse Embryonic Fibroblasts
MEM	Minimum Essential Medium Eagle

mESCs	mouse Embryonic Stem Cells
Mmu	*Mus musculus*
NBT	4-Nitro Blue Tetrazolium
NHEJ	Non Homologous End Joining
o/n	Over night
PACs	Parachordal Cells
PAM	Protospacer Adjacent Motif
PBS	Phosphate Buffer Saline
PBS-T	Phosphate Buffer Saline with Tween 20
PCR	Polymerase Chain Reaction
PCV	Posterior Cardinal Vein
PEI	Polyethylenimine
PFA	Paraformaldehyde
Ph	Pondus hydrogenii
PI3K	Phosphatidylinositol-3-kinase
PPIA	Cyclophilin A
PROX1	Prospero Homeobox protein 1
PTU	1-phenyl 2-thiourea
qRT-PCR	Quantitative Real Time Polymerase Chain Reaction
REF	Reference gene
rev	Reverse primer
RFP	Red Fluorescent Protein
RIPA	Radioimmunoprecipitation Assay Buffer
RNA	Ribonucleic Acid
RNAse	Ribonuclease
rpm	Revolutions per minute
RT	Room temperatura
RT-PCR	Real Time Polymerase Chain Reaction
SD	Standard Deviation
SD (X -LIF)	Spontaneous Differentiation (X days -LIF)
SDS	Sodium dodecyl sulphate
SDS-PAGE	Sodium dodecyl sulphate –polyacrylamide gel electrophoresis
SSC-T	Saline sodium citrate with Tween 20
TAE	Tris-buffered saline (buffer)
TBE	Tris/borate/EDTA buffer
TD	Thoracic Duct
TGF-β RI	Transforming Growth Factor beta Receptor I
TRE	TPA Responsive Elements
TSS	Transcription Start Site
UAS	Upstream Activation Sequence
V	Volts
VEGF-A	Vascular Endothelial Growth Factor A
VEGF-C	Vascular Endothelial Growth Factor C
VEGFR1	Vascular Endothelial Growth Factor Receptor 1
VEGFR2	Vascular Endothelial Growth Factor Receptor 2
VEGFR3	Vascular Endothelial Growth Receptor 3
vISVs	venous Intersegmental Vessel
WISH	Wholemount In Situ Hybridization

1 INTRODUCTION

1.1 JUNB, an AP-1 transcription factor

1.1.1 AP-1 signaling

1.1.2 Context-dependent JUNB function

1.1.3 Role of JUNB in vascular biology

1.2 Lymphatic vascular system

1.2.1 Functions and network structure

1.2.2 Lymphangiogenesis

1.3 Experimental models

1.3.1 Stem cells

1.3.2 *Danio rerio*

1.3.2.1 Vascular development in zebrafish

1.Introduction

An orchestrated spatiotemporal coordination of gene expression is necessary for proper embryo development as well as for the maintenance of tissue homeostasis. Dysregulation of these signals can lead to the development of pathologies.

Gene regulation occurs at different levels: i) transcriptionally at the DNA level, ii) post-transcriptionally at the mRNA level or iii) at the protein level during translation and the post-translational modifications.

At the DNA level, the transcription factors are the first regulators that activate or repress gene transcription becoming key players in development and differentiation processes.

1.1 JUNB, an AP-1 transcription factor

1.1.1 AP-1 signaling

The Activating Protein-1 (AP-1) transcription factors are considered “immediate-early” products that mediate gene expression in response of a plethora of extracellular stimuli including growth factors, cytokines, carcinogens, tumor promoters and physical stress such us UV irradiation and mechanical strain (Angel and Karin, 1991).

The AP-1 family comprises homo- and heterodimers of the JUN family (JUN, JUNB and JUND), FOS family (FOS, FOSB, FRA1 and FRA2), ATF family (ATF, ATF2,ATF3) and JDP subfamily (JDP1 and JDP2) and its members share structural and functional similarities.

All AP-1 members harbor conserved features like the bZip domain, a basic DNA-binding domain with a leucine zipper region. The leucine zipper enables and determines the dimer formation of the partners prior the DNA binding to the basic DNA motif. While some members of the family like FOS can only form heterodimers, JUN proteins can additionally form homodimers. The composition of the dimers ultimately affects their stability and transactivation potential. While JUN, c-FOS and FOSB are strong activators, JUNB, FRA1 and FRA2 are considered rather weak transactivators (Hess et al., 2004).

The DNA binding specifically occurs at some palindromic DNA recognition sites known as TRE (TPA Responsive Element) and dependent on the dimer composition, certain dimers are also able to recognize and bind the CRE (cAMP Response Element) sites.

AP-1 members have been described in many biological processes such as cell proliferation, differentiation and transformation (Angel and Karin, 1991).

1.1.2 Context-dependent JUNB function

JUNB is a transcription factor that is induced upon stress signals such as hypoglycemia (Textor et al., 2006), hypoxia (Schmidt et al., 2007) and growth factors among others.

Due to its weak transactivation potential, JUNB was once only considered as a transcriptional repressor of the JUN:FOS signaling. However, loss-of function approaches revealed that JUNB acts in a context-dependent manner holding both positive and negative functions required for physiological processes (Hess et al., 2004).

A clear example of its dual function is the regulation of the cell cycle: depending on the specific cell cycle phase, JUNB either promotes or blocks the cell cycle progression. During G_0/G_1 and G_2/M transitions, JUNB levels are very low but they increase upon mitogenic stimulations in G_1 and S phases (Piechaczyk and Farràs, 2008). At the G_1/S transition, JUNB prevents cell cycle entry via i) transactivation of cyclin-dependent kinase inhibitor *p16^{INK4a}* (Passegué and Wagner, 2000) and ii) repression of *Cyclin D1*, the key regulator of the G_1/S transition (Bakiri et al., 2000). Later on, during the G_2/M transition, JUNB promotes cell cycle progression by direct transactivation of *Cyclin A* (Andrecht et al., 2002). At G_2 phase, an accelerated JUNB decay by proteasomal degradation is required to reduce *Cyclin A* levels in transition towards mitosis (Farràs et al., 2008).

Apart from the cell cycle, the repressor functions of JUNB have been associated with inflammation and immune response. JUNB has been described to be required for the i) hematopoietic progenitor cells production, preventing myeloid malignancies (Passegué et al., 2001, 2004; Santaguida et al., 2009). ii) control of cytokines during wound healing (Florin et al., 2006), iii) suppression of IL-6 signaling in systemic lupus erythematosus phenotype (Pflegerl et al., 2009) and iv) regulation of chemokine expression in psoriasis via repression of SQSTM1/p62 (Zhang et al., 2015).

On the other side, the activator functions of JUNB have been associated with a variety of physiological functions such as i) T helper differentiation (Li et al., 1999; Hartenstein et al., 2002), ii) osteoclast differentiation (Hess et al., 2003; Kenner et al., 2004), iii) mast cell cytokine secretion and mast cell-endothelial cell cross-talk (Textor et al., 2007) and iv) vascular development which are described in detail in the section 1.1.3.

1.1.3 Role of JUNB in vascular biology

In mice, total loss of *Junb* led to embryonic lethality at midgestation (E8.5-E10.0) due to severe vascular defects. The *Junb*$^{-/-}$ embryos were grossly retarded in development and their premature death was associated to the insufficient exchange of nutrients through a defective feto-maternal communication. Several defects on the formation of the extra-embryonic tissues were observed during placentation: i) abnormal distribution of the trophoblast giants cells and subsequent decidua vascularization, ii) disorganized vascular network in the yolk sac and iii) absent vascularization in the labyrinth (Schorpp-Kistner et al., 1999).

Endothelial-specific deletion of *Junb* (Tie2-Cre) resulted in a similar outcome with embryonic lethality around E10. Again, the *Junb*-deficient embryos exhibited growth retardation and aberrant vasculature with abnormal branching and dilated vessels (Licht et al., 2006). In addition, using a mesenchymal-specific *Junb*-ablated mouse model (Coll1α2-Cre), a better characterization of adult endothelial cells was performed. *Junb*-deficient endothelial cells were described to display reduced sprouting capability in aortic explants and reduced tube formation in matrigel. JUNB direct target Core-Binding Factor beta (*Cbfß)* and CBFβ targets *Mmp2* and *Mmp13* were found to be required for endothelial cell morphogenesis (Licht et al., 2006).

Besides, several pro-angiogenic molecules have been described to be JUNB-regulated like Vascular Endothelial Growth Factor A (*Vegf-A)* and Heme Oxygenase (*Hmox)* (Hock et al., 2007). JUNB transactivates *Vegf-A* upon hypoglycemic (Textor et al., 2006) and hypoxic conditions via NF-κB (Schmidt et al., 2007).This hypoxia-induced *Vegf* regulation was proposed to be the cause for the reduced angiogenesis observed in *Junb*$^{-/-}$ teratocarcinomas.

Not only JUNB has been linked to developmental angiogenesis but also to the control of tissue homeostasis via transactivation of Myosin Regulatory Light Chain 9 *(Myl9),* a key player in the actomyosin contraction. Mesenchymal-specific ablated *Junb* mice displayed defects on arterial contractility making them unresponsive the deoxycorticosterone acetate DOCA-salt hypertension model. In addition, vascular smooth muscle cells isolated form these mice exhibited reduced stress fiber formation and motility (Licht et al., 2010).

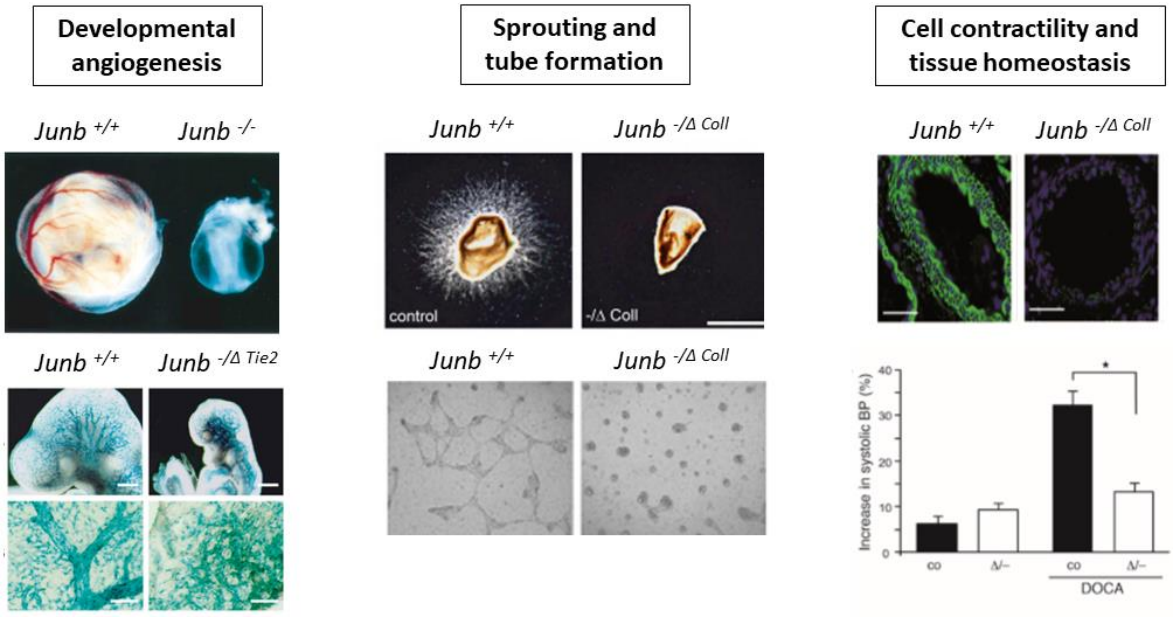

Figure 1-1. Vascular processes affected upon *Junb* loss.

Developmental angiogenesis (left panel): JUNB is required for proper vascularization in mouse embryos. Both total (Schorpp-Kistner et al., 1999) and endothelial cell specific loss of *Junb* (Licht et al., 2006) lead to embryonic death due to defects in vascularization. Sprouting and tube formation (middle panel): *Junb*-deficient cells display impaired cell sprouting in the aortic ring assay and impaired endothelial cell tube formation on matrigel (Licht et al., 2006). Cell contractility and tissue homeostasis (Right panel): *Junb*-defective cells are devoid of p-MYL9 expression, leading to a defect on arterial contractility upon DOCA-salt treatment (Licht et al., 2010).

Although, most of the known JUNB regulatory functions are based on direct regulation of its target genes (Figure 1-1), JUNB has also been described to regulate gene expression indirectly via regulation of microRNAs.

MicroRNAs comprise small non-coding RNAs that negatively regulate gene expression at the post-transcriptional level. MicroRNA expression profiling comparing *Junb* and *Junb*-deficient endothelial cells revealed that about 18% of the miRnome was altered upon *Junb* loss. MiR182 was found to be JUNB-regulated in endothelial cells, mouse embryonic fibroblasts and vascular smooth muscle cells. In addition, miR182 was described to be a lymphangiomiR required for proper lymphatic zebrafish development via attenuation of *foxo1* levels. Transient downregulation of zebrafish paralogues –*junba* and *junbb*– and their target miR-182 and *foxo1* in zebrafish embryos resulted in a failure in the formation of the first lymphatic structures so called parachordal cells (PACs) and the main lymphatic vessel, the thoracic duct (TD). Ectopic expression of miR-182 could successfully revert this effect. The axis Junb-miR182-Foxo1 was the first connection between JUNB and the development of lymphatic vessels ever described (Kiesow et al., 2015).

1.2 Lymphatic vascular system

1.2.1 Functions and network structure

The vascular network comprises two major circulatory systems: the circulatory blood and the linear lymphatic system. Although they resemble in some anatomical features, they harbor different functions and structures.

The lymphatic vasculature plays a role in several physiological functions: i) tissue homeostasis by collecting and transporting the interstitial fluid from the tissue back to the bloodstream, ii) fat absorption by the lacteal lymphatics in the intestinal villi (Tso and Balint, 1986; Harvey et al., 2005) and the iii) immune trafficking of antigens and activated antigen-presenting cells to the lymph nodes (Alitalo and Carmeliet, 2002).

The lymphatic vasculature includes lymphatic capillaries and collective lymphatic vessels. While the capillaries are blind-ended vessels formed by a thin single layer of endothelial cells (Leak and Burke, 1966, 1968)*;* the collective lymphatics additionally contain a perivascular muscle cell layer, a basement membrane and valves that guarantee the unidirectional flow of the lymph (Kampmeier, 1928; Smith, 1949).

Malfunction of the lymphatic vasculature leads to the onset of several pathologies associated with inflammation and fibrosis. The most severe diseases are the lymphedema and the lymphatic tumor-metastasis (Alitalo et al., 2005). Lymphedema is a condition characterized by the excessive accumulation of water and proteins in the tissues. Primary lymphedema is congenital and is associated with an abnormal vessel development. Secondary lymphedema is more common and occurs as a result of a physical damage in the lymphatics upon trauma, surgery or infection by filariasis (Szuba and Rockson, 1998). In addition, the formation of tumor-related lymphatic vessels is used by metastatic tumor cells to disseminate toward distant organs and lymph nodes (Cueni and Detmar, 2008). The presence of lymphatic metastasis in the patients is normally correlated with poor prognosis (Achen et al., 2005; Stacker et al., 2002; Tobler and Detmar, 2006).

Hence, a strong understanding of the signaling pathways involved in the proper formation and function of the lymphatic vasculature might shed some light in the development of novel targets or therapies for lymphatic-related diseases.

1.2.2 Lymphangiogenesis

Since the first observations of the existence of the lymphatic system by Hippocrates, it was not until the 20th century when two different theories for the origin of the lymphatic system were postulated. The anatomist Florin Sabin performed ink injections in pig embryos and suggested that the first lymphatic structures were stemming from the cardinal vein. These results led to the so-called "centrifugal model" in which lymphatics originate from venous structures (Sabin, 1902, 1904). Contrary to this theory, the anatomists George S. Huntington and Charles F.W McClure performed cat embryo wax reconstructions and proposed that the lymphatic sacs were formed from a cluster of mesenchymal cells. This study led to the "centripetal" model (Huntington and McClure, 1910).

Recent cell tracing experiments finally revealed that the lymphatics have a dual origin: while the first lymphatics arise from a special cluster of cells located within a venous structure; non-venous origins have been described for organ-specific lymphatics. Stanczuk et al., (2015) described that in mice, mesenteric lymphatic vessels derive from cKit^{+} hemogenic-endothelium cells and Martinez-Corral et al., (2015) proposed that murine dermal lymphatics form *de novo* during a lymphvasculogenesis process in which lymphatic endothelial cells (LECs) cluster together prior assembling the lymphatic networks. Klotz et al., (2015) also described a heterogeneous origin of heart lymphatics in which part of the lymphatic structures were formed independently of a venous source.

In general, lymphangiogenesis is the process of growth of lymphatic vessels from pre-existing lymphatics. It mostly takes place during embryonic development and during some pathological situations in adults such as wound healing or tumor metastasis.

In mammalian embryonic development and vasculogenesis, some mesodermal progenitors become "hemangioblasts", the common precursor cells of blood and vascular lineages. These precursors are characterized by VEGFR2 expression and they give rise to the endothelial cells that form the first vascular structures. Subsequently, a small population of venous endothelial cells acquire several molecular signatures and assume the lymphatic identity. Loss-of function studies in mice led to the identification of specific lymphatic markers like Vascular Endothelial Growth Factor 3 VEGFR3 (Kaipainen et al., 1995), Lymphatic Vessel Endothelial Hyaluronan Receptor 1 LYVE1 (Banerji et al., 1999), Prospero-related homeobox domain 1 PROX1 (Wigle and Oliver, 1999) and PODOPLANIN (Breiteneder-Geleff et al., 1999).

The first lymphatic structures are formed only when the blood vascular system has been previously established through two main processes: i) lymphatic endothelial specification of the vascular precursors and ii) formation of lymphatic structures.

LEC specification

In mouse embryos (E9.5-E10.5), a subpopulation of blood endothelial cells within the dorsolateral wall of the anterior cardinal vein acquires the competence to be lymphatic endothelial cell precursors by the expression of transcriptional regulators of the lymphatic endothelial fate: *Sox 18, Nr2fr (Coup-TFII)* and *Prox1*. SRY-related HMG-box 18 *(Sox18)* is a known marker required for arteriovenous specification and Chicken Ovalbumin Upstream Transcription Factor II *(Coup-TFII)* is a known as a vein marker. Both SOX18-dependent and COUP-TFII-dependent *Prox1* induction in the polarized venous compartment is observed during the lymphatic specification of the precursor cells (François et al., 2008; You et al., 2005; Srinivasan et al., 2010). Prospero-related homeobox domain 1 *(Prox1)* expression is necessary and sufficient to trigger lymphatic endothelial specification in these polarized cells (Srinivasan and Oliver, 2011; Wigle and Oliver, 1999; Wigle et al., 2002). Once the cells are committed to the lymphatic fate, they upregulate markers characteristic of lymphatic endothelial cells and downregulate blood endothelial markers.

Formation of lymphatic sacs

Around E10.5, PROX1-expressing progenitor cells are determined to the lymphatic lineage and start to express lymphatic markers like PODOPLANIN, VEGFR3 and NRP2. Then, the lymphatic cells sprout laterally from the vein and migrate in stream to form the primordial lymphatic structures called lymph sacs (Wigle and Oliver, 1999; Wigle et al., 2002). This process is mainly regulated by the signaling of VEGFR3 receptor expressed in the *Prox1*-specified cells and its ligand VEGF-C expressed by the mesenchymal cells (Makinen, 2001; Karkkainen et al., 2004; Tammela et al., 2005). A small cluster of PROX1-expressing cells remain in the veins to form the so called lymph-venous valves preventing the backflow of fluids (Srinivasan and Oliver, 2011). Subsequent sprouting from the lymphatic sacs and remodeling and maturation of the vessels generate more defined structures, the lymphatic plexus.

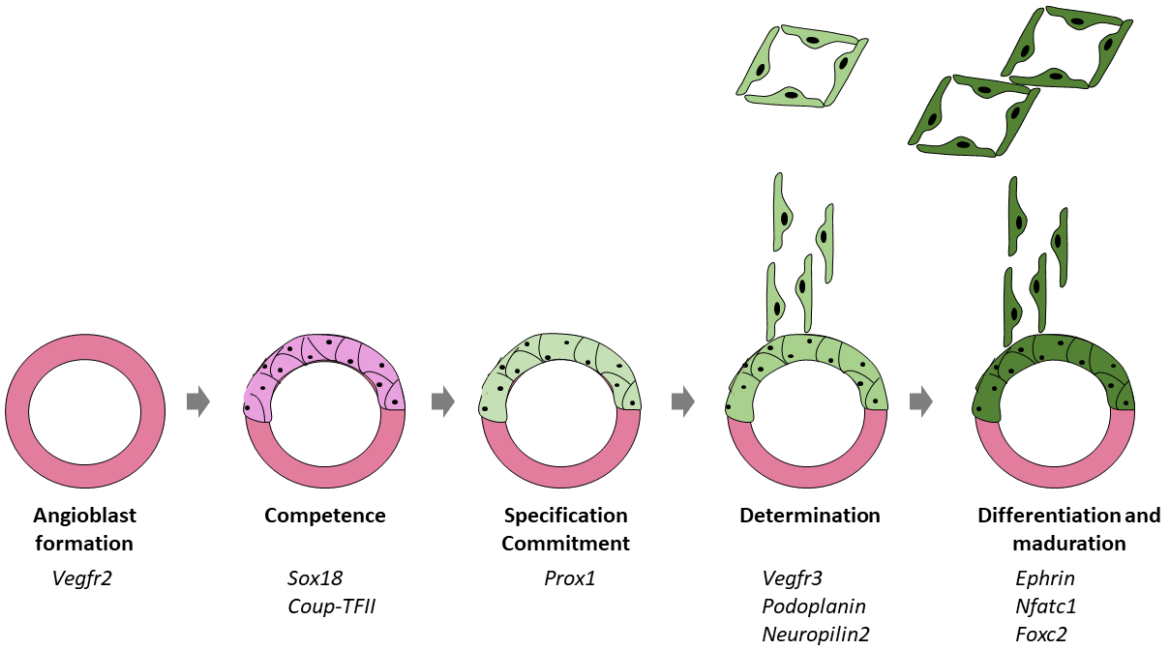

Figure 1-2. Lymphangiogenenesis in mammals

Schematic illustration depicting the key steps that take place during mammalian lymphatic endothelial cell differentiation. Angioblasts give rise to the blood endothelial cells and first vascular structures. A cluster of cells from the cardinal vein acquire competence and commit to the lymphatic fate by expressing a subset of lymphatic-specific genes. Upon mesenchymal stimulation, the LEC-specified cells bud off the vein and migrate to form the first lymphatic structures, the lymphatic sacs. Subsequent growth of the cells and lymphatic sacs leads to mature lymphatic vessels. The key genes have been included below each process. Adapted from (Oliver and Srinivasan, 2010).

1.3 Experimental models

The full understanding of the complex processes involved in the development of vessels requires experimentation with both *in vitro* and *in vivo* systems. While the *in vivo* study of animal models offers the possibility of visualizing processes as cell migration and tube formation; the *in vitro* systems are necessary to test conditions or treatments in a more controlled environment.

1.3.1 Stem cells

Stem cells are pluripotent cells that can give rise to cells of the three germ layers: endoderm-derived cells (inner organs), ectoderm-derived cells (skin and neural lineages) and mesoderm-derived cells (hematopoietic, cardiac, skeletal muscle and vascular lineages). They divide asymmetrically, renewing themselves in each division while generating another cell capable to respond to the environmental stimulus and undergo a differentiation lineage. Depending on the organ they belong to, they divide regularly to maintain the worn-out tissue or they divide only under special circumstances such as stress or tissue damage.

The stem cells can be found during embryonic development and adulthood but the main difference is their ability to differentiate into other cell types. The adult "somatic" stem cells are multipotent and can give rise only to a limited set of cells within their niche. They are difficult to isolate and they have a low division rate. On the contrary, the embryonic stem cells (ESCs) are pluripotent and can give rise to all the embryonic cells except the extra-embryonic tissues. They are isolated from the inner cell mass of the mammalian blastocyst and divide fast. Due the multiple differentiation possibilities, embryonic stem cells have been widely used for biomedical research.

Embryonic stem cells and the maintenance of pluripotency

The maintenance of the pluripotent state in embryonic stem cells is controlled by the expression of three main transcription factors: OCT 3/4 (Nichols et al., 1998; Niwa et al., 2000), SOX 2 (Avilion et al., 2003; Masui et al., 2007) and NANOG (Chambers et al., 2003; Mitsui et al., 2003). The collaboration between these three genes regulates gene expression in ESCs. In fact, a positive feedback in the activation of these genes is needed for stemness control. In addition, together they bind and recruit activators activating gene transcription in ESCs and repress lineage-specific regulators (Young, 2011).

In addition, Leukemia Inhibitory Factor (LIF) is an essential compound for the maintenance of the stemness properties and its role on LIF-gp130-STAT3 survival signaling has been described in murine stem cells (Boeuf et al., 2001; Niwa et al., 1998). LIF has to be supplemented in an *in vitro* system to guarantee that the ESCs remain in an undifferentiated state. Upon LIF withdrawal, the cells spontaneously differentiate (Smith et al., 1988; Williams et al., 1988).

Embryonic stem cells differentiation

The potential of the ESCs to give rise to cells of different lineages is used to study the development of cells from their progenitors. The differentiation protocols recapitulate the developmental key steps that occur in embryo development and allow the generation of differentiated cell populations (Murry and Keller, 2008).

During the step of gastrulation, the specification of the cells into these specific populations is timely and spatially controlled. Since the scope of the study is the development of the vascular system, my *in vitro* system is based on the generation of mesoderm-derived cells. The early steps of mesoderm induction are controlled by the expression of VEGFR2 in the hemangioblasts, precursors with hematopoietic and vascular potential (Choi et al., 1998; Ema et al., 2006).

Three basic methods for ESC differentiation have been mostly used: i) 3D aggregation of cells referred as embryoid bodies, ii) co- culture of cells in contact with supportive feeder cells and iii) monolayer culture in the presence of a matrix.

Although all of methods have been described to succesfuly differentiate the plutipotent cells into endothelial cells; the differentiation method is selected according to the conditions and suitability of each experimental setting.

Table 1-1.Summary of the published endothelial cell differentiation methods

Targeted differentiation	Differentiation model	Origin	Reference
Lymphatic endothelial cells	Embryid bodies	Mouse	(Kreuger et al., 2006)
Lymphatic endothelial cells	Embryid bodies	Mouse	(Liersch et al., 2006)
Hematopietic cells	Embryoid bodies	Mouse	(Obier et al., 2016)
Endothelial cells	Embryoid bodies	Human	(Costa et al., 2013)
Endothelial cells	Feeder cells	human	(Kusuma et al., 2013)
Lymphatic endothelial cells	Feeder cells	Human	(Nicenboim et al., 2015)
Endothelial cells	Feeder-cell	Mouse	(Blancas et al., 2008)
Endothelial cells	Matrix	Human	(Nguyen et al., 2016)

1.3.2 *Danio rerio*

Danio rerio is a freshwater fish commonly known as zebrafish and has been widely used in the recent years as a vertebrate model for vessel formation.

Zebrafish harbor a closed circulatory system and the main processes related to vessel formation as well as some of the regulatory cell signaling resemble to those described in mice and humans (Isogai et al., 2001, 2003; Ellertsdóttir et al., 2010). In addition, they display a separate lymphatic network similar to the one found in higher vertebrates with which they share functional and molecular features (Yaniv et al., 2006; Küchler et al., 2006).

Zebrafish present some unique advantages for *in vivo* experiments: i) easy husbandry and external fertilization, giving access to egg manipulation, ii) rapid development, iii) embryo transparency at early developmental stages allowing the imaging of internal anatomical structures and iv) availability of specific transgenic reporter lines to track vascular development in detail. One of the most used tools is the transgenic zebrafish line *Tg(fli:EGFP)^{y1},* a pan-endothelial reporter that expresses Enhanced Green Fluorescence Protein (EGFP) in all the endothelial cells and some neural cells (Lawson and Weinstein, 2002).

In addition, contrary to mammals, the small size of the embryos in the first steps of development allows them to uptake oxygen by passive diffusion and even develop for some days without a functional cardiovascular system (Stainier et al., 1996) or blood (Isogai et al., 2001).

1.3.2.1 Vascular development in zebrafish

In the first step of vascular development, mesoderm-derived angioblasts aggregate to form *de novo* the two axial vascular structures: the dorsal aorta (DA) and the posterior cardinal vein (PCV) within the first 24 hours post fertilization (hpf). During their assembly, the cells express distinct genetic programs and concomitantly acquire venous and arterial identity (Herbert et al., 2009; Swift and Weinstein, 2009). Subsequently, a process of sprouting and lumen formation starts, commonly referred as angiogenesis. Following the generation of the first vessels, a two-step process takes place to generate the intersegmental vessels (ISVs). Around 22 hpf, a primary sprouting phase starts from the dorsal aorta (DA) to generate arterial intersegmental vessels (aISVs). The aISVs sprouts migrate rapidly dorsally until they reach the surface of the neural tube, where they migrate rostrally and caudally to form the dorsal longitudinal anastomotic vessel (DLAV). Around 32 hpf, a secondary sprouting takes place to form venous intersegmental vessels (vISVs) from the posterior cardinal vein (PCV) in a similar fashion (Isogai et al., 2003). One half of the vISVs will connect to aISVs and turn them into vISVs. The other half of the formed vISVs will contribute to the formation of the lymphatic

system (Yaniv et al., 2006; Bussmann et al., 2010). These cells will migrate towards the horizontal myoseptum, a tissue partition of the dorsal and ventral muscle wall at the midline, and migrate rostrally and caudally to assemble the transient lymphatic structure of parachordal cells (PACs), which are the build-in blocks of the lymphatic system. Around 60 hpf, the intersegmental lymphatic vessels sprout from the PACs and migrate dorsally to form the dorsal lateral lymphatic vessel (DLLV) and ventrally to build the main lymphatic vessel, the thoracic duct (TD). These two vessels are complete by 5 days post fertilization (dpf) (Yaniv et al., 2006).

A novel model for lymphangiogenesis suggests that the lymphatic specification process starts as early as 24 hpf (Nicenboim et al., 2015). It was thought that the lymphatics cells derive from veins, but cell tracing experiments revealed that the lymphatics come from a cluster of precursor cells or angioblasts that locate anatomically within the plate of the ventral posterior cardinal vein (PCV). These precursors can give rise to cells of the venous, arterial and lymphatic fate (Nicenboim et al., 2015). The precursors divide asymmetrically and the Prox1^{+} specified cells migrate towards the dorsal part of the PCV prior budding off the vein towards the horizontal myoseptum (Koltowska et al., 2015) . A summary of the vascular development steps can be found in Figure 1-3.

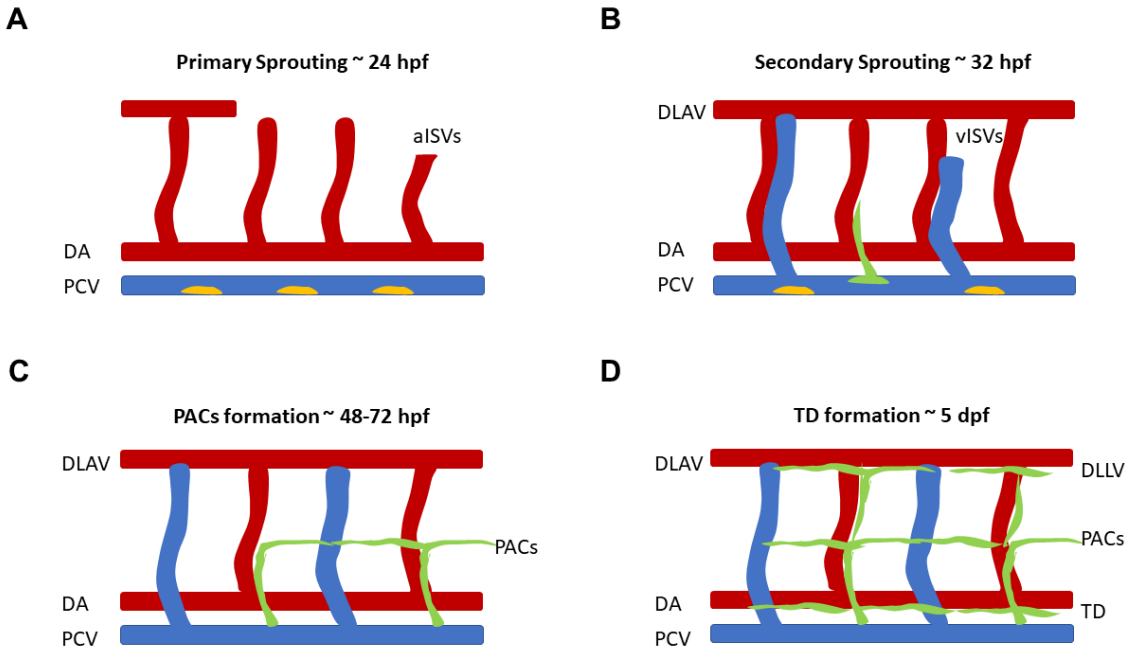

Figure 1-3. Vascular development in zebrafish.

Schematic illustration of the formation of the major blood and lymphatic vessels. DA:Dorsal Aorta, PCV: Posterior Cardinal Vein, DLAV: Dorsal Longitudinal Anastomotic Vessel; aISVs: arterial Intersegmental Vessel; vISVs: venous Intersegmental Vessel; PACs: Parachordal cells; DLLV: Dorsal Longitudinal Lymphatic Vessel; TD: Thoracic duct. Henceforth, red marks arterial identity, blue marks venous identity and green marks the lymphatic identity of the vessels. Yellow cells marked in panel A and B refer to the angioblasts. A) Around 24hpf the major vessels DA and PCV have been formed and aISVs sprout from the DA to form the DLAV. B) Around 32 hpf, the secondary sprouting generates vISVs. C) At 72hpf the PACs have been formed and aligned. D) By 5dpf two new lymphatic structures have been completed: the DLLV in the dorsal side and the TD in the ventral side. Adapted from (Padberg et al., 2017)

1.4 Objectives

The specification of cells into the vascular lineage and subsequent lymphatic fate is a very complex process in which many cell-specific differentiation programs as well as developmental signaling pathways are under strict control. The expression of specific genes is activated in a spatial and temporal manner and requires the appropriate expression of different gene regulators.

The AP-1 member JUNB, is a context-dependent transcription factor that has been demonstrated to play an essential role in vascular development in mouse embryos acting as an activator of pro-angiogenic molecules. Recently, a new role of JUNB in the regulation of lymphatic vasculature development in zebrafish via its target miR-182 was unraveled. This study also uncovered that transient loss of *junba* and *junbb* in zebrafish provoked a failure in lymphatic formation (Kiesow et al., 2015). Yet, the underlying mechanism still remains to be clarified.

According to the latest lymphangiogenesis model (Nicenboim et al., 2015; Koltowska et al., 2015), the defect on the development of lymphatics could be due to an impairment of any of the following biological processes: i) angioblast formation and proliferation, ii) lymphatic endothelial cell specification and differentiation, iii) sprouting of the lymphatic precursors from the posterior cardinal vein (PCV) and iv) lymphatic cell migration.

Thus, I aimed to investigate whether JUNB regulatory functions are needed during lymphatic vessel development and identify which developmental steps are altered upon *Junb* loss.

In order to answer these questions I will use a dual approach: i) an *in vitro* differentiation of murine embryonic stem cells (mESCs) into lymphatic endothelial cells (LECs) to investigate the angioblast formation and the early lymphatic endothelial cell differentiation steps and ii) *in vivo* generation and characterization of *junb*-ablated zebrafish mutants using imaging techniques to investigate the sprouting and migration of lymphatic cells.

For each of the approaches, the following specific questions will be addressed:

In vitro study of the JUNB regulatory functions in mammalian lymphangiogenesis:

1. Is JUNB implicated in mammalian lymphangiogenesis?
2. Which specific steps of LEC differentiation are altered upon *Junb* loss?
3. Is any lymphatic fate regulator deregulated upon *Junb* loss?

In vivo study of lymphangiogenesis in *junb*-ablated zebrafish mutants:

4. Can *junb*-ablated zebrafishes be generated?
5. Do *junb* mutant fishes exhibit lymphatic defects?

2 MATERIALS

2.1 Equipment

2.2 Consumables

2.3 Chemicals

2.4 Software

2.5 Molecular Biology reagents

2.6 Buffers and Solutions

2.7 Oligonucleotides

2.8 Plasmids

2.9 Antibodies

2.10 Cell lines and cell culture media

2.11 Zebrafish lines

2. Materials

2.1 Equipment

Bacteria Incubator Kelvitron©t	Heraeus Instruments, Hanau
Bacteria shaker HT Infors AG CH-4103	Infors, Bottmingen
Binocular M10	Leica, Wetzlar
Cell counter Z2 Coulter Particle Counter	Belckman Coulter, USA
Cell culture sterile hood SterilGard Hood	The Baker Company, USA
Cell incubator Binder Incubator 9140-0013 CB210	Binder, Tuttlingen
Cell incubator Heracell 240i CO2 incubator	Thermo Scientific, USA
Centrifuge Heraeus Megafuge 16	Thermo Scientific, USA
Centrifuge Heraeus Pico 17	Thermo Scientific, USA
Centrifuge J2-HS	Beckman, USA
Centrifuge Varifuge 3.OR Sephatech	Heraeus Instruments, Hanau
Chemical hood Airflow Controller RVC 90.1	Waldner, USA
Confocal microscope LSM 710	Zeiss, Oberkochen
Confocal microscope LSM 780	Zeiss, Oberkochen
Cooling centrifuge 5403, 5415R	Eppendorf, Hamburg
Cryo freezing container Nalgene	Thermo Fisher Scientific, USA
Developer Classic E.O.S.	Agfa, USA
Electrophoresis chamber for agarose gels	Serva, Heidelberg
Electrophoresis chamber for agarose gels	PeqLab, Erlangen
Electrophoresis chamber for SDS-PAGE	Bio-Rad Laboratories, Munich
Electrophoresis Power supply Power Pac 300/Pac 3000	Bio-Rad Laboratories, Munich
FACS CaliburTM	Becton Dickinson Biosciences, Heidelberg
FACS Canto	Becton Dickinson Biosciences, Heidelberg
Magnetic stirrer/Heater Heidolph MR2000	Heideloph, Schwabach
Micromanipulator/Injectior	World precision instruments
Microscope Nikon Eclipse Ti	Nikon, Düsseldorf
Microscope Olympus 1x51	Olympus,UK
Multiplate reader Clariostar	BMG Labtech, Ortenberg
NanoDrop 1000 Spectrophotometer UV-Vis	Thermo Fischer Scientific, USA
PCR Cycler PTC-200	MJ Research, USA
pH-meter	Knick, Berlin
Pipets	Gilson, USA
Pipettor Pipetboy	Integra Biosciences, Switzerland
Platform shaker Polymax 2040	Heidolph, Schwabach
Scale Model L2200S	Sartorius, Göttingen
Scale Model XS205	Mettler-Toledo, Giessen
Scales	Sartorius, Göttingen
Shaker mini Ika® Model MS1	Sigma-Aldrich, Munich
Shaker Multitron Infors	Bottmingen, Schweiz
Shaker Roto-shake Genie	Scientific Industries, USA
Shaker Thermomixer Confort	Eppendorf, Hamburg
StepOne Plus real time PCR System	Applied Biosciences,UK
Thermal Cycler MJMini Personal	Bio-Rad Laboratories, Munich
Thermocycler MJ Mini	Bio-Rad Laboratories, Munich
Thermomixer 5437	Eppendorf, Hamburg
UV-Stratalinker 2400	Stratagene, Heidelberg
Vortex	Bender+Hobein, Ismaning

Water baths	GFL, Burgwedel
Wet blot transfer system	Sigma, Deisenhofen
Zebrafish aqua culture system	Tecniplast, USA
Zebrafish breeding tanks	Tecniplast, USA

2.2 Consumables

Cell culture dishes 100mm	Sigma Aldrich, USA
Cell culture dishes 6-well, 12-well, 24-well, 96-well	Sigma Aldrich, USA
Cell scraper	Corning Incorporated, Mexico
Conical centrifuge tubes 15ml, 50ml	Corning, USA
Cover glasses	Menzel-Gläser, Braunschweig
Cryo vials	Thermo Fisher Scientific, USA
Elisa plate Microlon	Greiner Bio-One, Austria
Filter flask 0.22µm 200ml, 500ml	Sigma Aldrich, USA
Filter pipet tips 10 µl, 20 µl, 200 µl, 1000 µl	Neptune, USA
Luminac-200, flat bottom 96-well plates	Sigma Aldrich, USA
MicroAmp 96-Well Optical Adhesive Film	Applied Biosystems, UK
MicroAmp® fast optical 96-well reaction plate	Applied Biosystems, UK
Microflex powder-free nitrile examination Gloves	Microflex, USA
Mister Frosty TM Freezing Container	Thermo Fisher Scientific, USA
Object slides SuperFrost Plus	Thermo Fisher Scientific, USA
Opitran BA-S83 Nitrocellulose membrane	GE Helthcare, Munich
Parafilm PM996	Bemis flexible packaging, USA
Pasteur pipets	WU, Mainz
PCR reaction tubes (8-well stripes)	Nerbe plus, Winsen/Luhe
Pipet tips 10µl, 20µl, 200µl, 1000µl	Nerbe plus, Winsen/Luhe
Pipet tips (filtered)10µl, 20µl, 200µl, 1000µl	Neptune Rapton, USA
Pipets plastic 5 ml, 1 ml,	Sigma Aldrich, USA
Plastic container for cell counter	Nerbe plus, Winsen/Luhe
Polystyrene Round-Bottom Tube/ cell-Strainer cap 5ml	Falcon, Corining, USA
Reaction tubes 1.5 ml, 2 ml	Eppendorf, Hamburg
Serological pipette plastic 5ml,10ml,25ml,50ml	Costar Incorporation, USA
Syringe 10ml	Dispomed, Gelnhausen
Syringe filters 0.22 µm	Renner, Darmstadt
Western blot membrane Optitran BA-S83	Schleicher & Schüll, Dassel
Whatman 3 MM paper	Whatman, Dassel
X-ray films	Fuji, Düsseldorf

2.3 Chemicals

1-phenyl-2-thiourea (PTU)	Sigma-Aldrich, USA
3-amino benzoic acidethylester (Tricaine)	Sigma-Aldrich, USA
4-(2-hydroxyethyl)-1-piperazineethanesulfonic acid (HEPES)	Sigma-Adrich, Taufkirchen
5-Bromo-4-Chloro-3-Indolyl β-D-Galactopyranoside (X-Gal)	Thermo Fisher Scientific, USA
Acetic acid	Merck, Darmstadt
Acrylamid/Bisacrylamid Rotiphorese® (37,5:1)	Roth, Karlsruhe
Agar	Roth, Kalsruhe
Agarose	Roth, Karlsruhe
Ammonium peroxodisulfate (APS)	Sigma Aldrich, Taufkirchen
Ampicillin Sodium Salt	Sigma Aldrich, USA
ATX Ponceau S red staining Solution	Fluka Analytical, Munich
Boric acid	Sigma Aldrich,USA
Bovine serum albumine, fraction V (BSA)	PAA, Pasching, Austria
Calcium chloride (CaCl2)	Merck, Darmstadt
Chloroform	Sigma Aldrich, Munich
Coulter Isoton II Diluent	Belckmann Coulter, Krefeld
Dimethylsulfoxide (DMSO)	Sigma-Aldrich, Munich
Dithiothreitol (DTT)	AppliChem, Darmstadt
Enhanced chemoluminescence solution (ECL)	Perkin Elmer, USA
Ethanol (EtOH)	Fisher Scientific, UK
Ethanolamine	Merck, Darmstadt
Ethidiumbromide	AppliChem, Darmstadt
Ethylenediamine-tetraacetatic acid (EDTA)	Roth, Karlsruhe
FACS Clean/Flow/Rinse Solutions	BD Biosciences, USA
Formaldehyde	Roth, Karlsruhe
Formamide	Sigma-Aldrich, Munich
Gelatine	Merck, Darmstadt
Glycerol	Roth, Karlsruhe
Glycine	AppliChem, Darmstadt
Isopropanol (2-Propanol)	Sigma-Aldrich, Munich
Isopropyl-β-D-thiogalactoside (IPTG)	Sigma Aldrich, Munich
Kanamycin	Sigma-Aldrich, Munich
Litium Cloride	Roth, Karlsruhe
Magnesium sulfate (MgSO4)	Sigma-Aldrich, Munich
Magnesiumchloride (MgCl2)	Sigma-Aldrich, Munich
Manganchloride (MnCl2)	Sigma-Aldrich, Taufkirchen
Methanol	Merck, Darmstadt
Methylcelllulose	Sigma-Aldrich, Munich
Milk poder	Roth, Karlsruhe
Monosodium phosphate (NaH2PO4)	Sigma-Aldrich, Munich
Monosodium phosphate (NaH2PO4xH2O)	Merck, Darmstadt
N, N, N', N', Tetramethylethylenediamine (TEMED)	Roth, Karlsruhe
Paraformaldehyde	Roth, Karlsruhe
Phenol	Roth, Karlsruhe
Phenol Chloroform pH 4.0	Sigma-Aldrich, Munich
Phenol Chloroform pH 8.0	Sigma-Aldrich, Munich
Phenol red	Sigma-Aldrich, USA
Potassium chloride (KCl)	Roth, Karlsruhe
Potassium dihydrogen phosphate	Roth, Karlsruhe

Sodium chloride (NaCl)	Fluka Chemicals, Switzerland
Sodium deoxycholate	Sigma-Aldrich, Munich
Sodium dodecylsulfate (SDS)	Gerbu Biotechnik, Gaiberg
Sodium hydroxyde (NaOH)	VWR, Leuven, Belgium
Sodium phosphate dibasic dihydrate (Na2HPO4x2H2O)	Roth, Karlsruhe
Sodiumacetate-trihydrate (NaOAc)	Roth, Karlsruhe
Tergitol-type NP-40	Sigma-Aldrich, Munich
Tris-base	Roth, Karlsruhe
Tris-hydrochloride (Tris-HCl)	Roth, Karlsruhe
Triton-X-100	AppliChem, Darmstadt
Trypan blue	Sigma-Aldrich, Munich
Tryptone	Roth, Karlsruhe
Tween-20	AppliChem, Darmstadt
Xylol	AppliChem, Darmstadt
Yeast extract	Roth, Karlsruhe
β-Mercaptoethanol	Sigma-Adrich, Taufkirchen

2.4 Softwares

Adobe Illustrator	Adobe Systems,USA
Alibaba 2.1 http://gene-regulation.com/pub/programs/alibaba2/	open source, designed by Niels Grabe
ApE- A plasmid Editor http:// www.biology.utah.edu/jorgensen/wayned/ape/	open source, designed by M. Wayne Davis
BD CellQuest ProTM	Becton Dickinson Biosciences, Heidelberg
BD FACSDiva™ Software	Becton Dickinson Biosciences, Heidelberg
Cell A v.3.3	Olympus Soft Imaging Solutions
Chop-Chop(Labun et al., 2016) http://chopchop.cbu.uib.no	non-profit, Harvard University
Clustal Omega alignment(Sievers et al., 2011) https://www.ebi.ac.uk/Tools/msa/clustalo/	non-profit, EMBL-EBI, UK
CRISPR design tool (Hsu et al., 2013) http://crispr.mit.edu/Feng	non profit, Zhang group, MIT, USA
Zotero v5.0	open source, RRCHNM.org
FlowJo v.10	Tree Star, Inc., Ashland, USA
Graphpad Prism	GraphPad Software, Inc., La Jolla, USA
ImageJ	open source NIH, USA
In Silico PCR(Kent et al., 2002) http://genome.ucsc.edu/cgi-bin/hgPcr	open source, UCSC, USA
MARS Data-Analysis Software V3.00.R3	BMG Labtech, Ortenberg
Microplate Reader CLARIOstar V5.00.R4	BMG Labtech, Ortenberg
NIS Elements AR 4.13.04	Nikon, Darmstadt
Office 2010	Microsoft, USA
Primer blast (Ye et al., 2012) https://www.ncbi.nlm.nih. gov/tools/primer-blast/	open source NIH, USA
Snap Gene and Sanp Gene Viewer 4.1	Life Technologies, Darmstadt
StepOne Software v.2.2.2	Life Technologies, Darmstadt
Tm calculator	Thermo Scientific , USA
ZEN	Carl Zeiss AG, Oberkochen

2.5 Molecular reagents

4-Nitro Blue Tetrazolium (NBT)	Sigma-Aldrich, USA
7-AAD Viability Staining Solution	eBioscience, Frankfurt
Acc65I Fast Digest	Thermo Fisher Scientific, USA
Accutase® Cell Detachment Solution	Sigma Aldrich,USA
alpha-Digoxigenin Alkaline Phosphatase-conjugated Fab	Sigma-Aldrich, USA
BamHI Fast digest	Thermo Fisher Scientific, USA
Benzonase© Nuclease HC (90% purity)	Novagen, Darmstadt
Bradford MX Protein Assay	Expedeon, Cambridge, UK
Brdu Flow Kit	BD Biosciences, USA
Cas9 protein	Thermo Fisher Scientific, USA
Dako Fluorescence Mounting Medium	Dako North America Inc,USA
DH5α Competent Cells	Thermo Fisher Scientific, USA
DIG RNA Labelling Kit	Sigma-Aldrich, USA
DMEM/F12 medium	Gibco, USA
DNA ladders (50bp, 100bp, 1kb)	New England Biolabs, USA
DNA loading Dye (6x)	Thermo Fisher Scientific, USA
DNAseI (4000U/mg)	AppliChem, Darmstadt
dNTP mix (25 mM each)	Thermo Fisher Scientific, USA
Dual Glo® Luciferase Assay System	Promega, Mannheim
Dulbecco´s Modified Eagle´s Medium (high glucose)	Sigma-Aldrich, USA
Dulbecco´s Phosphate Buffered Saline (PBS)	Sigma-Aldrich, USA
eBioscience™ Annexin V Apoptosis Detection Kit APC	Invitrogen, USA
Endothelial Cell Growth Medium Kit C-22110	Promocell, Heidelberg
Endothelial Cell Growth Supplement (ECGS)	Promocell, Heidelberg
ESGRO (LIF) , 1 million units	Merck, Darmstadt
Fast Digest Buffer (10x)	Thermo Fisher Scientific, USA
Fetal Bovine Serum	Sigma-Aldrich, USA
Fetal Bovine Serum, embryonic stem cell-qualified	Life Technologies, USA
Forskolin	Sigma-Aldrich, Taufkirchen
FuGENE© HD Transfection Reagent	Promega, Mannheim
Gateway BP Clonase© Enzyme Mix	Invitrogen, USA
Gateway LR Clonase©II Plus Enzyme Mix (multi)	Invitrogen, USA
Gateway LR Clonase©II single	Invitrogen, USA
GENEART® Site Directed Mutagenesis System	Invitrogen, USA
GlutaMAX® Supplement	Life Technologies, USA
Goat serum	Sigma-Aldrich, USA
GoTaq® Green Master Mix	Promega, Mannheim
High Capacity cDNA Reverse Transcription	Applied Bioscience, USA
Hind III Fast Digest	Thermo Fisher Scientific, USA
Hoechst 33342	Biomol, Hamburg
Knockout® DMEM stem cell medium	Life Technologies, USA
L- Glutamine	Gibco, USA
LDS Sample Buffer (4x)	Thermo Fisher Scientific, USA
Ligation Buffer (2x)	Promega, Mannheim

MEGAshortscript T7 kit AM1354	Ambion, USA
Metaphor © Agarose	Lonza, Switzerland
Minimum essential medium - MEM Alpha Eagle	Biozol Diagnostica, Eching
miRNeasy Micro Kit	Qiagen, Hilden
miRNeasy Mini Kit	Qiagen, Hilden
Mycoplasma PCR Kit	Minerva Biolabs, Berlin
Non-essential Amino Acids (100x)	Gibco, USA
NotI	Thermo Fisher Scientific, USA
NucleoSpin® Gel and PCR Clean-up	Macherey Nagel, Düren
Oligo(dT)-Primer (0,5 µg/µL)	Thermo Fisher Scientific, USA
Opti-MEM Reduced Serum Medium	Thermo Fisher Scientific, USA
PageRuler™ Prestained Protein Ladder (10 to 180 kDa)	Thermo Fisher Scientific, USA
Penicillin/Streptomycin Solution	Sigma Aldrich,USA
Phosphatase Inhibitor Mix II Solution	Serva, Heidelberg
Plasmid Kit Nucleospin©	Macherey Nagel, Düren
Polyethylenimine (PEI)	Sigma-Aldrich,USA
Power SYBR® Green PCR Master Mix	Life Technologies, USA
Pre-Diluted protein assay standard: BSA Set	Thermo Fisher Scientific, USA
Protease Inhibitors Cocktail	Sigma Aldrich,USA
Proteinase K	Sigma Aldrich,USA
PureLink© HiPure Plasmid Maxiprep Kit	Invitrogen, USA
Q5 High-Fidelity Master Mix (2x)	New England Biolabs, USA
Qiazol Lysis Reagent	Qiagen, Hilden
Random Hexamer Primer (100 µM)	Thermo Fisher Scientific, USA
Rapid Ligation Buffer (2x)	Promega, Mannheim
Red Load Taq Master (5x)	Jena Bioscience, Jena
Reverse Transcription Buffer (5x)	Thermo Fisher Scientific, USA
RevertAid Reverse Transcriptase (200 u/µL)	Thermo Fisher Scientific, USA
RiboLock RNase Inhibitor (40 u/µL)	Thermo Fisher Scientific, USA
RNAse Zap	Ambion, Applera
RNase-free DNase-Set	Qiagen, Hilden
SB431542 TGF-β inhibitor	Merck, Darmstadt
Sodium Pyruvate Solution (100x)	Gibco, USA
T4 DNA Ligase (3U/µl)	Promega, Mannheim
TRI Reagent ©	Sigma Aldrich,USA
Trypsin-EDTA (0.25%) phenol red	Life Technologies, USA
VEGF-C murine recombinant	Sigma Aldrich,USA
Whatman paper (extra thick)	Thermo Fisher Scientific, USA
Wizard® SV Gel and PCR Clean-Up System	Promega, Mannheim
XL1Blue Competent Cells	Chem.Agilent, USA
X-Phosphate/5-Bromo-4-Chloro-3-indolyl-phosphate (BCIP)	Sigma-Aldrich, USA
β-Mercaptoethanol (100x)	Gibco, USA

2.6 Buffers

Table 2-1. Buffers and buffer composition.

Buffer	Buffer composition
Acrilamide gel/ running gel 12%	10-15 % acrylamide/bisacrylamide, 375 mM Tris- HCl pH 8.8, 0.1 % SDS, 0.1 % APS and 0.1 % TEMED
Acrilamide gel/ running gel 4%	4 % acrylamide/bisacrylamide solution, 125 mM Tris-HCl pH 6.8, 0.1 % SDS, 0.1 % APS and 0.1 % TEMED
Blue water	0.3g/l Instant ocean, 0.075 g/l calcium sulfate in distilled water
Danieau's solution 1x (pH 7.1)	58mM NaCl, 0,7mM KCl, 0,4mM $MgSO_4$, 0,6mM $Ca(NO_3)_2$, HEPES 5mM in distilled water
DNA Lysis Buffer for cells and tail biopsies	50mM Tris pH 8,0; 100mM NaCl, 100mM EDTA, 1% SDS and fresh 0,5 µg/µl proteinase k
DNA lysis: Extraction alkaline Buffer (pH 12)	25mM NaOH, 0.2mM EDTA
DNA lysis: Neutralizing Buffer (pH 5)	40mM Tris-HCl
Egg water	0,6 g/l aquarium salt in reverse osmosis water and 0,01 mg/l methylene blue
FACS Buffer	1% BSA in 1x PBS
LB-agar	20 g/l, Agar, 10 g/l, 10 g/l NaCl,Tryptone, 5 g/l Yeast extract pH 7.0
Methylcellulose mounting medium	3% methylcellulose in egg water
PBS 10x (pH 7.4)	1.37 M NaCl, 27 mM KCl, 80 mM Na_2HPO_4 x 2 H_2O Sodium phosphate dibasic dihydrate 20 mM KH_2PO_4 Potassium phosphate monobasic.
PBS-T	1X PBS in distilled water and 0.2% Triton
PFA 4% (pH 7.4)	4% PFA in distilled water
PTU 50x	1.5 mg/ml PTU in blue water
Ringer solution	55 mM NaCl, 1.8 mM KCl, 1.25 mM $NaHCO_3$ in distilled water
RIPA buffer	10 mM Tris-Cl (pH 8.0),150mM NaCl,1% NP-40, 0.5% sodium deoxycholate,0.1% SDS,140 mM NaCl.
SOC medium	2% tryptone, 0.5% yeast extract, 10 mM NaCl, 2.5 mM KCl, 10 mM $MgCl_2$, 10 mM $MgSO_4$, and 20 mM glucose.
SSC 20x (pH 7.0)	3M sodium chloride, 300mM tri-sodium citrate dihydrate in distilled water
TAE Tris-acetate-EDTA Buffer 1x	400mM Tris, 200mM acetic acid, 10mM EDTA
TBE Tris/Borate/EDTA 10x	1 M Tris base ,1 M Boric acid ,20 mM EDTA
TBS 10x (pH 8.1)	0.25 M Tris base, 1.37 M sodium chloride in distilled water
TBS-T	1x TBS in distilled water, 0,1% Tween-20
TE Buffer	10 mM Tris, 1 mM EDTA pH 8.0 in distilled water
Time lapse solution	250ml/l Danieau's solution, 50ml/l Tricaine 20x, 20ml/l PTU 50x in egg water
Tricaine 20x (pH 7.0)	400 mg/ml tricaine and 2,1ml/l 1M Tris in egg water
Western Blot Blocking Buffer	5% BSA in PBS-T or 5% milk powder in PBS-T
Western Blot Running Buffer 10x	250 mM Tris-base, 1.92 M glycine, 1% SDS
Western Blot Transfer Buffer 1x	25% methanol, 25mM glycine, 0,15% ethanolamine in distilled water
YT medium	16 g/L Tryptone, 10 g/L Yeast Extract

2.7 Oligonucleotides

Table 2-2. Primers used for genotyping.

Primers	Sequence 5'-3'	Size	Reference
mmu-*Junb* B2 for	GGGAACTGAGGGAAGCCACGCCGAG	685 bp	(Schorpp-Kistner et al., 1999)
mmu-*Junb* B10 rev	AAACATACAAAATACGCTGG		
dre-*junba*_for	TTTGTACGGTCGGAGCATCACAG	211 bp	
dre-*junba*_rev	TTGCAGCTGTTCAGGGTGGTGTA		
dre-*junbb*_for	CCAGCTGAACCACCGGTTTT	222 bp	
dre-*junbb*-rev	GGCCAGTTTGAGTGAGCCCA		
Kalt4 baitR1	CACTGTCCTCCTCCTGGATAT	208 bp	

Table 2-3. Primers used for qRT-PCR.

Primers	Sequence 5'-3'	Size	Reference
dre-*bactin2*_for	TGACAGGATGCAGAAGGAGA	101 bp	(Avraham-Davidi et al., 2012)
dre-*bactin2*_rev	GCCTCCGATCCAGACAGAGT		
dre-*junba*_for	TACACAGCGGCGACCGGAGA-	214 bp	(Kiesow et al., 2015)
dre-*junba*_rev	TCGGCGGGGGCATTTGGTTC		
dre-*junbb*_for	CGTGCTGACGACCCCCACAC	206 bp	(Kiesow et al., 2015)
dre-*junbb*_rev	CCGACTGCAGGGAGGAGCC		
mmu-*Junb*_Q1for	ACGCCGCCTGTGTCCCCCATCAA	175 bp	
mmu-*Junb*_Q2rev	CACTCGACAGCCCCGCGTTCTCAG		
mmu-*Lyve1*_for	GCCAACGAGGCCTGTAAGAT	106 bp	
mmu-*Lyve1*_rev	TCCAACCCATCCATAGCTGC		
mmu-*Nanog*_for	CAGGTGTTTGAGGGTAGCTC	223 bp	
mmu-*Nanog*_for	CGGTTCATCATGGTACAGTC		(Takahashi and Yamanaka, 2006)
mmu-*Oct3/4*_for	TCTTTCCACCAGGCCCCCGGCTC	224 bp	
mmu-*Oct3/4*_rev	TGCGGGCGGACATGGGGAGATCC		(Takahashi and Yamanaka, 2006)
mmu-*Pdpn*_for	AGAGAACACGAGAGTACAACC	203 bp	(Durchdewald et al., 2008)
mmu-*Pdpn*_rev	CAACAATGAAGATCCCTCCGAC		
mmu-*Prox1*_for	TCGCAGCTCATCAAGTGGTT	185 bp	
mmu-*Prox1*_rev	TCTGGAACCTCAAAGTCATTTGC		
mmu-*Rplp0*_for	CCCTGCACTCTCGCTTTCTGGAG	192 bp	
mmu-*Rplp0*_rev	CAGATGGATCAGCCAGGAAGG		
mmu-*Sox2*_for	TAGAGCTAGACTCCGGGCGATGA	297 bp	(Takahashi and Yamanaka, 2006)
mmu-*Sox2*_rev	TTGCCTTAAACAAGACCACGAAA		
mmu-*Vegf-C*_for	TGTGCTTCTTGTCTCTGGCG	148 bp	
mmu-*Vegf-C*_for	CCTTCAAAAGCCTTGACCTCG		
mmu-*Vegfr1*_for	TGCTAAGAGCCTGGACAGTG	190 bp	
mmu-*Vegfr1*_rev	GCAACAGGCTTTGAACAGCA		
mmu-*Vegfr2*_for	GACCCGGCCAAACAAGCCCG	208 bp	
mmu-*Vegfr2*_for	ACCCTCTCTCCTCGTCCCGC		
mmu-*Vegfr3*_for	AGATGCAGCCGGGCGCTGCGCT	143 bp	(Hamada et al., 2000)
mmu-*Vegfr3*_for	TAGGCTGTCCCCGGTGTCAATC		

Table 2-4. Primers used for zebrafish line generation.

Primers	Sequence 5'-3'
dre-*junba* crispr gRNA_for	TAGGACGGATTCGTCAAAGCGC
dre-*junba* crispr gRNA_rev	AAACGCGCTTTGACGAATCCGT
dre-*junbb* gRNA for	TAGGGTTACGGTCACAACGACG
dre-*junbb* gRNA rev	AAACCGTCGTTGTGACCGTAA
stop cassette *junba*	GAAATCGACTTCTACACAGCGGCGTCATGGCGTTTAAACCTTAATTAAGC TGTTGTAGACCGGAGACGTGGGCTCGCTGA
stop cassette *junbb*	TTGGGTTACGGTCACAACGAGTCATGGCGTTTAAACCTTAATTAAGCTGT TGTAGCGCGGCTCTACACGACTACA
junba 1A RF Kalt4_for	CACTAGTAACGGCCGCCAGTGTTGCTTATGGTCATCCAGACGCT
junba 1A RF Kalt4_rev	GGATATCTGCAGAATTCGCCCTTTTTCAGCGAGCCCACGTCTT
junbb 1b RF Kalt4_for	CACTAGTAACGGCCGCCAGTGTCCAGCTGAACCACCGGTTTTCAA
junbb 1b RF Kalt4_rev	GGATATCTGCAGAATTCGCCCTTGGCCAGTTTGAGTGAGCCCA
attb1 *junba*_for	GGGGACAAGTTTGTACAAAAAAGCAGGCTTCACCATGTCAACAAAAATG GAGCAACCG
attb2 *junba*_rev	GGGGACCACTTTGTACAAGAAAGCTGGGTAAAACGACTTGATCTTGGGC GTCAG
attb1 *junbB*_for	GGGGACAAGTTTGTACAAAAAAGCAGGCTTCACC ATGAGTACAAAAATGGAGCAGCCG
attb2 *junbB*_rev	GGGGACCACTTTGTACAAGAAAGCTGGGTAAAACGCCTCCATCTTACTG GTCAG

Table 2-5. Primers used for promoter cloning.

Primers	Sequence 5'-3'
dre-flt1-prom_rev	ATGTCATTGGTACCTCCGCCATTGTTACAGATATACAAG
dre-flt1-prom_rev	ATGTCATTAAGCTTCAAACTCCTGAAACCCTGCG
dre-flt1-CRE1 mut_for	CAAAGGGGGCTAATAATTCAGGGCTCCACTGTACACCAGTAAACAG
dre-flt1-CRE1 mut_rev	CTGTTTACTGGTGTACAGTGGAGCCCTGAATTATTAGCCCCCTTTG
dre-flt1-CRE2 mut_for	CATCGGGCTCGTGTAGGAGGGCTCCGTTGCGGGATGGGTGTGTC
dre-flt1-CRE2 mut_rev	GACACACCCATCCCGCAACGGAGCCCTCCTACACGAGCCCGATG
dre-flt1-CRE3 mut_for	GATGGGTGTGTCGATGAGGCTCCCGGAAGCTCCGGTGGCGG
dre-flt1-CRE3 mut_for	CCGCCACCGGAGCTTCCGGGAGCCTCATCGACACACCCATC
dre-flt1-TRE1 mut_for	CTCCGGTGGCGGTGGGAAAATGTTCCATCCCAGCCCGCGGTCATG
dre-flt1-TRE1 mut_rev	CATGACCGCGGGCTGGGATGGAACATTTTCCCACCGCCACCGGAG

Table 2-6. Primers used for sequencing.

Primers	Sequence 5'-3'
M13 uni (-21)	TGTAAAACGACGGCCAGT
pGL3 for	CTAGCAAAATAGGCTGTCCC
SP6	CATTTAGGTGACACTATAG
T7	TAATACGACTCACTATAGGG

2.8 Plasmids

Table 2-7. Plasmids used for cloning.

Plasmid name	Origin
5' E2A tag RFP	Gil Levkowitz Lab
5x mutated TRE-pGL3	Peter Angel Lab
5x TRE-pGL3	Peter Angel Lab
800bp dre-Flt1-pGL3	This work
800bp dre-Flt1-pGL3 CRE1 mutated	This work
800bp dre-Flt1-pGL3 CRE2 mutated	This work
800bp dre-Flt1-pGL3 CRE3 mutated	This work
800bp dre-Flt1-pGL3 TRE3 mutated	This work
DONR221	Invitrogen
DONR221-junba-no stop	This work
DONR221-junbb-no stop	This work
eGFPbait-E2A-KalTA4-pA (addgene #61069)	Filippo del Bene Lab (Auer et al., 2014)
p5E-UAS- 10x UAS element and basal promoter for Gal4	#327 Tol2kit Doug Campbell, Chien lab
pBSK junbA T7 antisense	Bettina Füssel, Peter Angel Lab
pBSK junbB T7 antisense	Bettina Füssel, Peter Angel Lab
pBSK junbB T7 sense	Bettina Füssel, Peter Angel Lab
pCR4 TOPO Zf-Junba IS	Atsushi Kawakami, TIT, Japan
pCR4 TOPO Zf-Junbb IS	Atsushi Kawakami, TIT, Japan
pDestTol2pAa destination vector	#392 Tol2kit Clemens Grabher, Look lab
Pgemt	Promega
pGEMT junbA T7 sense	Bettina Füssel, Peter Angel Lab
pGL3	Promega
PmaxGFP	Amaxa/Lonza
pT7-gRNA (addgene #46759)	Wenbiao Chen (Jao et al., 2013)
pU18 control plasmid	Thermo Scientific
TK renilla	Peter Angel Lab
UAS:junba-E2A-RFP	This work
UAS:junbb-E2A-RFP	This work

2.9 Antibodies

Table 2-8. Antibodies used for Western Blot.

Antibody	Source	Concentration	Company
CyclophilinA	rabbit polyclonal	1:1000	Cell signalling, #2175
Junb (210)	rabbit polyclonal	1:1000	Santa Cruz Biotechnology, sc-73
RFP	mouse monoclonal	1:10000	Sigma,SAB2702214
VEGFR1 (Y103)	rabbit monoclonal	1:2000	Abcam, ab32152
VEGFR2 (55b11)	rabbit monoclonal	1:1000	Cell signalling,#2478
anti-mouse HRP-conjugated	Horse	1:2500	Cell Signaling; #7076S
anti-rabbit HRP-conjugated	Goat	1:2500	Cell Signaling; #7074S

Table 2-9. Antibodies used for Flow cytometry.

Antibody	Source	Concentration	Company
anti-CD105-APC MJ7/18	Rat	1:100	Miltenyi Biotec 130-092-930
anti-CD31-APC	Mouse	1:100	Affymetrix eBioscience 17-0311
anti-rabbit APC IgG (H+L)	Goat	1:250	Thermo Fisher, A10931
APC-rat IG2a k isotype control	Rat	1:20	eBioscience 17-4321-71
VEGFR1 (Y103)	rabbit monoclonal	1:2000	Abcam, ab32152
VEGFR2 (55b11)	rabbit monoclonal	1:1000	Cell signalling,#2478

2.10 Cell lines and cell culture media

Table 2-10. Cell lines used for experiments.

Cell type		Species	Reference
MEFs	immortalized	Mouse	(Licht et al., 2006; Schorpp-Kistner et al., 1999)
Endothelioma	immortalized	Mouse	(Licht et al., 2006)
mESCs	primary	Mouse	(Schorpp-Kistner et al., 1999; Licht et al., 2006)

Table 2-11. Culture media for the different cell types.

Medium	Medium composition
Freezing medium	10% DMSO, 20% FCS, 70% medium
Frezing medium mESCs	10% DMSO, stem cell-qualified 25% FCS, 70% KNOCKOUT DMEM medium
Medium Endothelioma	DMEM (high glucose), 10% FBS, 1% Penicillin/Streptomycin, 2% L-Glutamine, 2nM Endothelial Cell Growth Supplement (ECGS), 1% Sodium Pyruvate, 1 % Non-essential amino acids
Medium F9 cells	F12/DMEM medium, 10% FBS, 1 % Penicillin/Streptomycin, 1% L-Glutamine, 1% Sodium Pyruvate, 1 % Non-essential amino acids and 0,1mM β-mercaptoethanol
Medium MEFs	DMEM (high glucose), 10% FBS, 1% L-Glutamine,
Medium mESC LEC-directed differentiation	Endothelial Cell Medium kit (0,02 ml/ml FBS, 0,004ml/ml endothelial cell growth supplement, 0,1 ng/ml epidermal growth factor, 1ng/ml basic fibroblast growth factor, 90 µg/ml heparine, 1µg/ml hydrocortisone, 100ng/µl of VEGF-C to and 10 µM SB431542
Medium mESC spontaneous differentiation	alpha-modified Minimum Essential Medium Eagle (alphaMEM), stem cell qualified 10% FBS, 1% Penicillin/ Streptomycin, 2mM Glutamax and 0,1mM β-mercaptoethanol
Medium mESC stem cells	KNOCKOUT DMEM, stem cell qualified 10% FBS, 1% Penicillin/ Streptomycin, 2mM Glutamax, 0,1mM β-mercaptoethanol and 1000 U/ml of murine Leukemia Inhibitory Factor (LIF)

2.11 Zebrafish lines

Table 2-12. Transgenic lines used for experiments.

Zebrafish line	Reporter tissue	Reference
Tg(fli1:EGFP)^{y1}	Pan-endothelial GFP expression	(Lawson and Weinstein, 2002)
Tg(fli1:gal4^{ubs3};uas:Kaede^{k8})	Endothelial expression of Gal4	(Herwig et al., 2011)
Tg(HuC/D:Gal4)	Neuronal expression of Gal4	(Faucherre and López-Schier, 2011)

3. METHODS

3.1 Molecular Biology

3.2 Protein methods

3.3 Flow Cytometry

3.4 Cloning

3.5 Cell culture

3.6 Luciferase Reporter Assay

3.7 Animal experiments

3.8 Imaging

3.9 Statistical analysis

3.1 Molecular methods

3.1.1 DNA extraction

The genomic DNA was extracted from cells and tail biopsies of mice. Samples were digested on fresh lysis buffer containing 0,5 µg/µl proteinase K at 56°C for two hours (cells) or overnight (tail biopsies) with gentle shaking. Proteins and SDS complexes were separated by adding 1/3 of the volume of saturated 6M sodium chloride, vigorous shaking and maximum speed centrifugation for 15 minutes. The DNA-containing supernatant was then precipitated by mixing it with 1 volume of propanol-2 and centrifuged at maximum speed for 20 minutes. The pellet was further washed with 70% ethanol. The final pellet was air dried to remove any residual alcohol and re-suspended in water according to pellet size.

The genomic DNA from zebrafish embryos and fin biopsies were isolated using the hot sodium hydroxide and Tris (HotSHOT) method (Truett et al., 2000) . In short, the tissue was digested in one volume of alkaline extraction buffer (pH 12) at 95°C for 1 hour. Subsequently, one volume of the neutralizing buffer (pH 5) was added.

3.1.2 RNA isolation

Cell samples were washed twice with cold 1x PBS to remove residual proteins from the medium supplements before starting the isolation protocol. For the zebrafish samples, around 30 embryos at different stages were manually dechorionated. They were anaesthetized and kept on ice for at least 10 min before proceeding to the lysis step.

Total RNA isolation from cells, tissues and zebrafish embryos was isolated using Trizol© reagent and TRI Reagent© respectively prior to mRNeasy minikit and microKit (< 500000 cells) according to manufacturer´s instructions. DNAse on-column treatment was included in all cases. Isolated RNA was stored at -80°C.

3.1.3 DNA/RNA quantification

DNA and RNA concentrations were measured by the Nanodrop ND-1000 UV VIS spectrophotometer. The concentration of the nucleic acids was calculated based on their absorbance readings at 260 nm considering that one optical unit at 260 nm ~ corresponds to 50µg/ml of DNA and ~40µg/ml of RNA.

The quality of the nucleic acids was controlled by the A260/A230 and A260/A280 ratios. A260/A280 ratio was used to assess the presence of proteins and A260/A230 for the presence of salts or organic contaminants. Pure DNA and pure RNA preparations were

considered when their A260/A280 ratio was equal or greater than 1.8 and 2.0 respectively and their A260/A230 ratio close to 1.8 (Green et al., 2012)

3.1.4 Reverse transcription

500ng to 1µg of RNA isolated from cells was reverse transcribed into cDNA using RevertAid M-MuLV Kit according to instructions of the manufacturer.

Reagent	Volume
RNA	500-1000ng
Oligo dT (0,5 µg/µL)	0,25µl
Random hexamers (10 µM)	0,25µl
Nuclease-free water	Up to 10µl
5x RT Buffer	4µl
25mM dNTPs	0,5µl
Ribolock (40 u/µL)	0,5µl
Reverse transcriptase (200 u/µL)	1µl

The RT reaction was performed using the following parameters:

Initial Denaturation	65°C	5 minutes
Reverse Transcription	42°C	1 hour
Final elongation	72°C	10 minutes
End	10°C	∞

For the zebrafish samples, 1µg of RNA was transcribed using the cDNA Kit: High Capacity cDNA Reverse Transcription, Applied Biosciences according to manufacturer´s instructions. Transcribed cDNA was stored at -20°C.

3.1.5 Polymerase Chain Reaction

PCR was performed routinely to genotype cells using the protocol below

Reagent	Volume
5x Red Load Taq	4µl
Forward primer (10µM)	0,3µl
Reverse primer (10µM)	0,3µl
DNA cells (25ng/µl)	1µl
Nuclease-free water	14,7µl

and the following parameters:

Initial Denaturation	95°C	2minutes
25-30 cycles		
-Denaturation	95°C	30 seconds
-Annealing (according to each primer set)	57°C	1 minute
-Elongation	72°C	30 seconds
Final elongation	72°C	5 minutes
End	10°C	∞

Go Taq Master Mix was used to genotype the zebrafish fin biopsies and embryos.

PCR amplicons were further analyzed by agarose gel electrophoresis. All primers sequences and corresponding melting temperatures are listed on Table 2-2.

3.1.6 Design and validation of quantitative Real Time PCR primers

All qRT-PCR primers were designed using Primer blast (Ye et al., 2012), a primer designing tool from the NCBI, and selected for their specificity, the exon-exon spanning location and efficiency. The efficiency of the qRT-PCR primers was determined by analyzing serial ten-fold dilutions of cDNA ranging from 100ng to 0,001ng. Only primers with efficiency in the range of 1.8-2.1 were used in this study. Primer specificity was assessed by the analysis of the melting curve and the verification of the amplicon size by gel agarose electrophoresis.

The efficiency of the primers was calculated according to equation 1:

Equation 1. Calculation of real time PCR primers efficiency.

$$Efficiency\ (E) = 10^{\left(\frac{-1}{slope}\right)}$$

The slope value is taken from the linear standard curve of the graph log cDNA input vs Ct mean.

All primer information can be found in Table 2-3.

3.1.7 Quantitative Real Time-PCR

The quantitative Real Time PCR was performed using the StepOne Plus real time PCR System (Applied Biosciences). All samples were measured in technical duplicates containing 2,5ng of cDNA as template in a PowerSYBR© PCR Master Green mix as it follows:

Reagent	Volume
Power SYBR Green PCR Mix (2x)	6.25 µl
Forward Primer (50 µM)	0.075 µl
Reverse Primer (50 µM)	0.075 µl
Nuclease-free water	2.25 µl
cDNA template (1 ng/µl)	2.50 µl

Since the RT-PCRs were designed to work at 60°C using the following parameters:

Initial Denaturation	95°C	10 minutes
40 cycles		
-Denaturation	95°C	15 seconds
-Annealing	60°C	30 seconds
Melt Curve (Temperature increment 0,3°C)		
	95°C	15 seconds
	60°C	1 minute
	95°C	15 seconds

All data was analyzed using StepOne software v2.3 The relative expression was calculated applying the ΔΔCt method (Pfaffl, 2001).In short, variations on the initial sample were corrected by normalizing the cycle of threshold (Ct) of the gene of interest (GOI) to the cycle of threshold of the reference gene (REF) according to equation 2:

Equation 2. Mathematical model used for relative quantification.

$$Relative\ expression = \frac{E_{GOI}^{\Delta Ct_{GOI}(mean_{control} - mean_{sample})}}{E_{REF}^{\Delta Ct_{REF}(mean_{control} - mean_{sample})}}$$

E_{GOI} = Real time efficiency of the Gene of interest transcript

E_{REF} = Real time efficiency of the Reference transcript

ΔCt_{GOI} = Ct - deviation of Gene of interest transcript between control and sample

ΔCt_{REF} = Ct - deviation of Reference transcript between control and sample

3.1.8 Gel agarose electrophoresis

DNA fragments were separated according to the size in 0.8% agarose gels (for restricted plasmids), 1,5% agarose gels (for PCR amplicons) or 3% (zebrafish mutant genotyping) stained with 5% Ethidium Bromide solution at constant voltage of 100V. Depending on the amplicon size, DNA ladders of certain range were used as reference of molecular weight.

3.1.9 Nucleic acids purification

DNA purification for further downstream application such as cloning was purified with the kit NucleoSpin® Gel and PCR Clean-up (amplicons after PCR) or with Wizard® SV Gel and PCR Clean-Up System (from gel) according to manufacturer´s instruction.

DNA used for injections in zebrafish embryos needed to go through an extra step of purification by phenol/chloroform/isoamylalcohol 25:24:1 (Chomczynski and Sacchi, 1987). In short, DNA solution was mixed with 1 volume of phenol/chloroform and vigorously mixed. The upper aqueous phase was then mixed with one volume of chloroform and finally the upper phase was mixed with 1 volume of propanol-2 to precipitate the nucleic acids. Since the pH of the phenol-chloroform determines the presence of certain nucleic acids on the aqueous phase, acidic phenol/chloroform pH 4.0 was used for RNA purification and pH 8.0 for plasmid purification.

3.1.10 Sequencing

15µl of 0,7-1 µg DNA solution containing 10pmol/µl of primer was sequenced using the Sanger method (Sanger et al., 1977) by Eurofins or the Sequencing Unit from the Weizmann Institute. More information about the sequencing primers can be found in Table 2-6.

3.2 Protein analyses

3.2.1 Whole cell protein isolation

The cultured cells were washed several times with cold 1x PBS prior harvesting to reduce contamination from proteins present in the medium and its supplements. The cell lysates were incubated on ice in freshly prepared RIPA lysis buffer containing 1mM DTT, 1% of protease inhibitors, 1% phosphatase inhibitors plus 250U benzonase© for 20 minutes. After three freeze-thaw cycles and maximum centrifugation of the lysates for 15 minutes, the protein-containing supernatant was collected and stored at -80°C until further applications.

3.2.2 Protein quantification

The Bradford method was used to determine the protein concentration of the lysates (Bradford, 1976). For this purpose, a dilution of the lysates was mixed with Bradford MX© solution. A BSA set containing Pre-Diluted BSA standard concentrations within a range of 125 to 2000µg/ml were analyzed in parallel to create the standard curve. The absorbance of the samples was measured at 595nm using the Clariostar microplate reader and the Clariostar software V5.00.R4 and the final protein concentrations were calculated using the MARS Data Analysis Software V3.00.R3.

3.2.3 SDS-PAGE electrophoresis

The proteins were separated according to their molecular weight by sodium dodecyl sulfate polyacrylamide gel electrophoresis (SDS-PAGE). In short, 20 µg of the protein lysates were mixed with 4x Laemmli Buffer and boiled for 5 minutes to denature proteins (Laemmli, 1970). The lysates were then loaded into a 12% poly-acrylamide gel in 1x SDS running buffer at 120V for 90 minutes. Protein ladder was used as reference for protein size verification.

3.2.4 Western Blot (Towbin et al., 1979)

Proteins were transferred from the acrylamide gel onto a nitrocellulose membrane using a wet blotting system in transfer buffer at 175A for 2h at 4°C. After disassembling the transfer cassette, the membrane was stained with Ponceau S for rapid and reversible staining of the proteins to check for proper and equal amount of protein for each lane. After that, the membrane was quickly rinsed in 1x PBST buffer until the Ponceau staining was no longer perceptible. Then, the membrane was incubated in blocking buffer containing 5% BSA or 5% dry milk (depending on the primary antibody) for 1h at room temperature. Primary antibody was diluted accordingly in blocking buffer and the membrane was kept in rotation overnight at 4°C. Next, it was washed 3 times for 15 minutes each to remove the traces and the unspecific binding of the antibody. Thereafter, the membranes were incubated in the diluted Horseradish peroxidase (HRP)-linked antibodies. Further on, the membrane was washed again 3 times for 15 minutes and subsequently incubated for 1 minute with a chemiluminiscence agent. Finally, the signal was detected using X-ray films and developer Classic E.O.S (Agfa). All the primary and secondary antibodies are listed in Table 2-8.

3.2.5 Western blot quantification

In order to quantify the amount of proteins, original X-Ray films exposed at similar time points were scanned and transferred into an image file. Using the gel plugging from ImageJ, equal areas of the bands were measured for intensity and corrected with a background control. For the calculations, the pixel density values were inverted. The inverted value was expressed as 255-X being X the pixel density by the gel plugin. The final calculation was the ratio between the net value of the band and the net value of the loading control (Equation 3).

Equation 3. Quantification of western blot signals.

$$\frac{((255 - protein\ of\ interest\ pixel\ density) - (255 - background\ pixel\ density))}{((255 - loading\ control\ pixel\ density) - (255 - background\ pixel\ density))}$$

3.3 Flow Cytometry

Prior to the staining, cells were washed twice with 1x PBS, harvested using 0,25% accutase solution and re-suspended until they were a homogeneous one cell suspension. Cells were quantified using the cell counter Z2 (Beckmann Coulter) and around 250000 cells were used per staining condition.

For direct staining, the fluorophore-coupled antibody was incubated in FACS buffer for 20-30 minutes on ice, light protected and with gentle shaking. For indirect staining, the first antibody was incubated as previously described. After the incubation period, the cells were centrifuged, and the pellet was washed to get rid of the unbound antibody. Secondary fluorophore-coupled antibody was then incubated 1:200 as previously described.

Most of the used antibodies in this study were membrane proteins but some of the epitopes recognized by the antibodies were in the cytoplasm. For those cases, prior the staining procedure, a fixing and permeabilization step was added to allow the antibody to penetrate the cells. The antibodies were diluted in permeabilization buffer to maintain the permeability. In all cases, unstained control and isotype control were analyzed in parallel to assess the specificity of the antibodies and the gating. The samples were analyzed using the FACS Calibur™. All the antibodies and their working concentrations can be found in Table 2-9.

3.4 Cloning methods

3.4.1 pGEM®-T cloning

pGEM®-T easy vector was used to clone PCR amplicons prior to sequencing. pGEM®-T plasmids are linearized plasmids containing 3´T-overhangs which facilitate the ligation of PCR products which avoid re-circularization of the vector. In addition, the vector contains the enzyme β-galactosidase (LacZ operon) which allows blue-white screening for recombinant colonies. For that purpose, IPTG (Isopropyl β-D-1-thiogalactopyranoside), a non-metabolizable inducer of β-galactosidase, and X-Gal, a chromogenic substrate, were added to the agar plates.

β-galactosidase is an enzyme that cleaves lactose into glucose and galactose. In the presence of an analogue of galactose such as IPTG, the β-galactosidase is induced. If β-galactosidase is produced, X-Gal produces a blue pigment called 5,5'-dibromo-4,4'-dichloro-indigo. Therefore, colonies formed by non-recombinant cells will appear blue while the recombinant cells will appear white. Only white colonies were selected for further analysis.

For the ligation, the following mixture was prepared and incubated 1h at room temperature according to manufacturer´s instructions.

Reagent	Volume
pGEM®-T easy (50ng/µl)	1 µl
2x Ligation Buffer	5 µl
T4 DNA Ligase (3U/µl)	1 µl
PCR clean product	0,3 µl
Nuclease-free water	9,7 µl

The volume of the PCR clean product was adjusted for each experiment according to the insert size and concentration (Equation 4).

Equation 4. Calculation of the insertion volume for pGEM-T ligation

$$\frac{insert\ (ng)}{PCR\ product\ concentration\ (ng/\mu l)}$$

3.4.2 Generation of *dre-flt1* 800bp-pGL3 construct

The resulting vector containing 800bp of the promoter region of the zebrafish Flt1 in a pGL3 backbone was obtained by restriction enzyme cloning. pGL3 Luciferase Reporter Vector® is a reporter construct designed for quantitative analysis of gene expression in mammalian cells and contains a region coding for firefly *(Photinus pyralis)* luciferase.

In order to clone the promoter region of interest into the pGL3 vector, the promoter fragment and the vector were treated with the same restriction enzymes to create compatible ends. For this case, the plasmid was linearized with two enzymes of the Multiple Clonal Site (MCS) (*Acc65*I (+1) and *Hind*III (+53)). In addition, specific primers amplifying the targeted 800bp region were designed using ApE software. Flanking sequences recognized by *Acc65*I and *Hind*III were included to the primers.

The zebrafish promoter region was amplified using a proofreading Taq polymerase and zebrafish gDNA as it follows:

Reagent	Volume
2x Q5 High-Fidelity Master Mix	12,5µl
Zebrafish genomic DNA (1ng/µl)	2µl
Primer F (10µM)	1,25µl
Primer R (10µM)	1,25µl
Nuclease free water	8µl

Initial Denaturation	98°C	2minutes
25-30 cycles		
-Denaturation	98°C	30 seconds
-Annealing	65°C	30 seconds
-Elongation	72°C	1 minute
Final elongation	72°C	2 minutes
End	10°C	∞

PCR amplicons were resolved in a 2% agarose gel and purified as described before. PCR amplicon and plasmid were both digested for 1h at 37°C using *Acc65*I and *Hind*III as it follows

Reagent	Volume
Amplicon/pGL3 vector	27 µl
FD Acc65I	2 µl
FD HindIII	2 µl
10x FD Buffer	4 µl
Nuclease-free water	5 µl

Digested PCR amplicon and plasmid were resolved in a 1,5% agarose gel and purified as previously described in section 3.1.9.

Purified amplicons and plasmid were ligated as it follows for more than 2h at RT.

Reagent	Volume
pGL3 (*Acc65*I + *Hind*III)	1 µl
Flt1a/promoter (*Acc65*I + *Hind*III)	1 µl
2x Rapid Ligation Buffer	5 µl
T4 DNA ligase	1 µl
Nuclease-free water	2 µl

5µl of the ligation reaction were transformed in competent bacteria as described in section 3.4.4. Minipreps and maxipreps were prepared as in 3.4.5 and sequenced as in 3.1.10.

3.4.3 Site-directed mutagenesis

Zebrafish *flt1* promoter regions harboring mutated sites were generated according to the GENEART® Site-Directed Mutagenesis System from Invitrogen. 4 potential binding sites were mutated: a consensus CRE site (-196 -188), a CRE site with a variation (-105 -97), half CRE binding site (-72 -67) and one TRE site (-42 -35). Specific primers with the desired modifications were designed according to the manufacturer´s instructions. More information about the mutagenesis strategy can be found in Table 2-5.

In short, the target DNA (the previously generated 800bp *dre-fl1*-pGL3 vector) was methylated by a DNA methylase. The complementary primers harboring the mutated binding sites anneal to the targeted area and recombine. After degradation of methylated DNA, the resulting construct contains the desired modifications. Mutated versions of the construct were transformed into bacteria as described in 3.4.4 Minipreps and maxipreps were prepared as in 3.4.5 and sequenced as in 3.1.10.

3.4.4 Bacterial transformation

Bacterial transformation was used to propagate plasmid DNA. Depending on the plasmid size and the application, Top 10, DHL5 alpha or XL1blue *E.coli* competent bacteria were used. In short, a small amount of ligation product or plasmid (~200ng) was incubated with the bacteria for 20 minutes on ice. After this time, heat shock was performed: bacteria were incubated for 45 seconds at 42°C and then 2 minutes on ice. Between 250-500µl of SOC medium was added and subsequently was incubated for at least 1h at 37°C with gentle shaking. A small volume of this preparation was then seeded onto agar plates (containing the appropriate antibiotic) for selection. Positive colonies were picked and grown into 5ml medium (for mini preps) or in 200ml (for maxi preps). Commercial pU18 plasmid and water were used as positive and negative controls respectively.

3.4.5 DNA isolation from plasmids: minipreps and maxipreps

The plasmids were isolated from minipreps (5ml) or maxipreps(200ml). For small scale isolation, Nucleospin© Plasmid kit was used according to manufacturer´s instructions. For the large-scale purification, PureLink© HiPure Plasmid Maxiprep Kit was used according to manufacturer's instructions. Both kits were based on the same principle. First the bacteria were sedimented from the medium by centrifugation. Then they were re-suspended in alkaline lysis buffer containing RNAse. The suspension was neutralized and clarified by centrifugation to remove proteins, cell debris and genomic DNA. Next, the upper soluble phase was purified on a column containing a silica resin that selectively binds RNA. After several washes with alcohol-based buffers, the plasmids were eluted in water. DNA quality and quantity were assessed with the nanodrop (3.1.3) and sequenced as explained on section 3.1.10.

3.5 Cell culture methods

3.5.1 Culture conditions and maintenance: Murine Embryonic Fibroblasts (MEFs), endothelioma cells, F9 and mouse embryonic stem cells (mESCs)

Mouse Embryonic Fibroblasts *Junb* $^{+/+}$ and *Junb* $^{-/-}$and Endothelioma *Junb*$^{-/-}$ and *Junb* $^{+/-}$ (Schorpp-Kistner et al., 1999; Licht et al., 2006) were cultured on Dulbecco´s Modified Eagle´s Medium (DMEM) with 10% Fetal Bovine Serum (FBS) medium at 37°C and 5% CO_2 and passaged every 3-4 days. Cell-specific medium was changed every other day if not specified otherwise. For each passage, the cells were washed twice with 1x PBS and detached from the surface using Accutase© or 0,25% Trypsin. After a short incubation at 37°C, the cells were counted and seeded accordingly. Murine teratocarcinoma F9 cells were cultured in F12/DMEM based medium and passaged every other day. The medium was changed twice a day and they were treated with 0.025% trypsin prior passaging. mESCs were culture into gelatin-coated dishes, the medium was changed daily and they were passaged every other day. mAll the cells were cultured in sub-confluent conditions and checked regularly. All the cells were manipulated under sterile conditions.

3.5.2 Differentiation of stem cells

Mouse embryonic stem cells were differentiated into lymphatic endothelial cells according to the previously described instructions in human stem cells with several adaptations (Kusuma et al., 2013). Shortly, the cells were subjected to a three-step differentiation protocol. In the first step, the stem cells were cultured on 0,1% gelatin-coated dishes with Knockout DMEM Medium (Gibco) supplemented with 10% stem cell-

qualified Fetal Bovine Serum (Gibco), 1% Penicillin / Streptomycin, 2mM Glutamax (Life Technologies), 0,1mM β-mercaptoethanol (Sigma) and 1000 U/ml of murine Leukemia Inhibitory Factor (LIF) (Millipore). The cells were cultured in the presence of LIF to maintain their stemness property and under feeder-free conditions for three passages. Cells were passaged every other day to low density (30-50%) and medium was changed daily. Thereafter, the cells were succumbed to a mesodermal-derived spontaneous differentiation by culturing the cells in alpha-modified Minimum Essential Medium Eagle (alphaMEM) medium supplemented with 10% stem cell-qualified Fetal Bovine Serum, 1% Penicillin / Streptomycin, 2mM Glutamax (Life Technologies), 0,1mM β-mercaptoethanol (Sigma) yet in the absence of LIF. The cells were plated at a density of 6 x 10^3 cells / cm^2 in absence of LIF to promote spontaneous differentiation , passaged every other day and medium was changed daily. Upon spontaneous differentiation for 6 consecutive days, the cells were subjected to the third step of lymphatic endothelial cell directed differentiation. For this last step, the cells were detached, counted and seeded to the density of 1,25 x 10^4 cells/cm^2 in Endothelial Cell Medium kit supplemented with 100ng/µl of VEGF-C to and 10 µM SB431542, an TGF-β RI (Transforming Growth Factor beta Receptor I) inhibitor (Oka et al., 2008; Clavin et al., 2008; Avraham et al., 2010). The cells were cultured in this medium for another 4 days and the medium was changed every other day. The cells were maintained at 37°C and 5% CO_2.

3.5.3 Freezing and thawing of cells

mESC were dissociated using 0,25% trypsin and separated into a one-cell suspension. They were counted using Cell counter Z2 (Beckmann Coulter) and frozen into 1 million cells/ml cryovials. The freezing medium consist of: 10% Fetal Bovine Serum,10% Dimethyl Sulfoxide (DMSO) and 80% culture medium. mESC freezing medium containing: 65% stem cells medium, 10% Dimethyl Sulfoxide (DMSO) and 15% stem cell qualified Fetal Bovine Serum.

3.5.4 Mycoplasma check

All cells were routinely tested for mycoplasma contamination using Mycoplasma PCR Kit (Minerva Biolabs) according to manufacturer´s instructions.

3.5.5 Transient transfection of cells

For transfection experiments, the cells were seeded 24 hours prior the experiments. Transfection of plasmids into MEFs was performed using polyethylenimine (PEI) and plasmid in a 1:3 (Boussif et al., 1995) Plasmid DNA: PEI ratio and using FuGENE®HD transfection agent for F9 cells using 1:2.5 ratio following manufacturer's instructions. In short, cells were washed with serum-free medium and added the plasmid: transfection reagent complex mixtures in a dropwise manner. Medium of the transfected cells was refreshed after 24 hours. Analyses and harvesting of the cells were performed 48 hours post-transfection.

For the transfection of MEFs using PEI:

Format	# cells	Optimem	Plasmid (1µg/µl)	PEI
12-well dish	25.000 cells	100 µl	1 µl	3 µl

For the transfections of F9 cells using FuGENE®HD

Format	# cells	Serum-free DMEM	Plasmid (1µg/µl)	FuGENE®HD
12-well dish	40.000 cells	100 µl	1µ	2.5 µl
6-well dish	80.000 cells	200 µl	2 µl	5 µl
10 cm dish	800.000 cells	500 µl	5 µl	12.5 µl

3.6 Luciferase Reporter Assay

25000 MEFs were plated in 12-well plates 24 hours prior the transfection. 3 independent transfections using PEI as transfection reagent were carried out in parallel as described in Section 4.3.1. For the luciferase experiment, all the experimental conditions were transfected with 1µg of promoter construct and normalized by co-transfection of 0.05 ng/µl of RSV-Renilla construct. In addition, 5X TRE and mutated 5X TRE vectors were used as internal controls and transfected to assess the efficacy of the luciferase experiment. Transfection efficiency was assessed by transfecting GFPmax construct and controlling GFP expression by fluorescence microscopy. Only transfection rates of 80-90% were considered acceptable to continue with the experiments. 48 hours after transfection, the medium was removed and washed twice with cold 1x PBS prior using Dual-Glo® Luciferase Assay System (Promega). In short, 150 µl of Passive Lysis Buffer was added to the surface of the wells and incubated for 20 minutes with gentle shaking. The protein containing buffer was collected and shortly centrifuged to precipitate cell membranes. 50 µl of the protein isolates were loaded into a white-bottom 96-well plate. For the luciferase Assay, a luminescence program was designed, and the bioluminescence was measured in a Clariostar multiplate reader equipped with injectors primed with the luciferase reagents.

In this program, the multiplate reader inject 100 µl of the Luciferase Reagent and measure the bioluminescence for 10 consecutive seconds. Subsequently, 100 µl of the Stop and Glow reagent was injected in the same well prior bioluminescence measurement.

The data were normalized according to their transfection efficiency by calculating the ration between the sum of the luciferase and renilla signal among the three technical replicates. The ratios of the conditions with transfected promoter vectors were normalized to the condition of the transfected empty pGL3 vector that was set to 1. The statistical analysis was performed among three independent biological replicates.

3.7 Animal experiments in zebrafish

3.7.1 Maintenance and breeding

Zebrafish husbandry and handling during the experimental procedures were performed according to the guidelines of the Weizmann Institute Animal Care and Use Committee (Avraham-Davidi et al., 2012).

All the zebrafish transgenic lines used in this study were previously described: *Tg(fli1:EGFP)*^{y1} (Lawson and Weinstein, 2002), *Tg(fli1:gal4*^{ubs3}*;uas:Kaeder*^{k8}*)* (Herwig et al., 2011) and *Tg(flt1_9a_cFos:GFP)*^{wz2} (Nicenboim et al., 2015). d *Tg*(HuC/D:Gal4) (Faucherre and López-Schier, 2011)

Zebrafish were raised and maintained as previously described in Westerfield, M The Zebrafish Book. A Guide for the Laboratory Use of Zebrafish (*Danio rerio*). In short, larvae and adult zebrafish were kept at 28°C in a 14h light/10h darkness cycle in an aquaculture system (Tecniplast).

All the embryos used in this study were collected from natural spawning. For the natural breeding to take place, females and males were placed separately in false-bottom mating tanks in the evening. The next morning, the transparent divider was removed since the morning light is a natural stimulus to breed. 15-20 minutes after the removal of the separator, the fertilized eggs could be collected in egg water and be ready for injection or kept at 28°C till later stages. Around 4-6 hpf, the embryos were checked under the binocular and only viable eggs were selected for further experiments. Dead embryos were discarded. Depending on the purpose of the experiment, the embryos were raised in different water solutions: if the offspring needed to be raised till adulthood; the embryos were grown in zebrafish embryo medium containing methylene blue that inhibits mold growth in water. When the embryos were used for wholemount immunofluorescence of *in situ* hybridization, they were placed in 0,003% PTU (1-phenyl-

2-thiourea) to inhibit pigmentation. PTU is a chemical that blocks all the tyrosinase-dependent steps during melanin synthesis.

All the embryos used in the study were staged according to the somite number (Kimmel et al., 1995).

3.7.2 Preparation of injection needles and plates

The molds for injection wells were placed on top of petri dishes filled with 1% agarose in blue water and kept at 4°C till the injections.

The needles were prepared from 1mm capillaries tubes with filament that were prepared using the needle puller to obtain an optimum shank.

3.7.3 Injections

For the injections, fine capillaries tubes, injection plates, micromanipulator and microinjector were used. First, the injection solution was loaded into the capillary and placed into the micromanipulator. The needle was broken using a gated pressure in the microinjector. The opening of the tip of the capillary was calibrated and the pressure time was modified accordingly till the injection volume was 1nl. The freshly collected embryos were arranged in the injection wells, oriented in a way that animal pole is opposite to the needle and injected at one-cell stage.

The DNA constructs, Cas9 protein and transposase solutions were injected directly into the cell. RNA was injected into the yolk of the egg since it diffuses into the cell by cytoplasm streaming.

3.7.4 Wholemount In situ Hybridization

Probe synthesis

Sense or antisense probes of *junba* or *junbb* (Ishida et al., 2010) were cloned into BSK plasmids, *in vitro* transcribed and DIG labelled using digoxigenin DIG RNA Labelling Kit (SP6/T7) according to manufacturer´s instructions. Newly transcribed RNA was then sedimented using 4M Lithium Chloride and cleaned by 70% alcohol washes at -20°C. RNA probes were loaded into an agarose gel for stability check and re-suspended in formamide-containing buffer. All probes were stored at -20°C.

Embryo preparation

PTU-treated embryos staged at the age of interest were manually dechorionated and anaesthetized. They were placed on ice for 10 minutes and then fixed in cold 4% paraformaldehyde (PFA) in PBS-T overnight at 4°C with gently shaking. The day after, the embryos were quickly rinsed in PBS-T and dehydrated through a methanol/PBS-T gradient (25%, 50%, and 75%) for five minutes and stored in 100% methanol at -20°C.

Probe Hybridization

The wholemount protocol was based on the published protocol (Thisse et al., 2004). In short, the embryos were hydrated through a methanol gradient (75%, 50%, and 25%) and washed in PBS-T. The embryos were permeabilized with Proteinase K as follows.

Stage	Final Proteinase K	Digestion time
20 hpf	10 µg/µl	6 minutes
24 hpf	10 µg/µl	6 minutes
30 hpf	30 µg/µl	10 minutes

The embryos were fixed again in 4% PFA and incubated in formamide-containing hybridization buffer for two hours. The probes were diluted accordingly in hybridization buffer and incubated at 68°C overnight. The embryos went through a series of washing steps at 68°C to remove the formamide (2x Saline sodium citrate Tween 20) SSCT-50% formamide, 2xSSC-T, 0,2x SSC-T) and incubated in blocking buffer with goat serum for 1 hour at room temperature. 1:5000 sheep alpha-Digoxigenin Alkaline Phosphatase-conjugated Fab fragments were then incubated with the embryos for 2 hours at room temperature with gentle shaking. Subsequently, the embryos were washed overnight. On the next day, later the embryos were shortly calibrated in staining solution before being developed in staining solution with NBT (4-Nitro Blue Tetrazolium)/BCIP(X-Phosphate/5-Bromo-4-Chloro-3-indolyl-phosphate). The staining was controlled every half an hour and stopped according to the intensity of the staining.

The embryos were washed and fixed and stored in glycerol until their imaging. Embryos were oriented in 1% methylcellulose and imaged using a binocular (Leica).

3.7.5 CRISPR design and mutant generation.

Since zebrafish genes *junba* and *junbb(junb-like)* genes consist solely of one exon; the targeted area was designed to be at the beginning of the coding sequence using the CRISPR tool from the Zhang Lab (http://crispr.mit.edu/) and CHOP-CHOP design tool (http://chopchop.cbu.uib.no)(Labun et al., 2016). In addition, extra care was taken in order not to target highly conserved regions of other Jun family members and select CRISPR guide with less predicted off- targets effects.

I designed individual oligos guide RNAs for each gene and oligos were annealed and ligated into pT7-gRNA plasmid (pT7-gRNA was a gift from Wenbiao Chen (Addgene plasmid # 46759, Jao et al., 2013). CRISPR gRNAs were *in vitro* transcribed using MEGAshortscript T7 kit AM1354 according to manufacturer's instruction and checked in an agarose gel for stability check.

200 pg of guideRNAs were co-injected with Cas9 protein in one-cell stage embryo. A sample of the injected embryos was selected, and their genomic DNA was isolated prior PCR amplification using specific primers. Amplicons were separated into a high resolution 3% MetaPhor© agarose gel and injection was only considered successful when small differences in the amplicon size were observed as smear. Only then, the embryo batches were raised until adulthood. When the fish reached the age of 3 months, and thus puberty, they were backcrossed to wildtype animals and their progeny was analyzed for germline transmission of the mutated *junb* allele. Single 24 hpf embryos were genotyped as described before. PCR amplicons were cloned into pGEMT plasmids and sequenced. Only fish carrying mutations resulting in a frameshift and premature STOP codon were selected as founders and were outcrossed to vascular reporter lines.

3.7.6 *junb*-kalt4 reporter mutant

A fragment of the *junba* sequence containing the CRISPR targeted area was amplified with specific primers and cloned into eGFPbait-E2A-KalTA4-pA donor vector addgene #61069 (Auer et al., 2014) by restriction enzyme free cloning. Successful insertion of the sequence was assessed by restriction enzyme digestion.

This *junba*-Kalt4 construct was co-injected with Cas9 protein and *junba* gRNAs into one-cell *Tg(UAS:Kaede)* zebrafish embryos. After Cas9 nuclease activity, concurrent cleavage of the genomic locus and the *junba*-Kalt4 plasmid occurred and the *junba-Kalt4* donor plasmid was integrated into the genome by the homology-independent DNA repair machinery.

3.7.7 Generation of overexpression vector

junba and *junbb* coding frame was amplified from pGEMT vectors containing the *junba* and *junbb* sequences from zebrafish embryos. Specific primers were designed with flanking attB1 and attB2 sites. The amplicons were used in BP recombination with DONR221 plasmid. *junba/junbb*-DONR221 vectors were purified and sequenced. Previously designed constructs: 3' attL4 UAS promoter attR1 vector, 5' aatR2 E2A linker-RFP attL3 vector and attL1 gene of interest attL2 DONR221 vector were LR recombined into a destination vector containing flanking Tol2 sites. This Tol2 sites allow the integration of the vector into the genome by the transposase action.

Concurrent injection of 30µg the final construct UAS:GOI-E2A-RFP and 30µg transposase was injected into *Tg(fli1:gal4^{ubs3})* one-cell stage embryos. Efficacy of the construct injection was validated by fluorescence.

3.7.8 Scoring and Morphological analyses of the embryos

The quantification of the number of PACs, TD fragments and the analysis of the ectopic sprouts present in the embryos were performed analyzing the pictures of 3 dpf and 5 dpf embryos. The embryos were raised in PTU and kept at 28ºC for their optimum development. Before the imaging, the embryos were shortly anaesthetized in 0.25% tricaine and immobilized and oriented in 6% methylcellulose. Confocal pictures of the trunk vasculature (the seven somites over the extension yolk) were taken for their analysis.

PACs and TD fragments were considered complete when the structures could be easily identified and tracked between the somites. Absent PACs and TD fragments were considered when the lymphatic sprouts did not reach the horizontal myoseptum or when the structure looked incomplete respectively.

The number of ectopic sprouts was quantified considering the dorsal part of the ISVs only. The sprouts were considered complete only when the sprout link to the neighboring somite was visible or disconnected when a space between the sprout tip cell and the neighboring ISV was observed. aISVs and vISVs were quantified tracking each ISVs to their origin. aISVs were considered when the ISVs were originated from the dorsal aorta and vISVs were considered when the ISVs was originated from the posterior cardinal vein.Blind quantification was performed in a single embryo basis prior genotyping of the analyzed embryos.

3.8 Imaging and imaging processing

Zebrafish embryos submitted to WISH were imaged using a Leica M165 FC binocular.

Zebrafish embryo confocal imaging was performed using a Zeiss LSM 710 and LSM 780 upright confocal microscope with a W-Plan Apochromat 20x objective NA 1.0 and excited with a 488nm laser. *In vivo* time-lapse of the embryos was performed as previously described (Ben Shoham et al., 2012). A plastic chamber linked to a perfusion pump that regularly circulated temperature-controlled medium was placed in the stage of the microscope. In short, the dechorionated embryos were shortly anaesthetized in 0.25% tricaine and oriented and immobilized in the plastic chamber containing 0.25% low melting agarose. Subsequently, the embryos were raised for 1 or 2 days in contact to a constant flow buffer containing tricaine and PTU and maintained at 28ºC to guarantee their proper development. Z-stacks of the embryo trunk were taken every 10 minutes for 1-2 days.

Fluorescence cell imaging of F9 cells was performed using a Nikon Eclipse Ti microscope and a 40x objective. Brightfield imaging of the mESCs was performed in an Olympus 1x51

ZEISS ZEN microscope software and Fiji is Just Image J (FIJI) were used to analyze the time-lapse and the confocal pictures respectively. Z-projections based on the maximum intensity point were created for each confocal image. Brightness and contrast were modified accordingly and were performed equally in all the experimental groups. Grey LUT was modified when indicated in the text

3.9 Statistical analysis

The data were analyzed using unpaired two-tail Student test: ns (not significant) $p>0.05$, * $p<0.05$, ** $p<0.01$, *** $p<0.001$, ****$p<0.0001$. For *in vitro* cells, the analyses were performed among three biological replicates. For *in vivo* experiments, the sample number was selected considering previous experimental variability.

For the *in vivo* data, the normal distribution and similar variance was assumed. For the analysis of fold change and relative gene expression, the data was normalized using a logarithmic transformation. For the luciferase reporter assay analysis, serial comparison of the mutant versions of the promoter respect the wildtype promoter was done with t-test and Dunnett's multiple comparison test.

All startistical analysis was performed with Graph Pad software. All the data in graphs are displayed as mean ± SD.

4 RESULTS

4.1 Role of JUNB in an *in vitro* LEC differentiation model.

4.1.1 Optimization of a mESC differentiation protocol into LECs

4.1.2 JUNB activity is increased during *"in vitro"* LEC differentiation

4.1.3 *Junb*$^{-/-}$ mESC fail to form LEC-like cells

4.1.4 *Junb*$^{-/-}$ mESC fail to upregulate VEGFR2 during LEC differentiation

4.1.5 Surviving *Junb*$^{-/-}$ mESCs form immature LEC-like cells.

4.2 Impact of *Junb* in lymphangiogenesis in Zebrafish

4.2.1 *junba* and *junbb* are differently expressed in zebrafish development.

4.2.2 CRISPR-Cas-mediated generation of *junb* mutants

4.2.3 CRISPR-Cas junb mutants are fertile and reach adulthood.

4.2.4 *junb* mutants partially phenocopy the morphants

4.2.4.1 *junb* mutants display an allele-dependent loss of PACs

4.2.4.2 *junb* mutants develop a normal thoracic duct

4.2.5 *junb* mutants generate ectopic sprouts from 3 dfp until 5 dpf

4.3 Outlook

4.3.1 *flt1* is a JUNB-direct target

4.3.2 Generation of a gain of function mutant

4.1 Role of JUNB in an *in vitro* LEC differentiation model

4.1.1 Optimization of a mESC differentiation protocol into Lymphatic Endothelial Cells

Since both total and endothelial-specific *Junb* deletion results in embryonic lethality before lymphatic endothelial specification takes place (Schorpp-Kistner et al., 1999; Licht et al., 2006); an *in vitro* system of mESCs differentiation into LECs was implemented to investigate the role of JUNB in LEC specification.

In vitro LEC differentiation has not been as widely attempted in the community as the differentiation of stem cells into other cell lineages. However, several teams have succeeded using different strategies such as the generation of embryoid bodies (Liersch et al., 2006; Kreuger et al., 2006) and the co-cultures of the stem cells with feeder-cells (Kusuma et al., 2013; Nicenboim et al., 2015). Unfortunately, neither of the published approaches were optimal for my aim: the variety of cells within the embryoid bodies hampers the study of specific cells throughout the process. Besides, the high basal JUNB expression levels in the feeder cells complicates the monitoring of the JUNB induction kinetics during LEC differentiation.

Therefore, since maintaining mESCs under feeder-free conditions does not affect their proliferation or differentiation potential (Tamm et al., 2013), I aimed to develop a feeder-free LEC differentiation protocol.

Similarly to other described methods, this *in vitro* protocol targets the lymphatic differentiation via a mesoderm differentiation step recapitulating the *in vivo* process. In short, the presented protocol consists of three steps: i) expansion of stem cells under undifferentiated conditions, ii) spontaneous differentiation towards mesoderm and angioblast formation and iii) LEC-directed differentiation (Figure 4-1)

In the first step, the mESCs were cultured under stem cells conditions for 3 passages. During this period, the cells were maintained at low confluency to avoid cell-cell contact and further differentiation in the presence of Leukemia Inhibiting Factor (LIF). Thus, mESCs were passaged every other day and LIF-containing medium was changed daily.

After this first period, the cells were deprived from LIF for 6 consecutive days to trigger a spontaneous differentiation towards mesoderm. The cell density was adapted in comparison with other reports so the culture could be passaged every other day and medium was daily refreshed.

Finally, the last part of the protocol aimed for a lymphatic endothelial specific differentiation step with a combination of stimuli from different protocols.

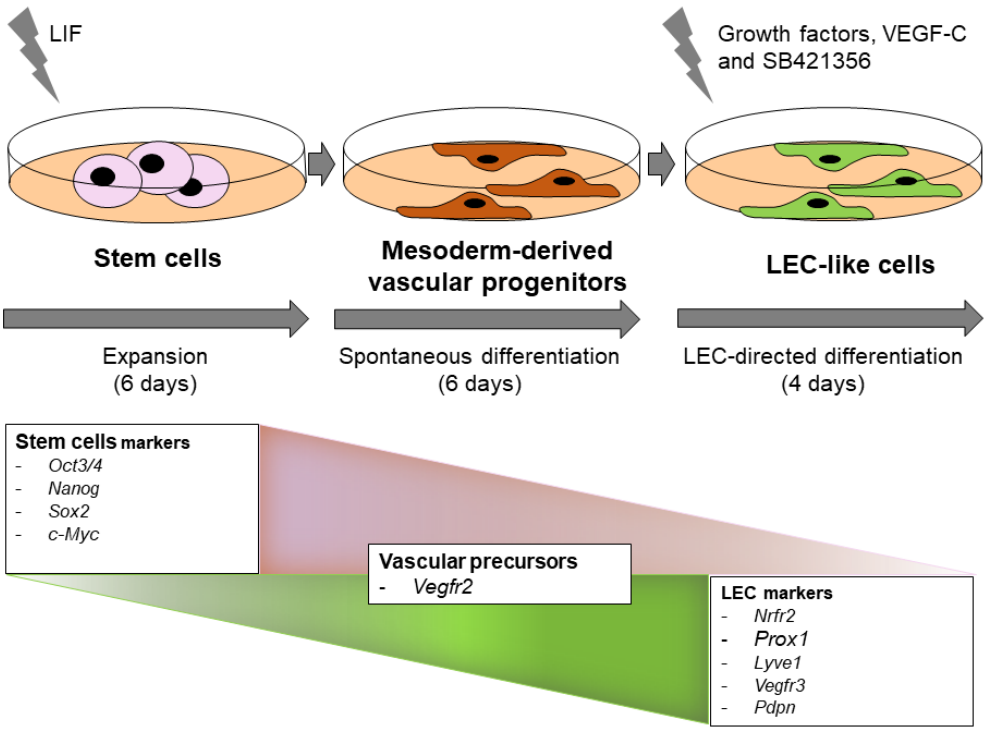

Figure 4-1: Feeder-free mESC differentiation protocol into Lymphatic Endothelial Cells.

Schematic representation of the feeder-free LEC differentiation protocol. mESCs were expanded for six days in the presence of LIF prior differentiation towards mesodermal vascular precursors. Vascular progenitors were subjected to a growth factor and inhibitors cocktail to trigger a LEC-specific differentiation.

Kreuger et al., (2006) described that solely addition of either VEGF-A or VEGF-C lead to the formation of a LYVE1$^+$ cells, although a combination of these two stimuli resulted in a synergistic effect. In addition, Vittet et al., (2012) showed that TGFβ1 reduced the expression of key lymphatic transcriptional regulators *Nr2f2 (Coup-TfII)* and *Sox18* in a stem cell model. This effect could be chemically reverted by adding an inhibitor of the TGFβ1 signaling, SB421356, to the medium. Thus, in order to potentiate the LEC differentiation, the cells were kept in culture in endothelial-specific medium supplemented with a cocktail of growth factors, 100ng/ml of VEGF-C and 10µM of SB421356 every 48 hours.

Visual control of the cells by phase-contrast microscopy revealed that the cells adapted well to the surface of the dishes throughout the experiment. During the first expansion step, the cells grew as organized colonies feeder-free on the gelatin-coated dishes. Later on and in the absence of LIF, the cells at the edges of the colonies began to differentiate and by the fourth day, they lost their 3D structure and remained as a monolayer morphologically resembling to mesenchymal stem cells. After the addition of the stimuli for the endothelial cell-directed differentiation, most cells displayed a more cobblestone morphology, more endothelial-like appearance and endothelial cell islands were observed (Figure 4-2 A).

It has been reported that a population of mesodermal cells spontaneously expresses VEGFR2 after 4 days without LIF (Hirashima et al., 2003). These VEGFR2$^+$ cells are considered to be the vascular progenitors or angioblasts that are stimulated by mesenchymal signals. The presence of these VEGFR2$^+$ cells is then a key step to guarantee that the cells will be stimulated during the endothelial cell-specific differentiation.

In order to analyze the purity of the VEGFR2$^+$ population, cells deprived of LIF for four days (SD 4-LIF) were stained for VEGFR2 and analyzed by flow cytometry. Around 60% of the analyzed cells exhibited a high expression of VEGFR2 indicating the high efficiency of the protocol and excluding the necessity of an additional purification step as suggested in other protocols (Figure 4-2 B).

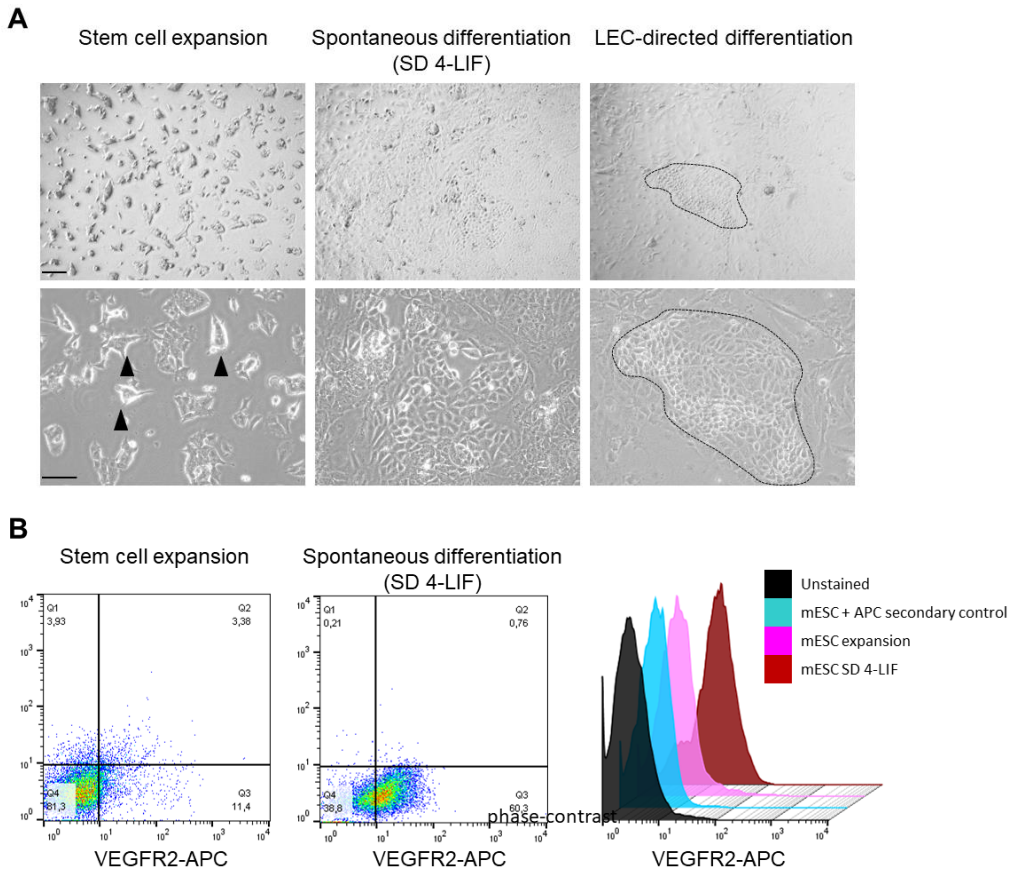

Figure 4-2: Validation of a feeder-free three-step mESCs differentiation protocol into LECs.

A) Representative phase-contrast pictures of the mESCs throughout the differentiation process: mESCs expansion, day 4 of the spontaneous differentiation (SD 4-LIF) and endpoint of the LEC differentiation. Black arrowheads point to the mESCs colonies and dashed lines mark the EC island.Scale bar 200 µm upper panel and 100 µm lower panel B) Flow cytometry density plot showing a shift in the VEGFR2$^+$ population at the expansion step and after 4 days in the absence of LIF. Histograms depict the increase in the VEGFR2$^+$ population at the mESC expansion step and at the fourth day of the spontaneous differentiation step (SD 4-LIF).

To further prove that the protocol successfully led to cells of the lymphatic lineage, the expression of several markers from undifferentiated and differentiated LECs were investigated throughout the process. As expected, a gradual decrease of the markers indicative for undifferentiated ES cells (*Oct3/4, Sox2, Nanog* and *c-Myc*) was detected during the spontaneous differentiation and their expression was minimal at the endpoint of the experiment (Takahashi and Yamanaka, 2006) (Figure 4-3A). In addition, expression of early LECs markers such as *Nr2f2* (*Coup-tfII)*, *Sox18* and *Prox1* were detected prior to the known late markers *Lyve1, Vegfr3* and *Podoplanin*. *Prox1* levels significantly rose during the spontaneous differentiation (SD 4-LIF) and were significantly maintained (15x fold higher compared to the undifferentiated mESCs) at the LEC endpoint step. As expected, *Lyve1* and *Podoplanin* expression levels significantly peaked (40x fold and 7x fold respectively) at the endpoint of the experiment (Figure 4-3 B).

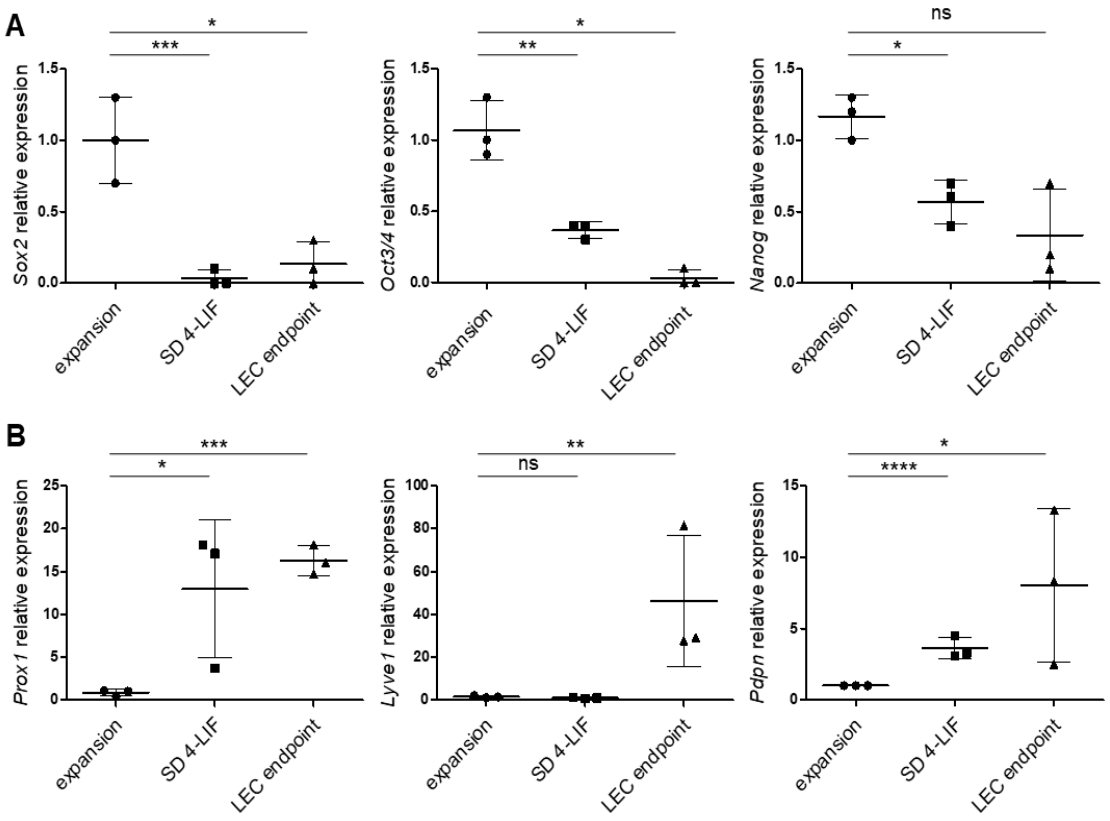

Figure 4-3: Expression switch from stem cells to lymphatic markers during the *"in vitro"* LEC differentiation.

A) Relative expression of stem cells markers : *Sox2, Oct3/4* and *Nanog* and B) LEC markers: *Prox1, Lyve1* and *Podoplanin* at three different steps of the differentiation protocol: end of mESCs expansion, day 4 of the spontaneous differentiation (SD 4-LIF) and LEC endpoint. mRNA levels of the genes of interest were analyzed by qRT-PCR and normalized to the expression of *Rplp0*. Fold change is shown relative to their expression at the expansion step which was set to 1.The lines and error bars refer to mean ± SD of three independent experiments N=3. Statistical analysis was performed using unpaired two-tailed t-Student test. ns (not significant) p>0.05, * p<0.05, ** p<0.01, *** p<0.001, ****p<0.0001.

In summary, differentiation of feeder-free mESCs into LEC was possible and the applied cell densities and chosen stimuli and concentrations were appropriate to achieve LEC-like cells that express LEC-specific markers.

4.1.2 *Junb* levels are increased during *in vitro* LEC differentiation

In order to assess whether JUNB is important for LEC differentiation, its induction levels were monitored at different stages of the process. For this purpose, total RNA and whole cell protein were isolated and subjected to gene expression and protein analyses, respectively.

Both *Junb* transcript and protein levels were significantly upregulated during the differentiation process although they presented different intensity and induction kinetics. *Junb* transcripts continuously increased throughout the entire process in a moderate manner (around 2x fold during the spontaneous differentiation and 3x fold in the endpoint). JUNB protein, was first undetectable in undifferentiated cells and then displayed a sudden and strong induction upon deprivation of LIF for 4 days during the spontaneous differentiation (SD 4-LIF). These high protein levels were maintained throughout the spontaneous differentiation process. In the last step, JUNB levels diminished although the phosphorylated isoform was still detectable (Figure 4-4).

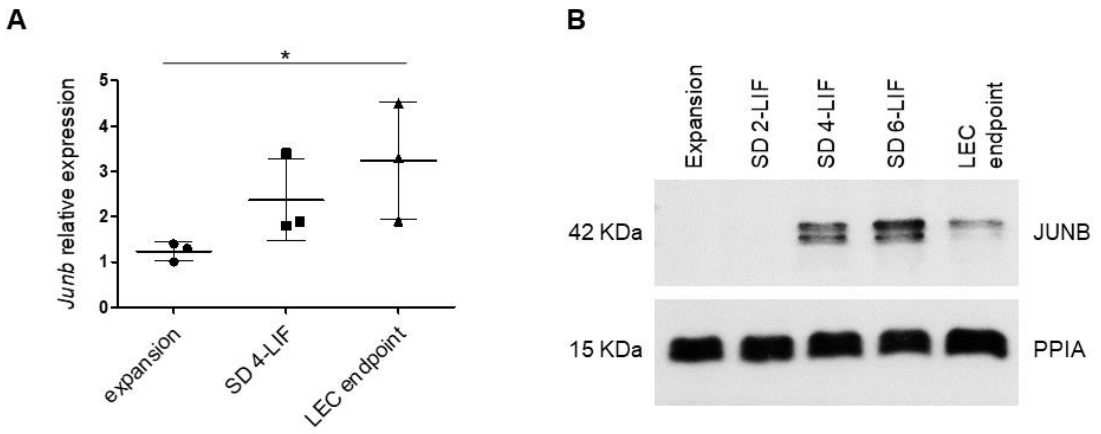

Figure 4-4: JUNB is induced during *in vitro* LEC differentiation at the transcript and protein level.

A) Relative *Junb* expression in mESCs differentiated to LECs determined by qRT-PCR. *Junb* mRNA levels were normalized to *Rplp0* expression and depicted as fold change relative to the starting point at which *Junb* expression was set to one. The lines and error bars refer to mean ± SD of three independent experiments N=3. Statistical analysis was performed using unpaired two-tailed t-Student test. p-value * $p<0.05$. B) Representative western blot of JUNB levels in mESCs submitted to *in vitro* LEC differentiation: mESC expansion, spontaneous differentiation (SD 2-LIf), (SD 4-LIF) and (SD 6-LIF) and LEC endpoint. Cyclophilin A (PPIA) was used as control for equal quality and loading of protein extracts.

These results are consistent with the starting hypothesis of JUNB controlling LEC formation. The protein data suggest that JUNB is even playing a role at earlier time points since JUNB is induced during the spontaneous differentiation (SD 4-LIF) when the vascular progenitors express VEGFR2.

4.1.3 *Junb*$^{-/-}$ mESCs fail to form LEC-like cells

Next, I asked whether the presence of *Junb* is essential for the generation of the vascular progenitors in the first place and ultimately on fully differentiated LEC cells. In order to assess this, parallel studies were performed on *Junb*$^{+/+}$ and *Junb*$^{-/-}$ mESCs (Schorpp-Kistner et al., 1999; Schmidt et al., 2007)

Morphological inspection of the cells by phase-contrast microscopy revealed that *Junb*$^{+/+}$ and *Junb*$^{-/-}$ mESCs were visually indistinguishable in the non-differentiated status until the spontaneous differentiation (SD 4-LIF) (Figure 4-5).

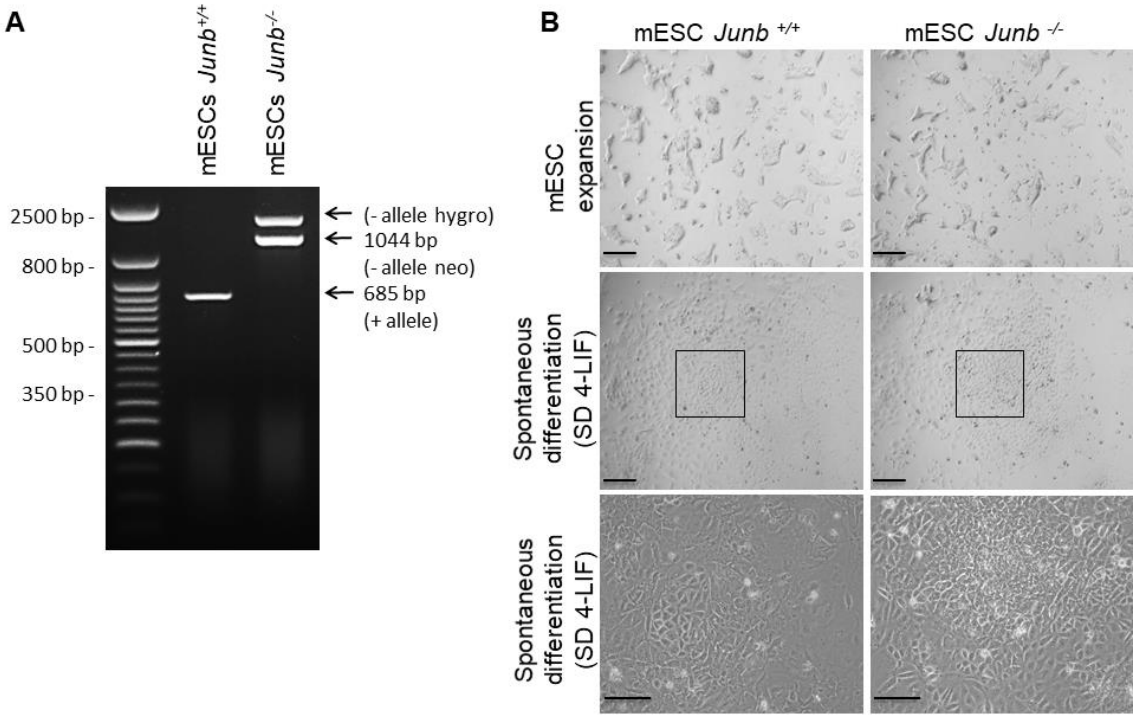

Figure 4-5: *Junb*$^{+/+}$ and *Junb*$^{-/-}$ mESCs behaved similarly during the first steps of LEC differentiation.

A) Genotyping of the mESCs by PCR amplification of the *Junb* locus. Neomycin/Hygromycin cassettes insertion in the *Junb*$^{-/-}$ cells are detected. B) Representative phase-contrast microscopy pictures showing no morphological differences between the two cell types at several stages of the differentiation: undifferentiated mESC expansion and day 4 of the spontaneous differentiation (SD 4-LIF). Lower panels are magnifications of the middle panels. Scale bar 200 µm upper and middle panel and 100 µm lower panel

Since JUNB is known to control the cell cycle in different phases by activating *p16* and and *CyclinA* and repressing *CyclinD1* (Passegué and Wagner, 2000; Andrecht et al., 2002; Bakiri et al., 2000) a closer look into the proliferation rate was given. For that, the cell number was measured every 2 days and doubling time was calculated. No difference in the doubling time in the analyzed cells from the undifferentiation step up to day 4 of the spontaneous differentiation (SD 4-LIF) was appreciated.

These data were in line with other publications which showed that loss of *Junb* did not affect the overall turnover of the population (Passegué et al., 2001).

Surprisingly, there was a very striking difference between the cells at day 6 of the spontaneous differentiation (SD 6-LIF). At that time, *Junb*$^{-/-}$ cells succumbed to a major cell crisis manifested by a very abrupt drop of cell numbers (Figure 4-6 A).

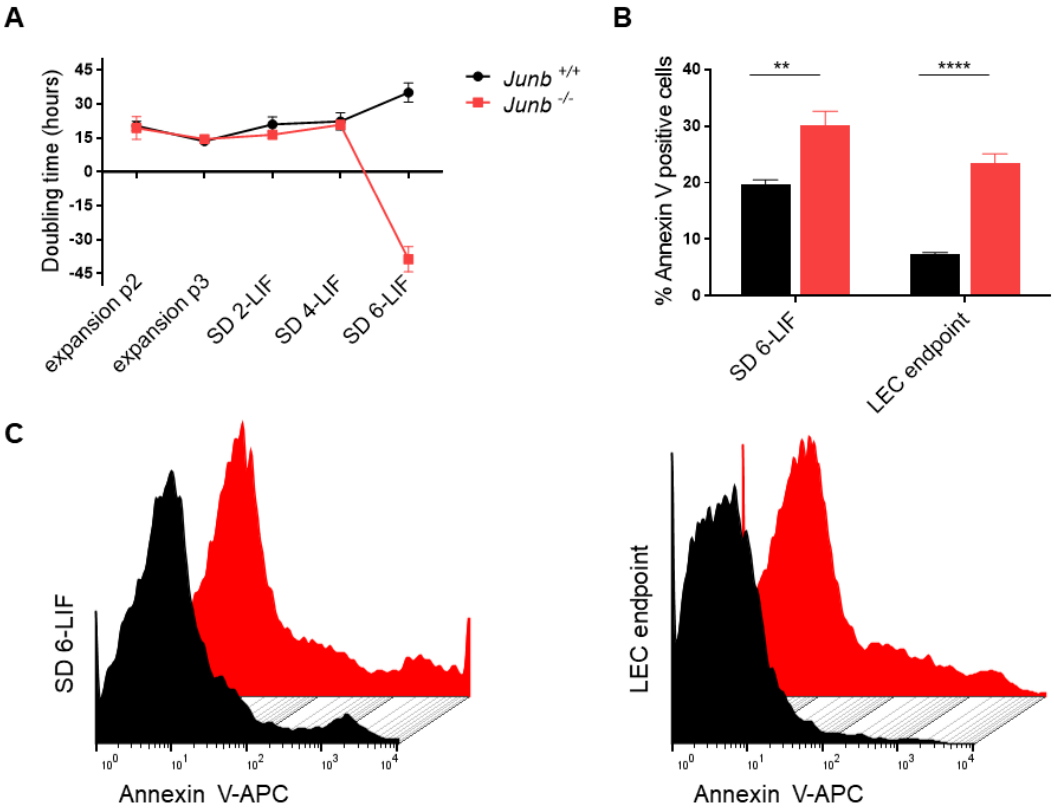

Figure 4-6: *Junb* $^{-/-}$ mESCs exhibited increased apoptosis rate during LEC differentiation.

A) Cell doubling time of *Junb* $^{+/+}$ and *Junb* $^{-/-}$ mESCs during early LEC differentiation. Each point represent the mean±SD of biological triplicates. B) Quantification of the apoptotic cells at day 6 of the spontaneous differentiation (SD 6-LIF) and at the endpoint of the LEC differentiation. Bars represent mean±SD of biological triplicates. Asterisks mark statistical significance $p<0.05$ unpaired student t-test ** $p<0.01$ and ****$p<0.0001$ C) Flow cytometry histograms of Annexin V$^+$ populations in differentiating *Junb*$^{+/+}$ and *Junb*$^{-/-}$ cells respectively. In all cases, black dots and graphs refer to *Junb*$^{+/+}$ and red dots and graphs refer to *Junb*$^{-/-}$ cells.

To further investigate this loss in *Junb*$^{-/-}$ cells, the presence of apoptotic/Annexin V^{+} cells was analyzed by flow cytometry.
Serial comparison of Annexin V^{+} populations between *Junb*$^{+/+}$ and *Junb*$^{-/-}$ cells showed no difference in the apoptosis rate during the expansion of the undifferentiated cells. However, there was a significant increase in the apoptotic cell population at the day 6 of the spontaneous differentiation (SD 6-LIF). This difference was more pronounced when the surviving *Junb*$^{-/-}$ cells were submitted to the LEC directed differentiation step and analyzed at the end point of the differentiation (Figure 4-6B C).
These data suggest that *Junb* induction at day 4 of spontaneous differentiation is rather necessary for cell survival than for cell proliferation.

4.1.4 *Junb*$^{-/-}$ mESC fail to upregulate VEGFR2 during LEC differentiation

Since *Junb*$^{-/-}$ mESCs showed an increased apoptosis rate during LEC differentiation; a closer look on the main survival signaling pathways in endothelial cells was taken. In endothelial cells, the survival cascade is mediated by PI3K/AKT phosphorylation via stimulation of Neuropilin, Fibroblast Growth Factor Receptors or Vascular Endothelial Growth Factor Receptors (Gerber et al., 1998).

Since the growth factors VEGF-A and VEGF-C were used as specific stimuli used in the differentiation protocol, the focus was directed towards their respective tyrosine kinase receptors. VEGF-A is a ligand of VEGFR1 and VEGFR2 and VEGF-C is able to bind and activate both VEGFR2 and VEGFR3. While VEGFR1 and VEGFR2 are key regulators for vasculogenesis as well as blood endothelial differentiation, VEGFR3 is critical for lymphatic endothelial differentiation (Shibuya, 2011; Alitalo et al., 2005).

Thus, the focus was on these receptors and I aimed to investigate whether there is any imbalance in the expression levels of these receptors during the differentiation process. Therefore, *Vegfr1* and *Vegfr2* RNA and protein levels were assessed by qRT-PCR and western blot respectively.

In *Junb*$^{+/+}$ mESCs, VEGFR1 and VEGFR2 were detected as expected from literature and my previous optimization experiments, thus, confirming the correct course of the differentiation process. Importantly, in *Junb*$^{-/-}$ mESCs the expression of both receptors was found to be impaired when compared to the wildtype cells. *Vegfr1* transcript levels in both *Junb*$^{+/+-}$ and *Junb*$^{-/-}$ cells were similar at the SD 4-LIF phase. However, VEGFR1 protein levels were already reduced in the expansion phase but still induced upon spontaneous differentiation, yet to a slightly lesser extent when compared to wildtype cells.

Intriguingly, *Vegfr2* was not induced upon differentiation on both RNA and protein levels in *Junb*$^{-/-}$ cells. *Vegfr2* transcript levels were significantly reduced (4x) in *Junb*$^{-/-}$ cells. At the protein level, no induction of VEGFR2 was observed at the spontaneous differentiation step suggesting that *Junb*$^{-/-}$ mESCs are impaired to generate VEGFR2^{+} vascular progenitors during spontaneous differentiation (Figure 4-7).

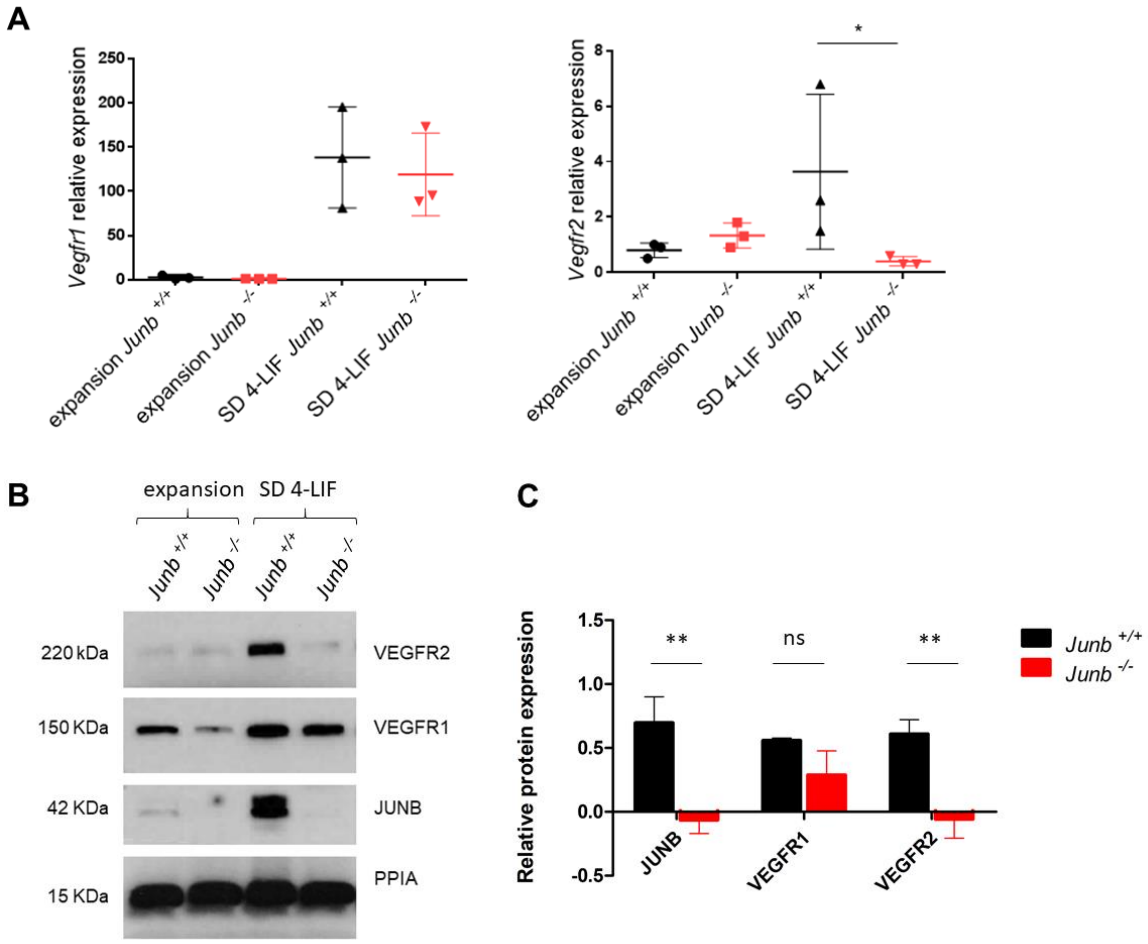

Figure 4-7: Expression of both VEGFR1 and VEGFR2 is affected in *Junb*$^{-/-}$ mESCs during spontaneous differentiation.

A) *Vegfr1/Vegfr2* transcript levels were assessed by qRT-PCR and normalized to the expression of *Rplp0*. Expression levels were normalized to those of *Rplp0* and wildtype levels at the expansion time point were set to 1. Black and red dots refer to *Junb*$^{+/+}$ cells and *Junb*$^{-/-}$ cells respectively. The lines and error bars mark the mean± SD of biological triplicates N=3. B) Representative western blot for VEGFR1,VEGFR2 and JUNB during LEC differentiation. Cyclophilin was used as loading control for equal quality and quantity of loaded proteins.C) Quantification of the protein levels in the western blots among biological triplicates at the spontaneous differentiation step (SD 4-LIF). Bars and error lines mark the mean± SD. Asterisks mark statistical significance by unpaired student t-test: ns (not significant), * $p<0.05$ and ** $p<0.01$.

In order to assess whether the impairment in *Vegfr1* and *Vegfr2* expression could be due to the loss of the transcriptional regulator function of JUNB, I first aimed to recapitulate these results in a distinct cell type, namely murine endothelioma cells. These cells are fully differentiated immortalized endothelial cells in which either one or two alleles of *Junb* were deleted (END72 *Junb*$^{+/-}$ and END70 *Junb*$^{-/-}$*).* They were previously generated in the lab from the *Junb* embryos isolated at midgestation and subsequently immortalized by retroviral transduction of PymT (Licht et al., 2006).

These cells displayed similar expression of endothelial surface markers CD31 and CD105 regardless of their genotype and have been used for validation of other JUNB targets in the past (Licht et al., 2006) (Figure 4-8).

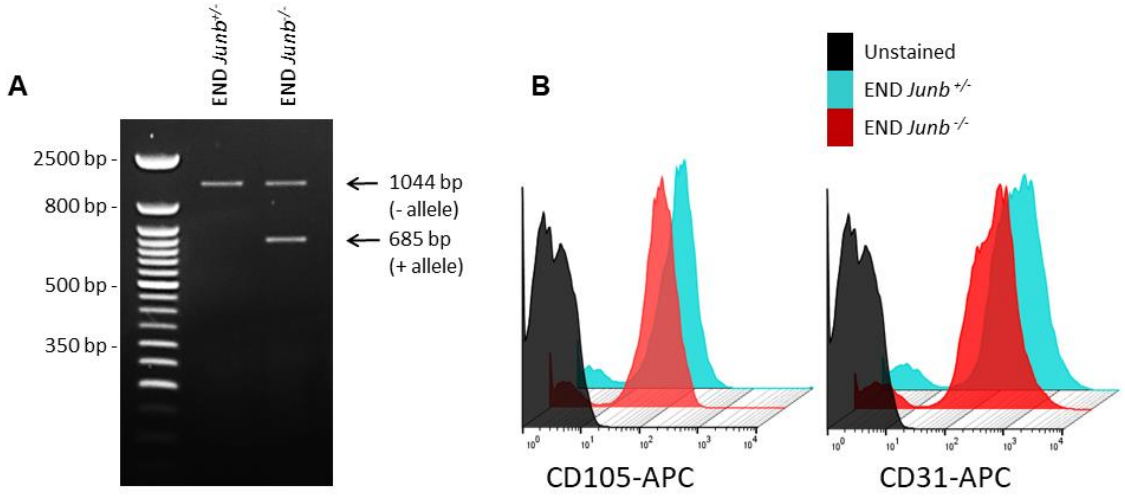

Figure 4-8: Transformed murine endothelioma cells lacking one or two *Junb* alleles display similar expression of endothelial markers CD105 and CD31.

A) Genotype of the endothelioma cells (END 72 *Junb*$^{+/-}$ and END 70 *Junb*$^{-/-}$*)* used in this study by PCR amplification of the *Junb* locus. Neo cassette insertion in the *Junb* $^{+/-}$ was detected. B) Flow cytometry histograms for CD105 and CD31 endothelial markers in comparison with unstained control.

Total RNA and protein isolates from these cells were obtained and analyzed for *Vegfr1* and *Vegfr2* expression.

Indeed, endothelioma cells lacking *Junb* expressed lower levels of both receptors at the transcript and protein level. Similarly to the observations in mESCs, both *Vegfr1* and *Vegfr2* transcripts levels were significantly reduced in *Junb*$^{-/-}$ endothelioma cells in comparison to *Junb*$^{+/-}$ cells. At the protein level, the results confirmed the mESCs data: while a mild although significant VEGFR1 decrease was observed, VEGFR2 protein levels were diminished by more than 50% in *Junb*-deficient endothelioma cells (Figure 4-9).

Taken together, these data strongly suggest that *Vegfr1* and *Vegfr2* are JUNB-regulated.

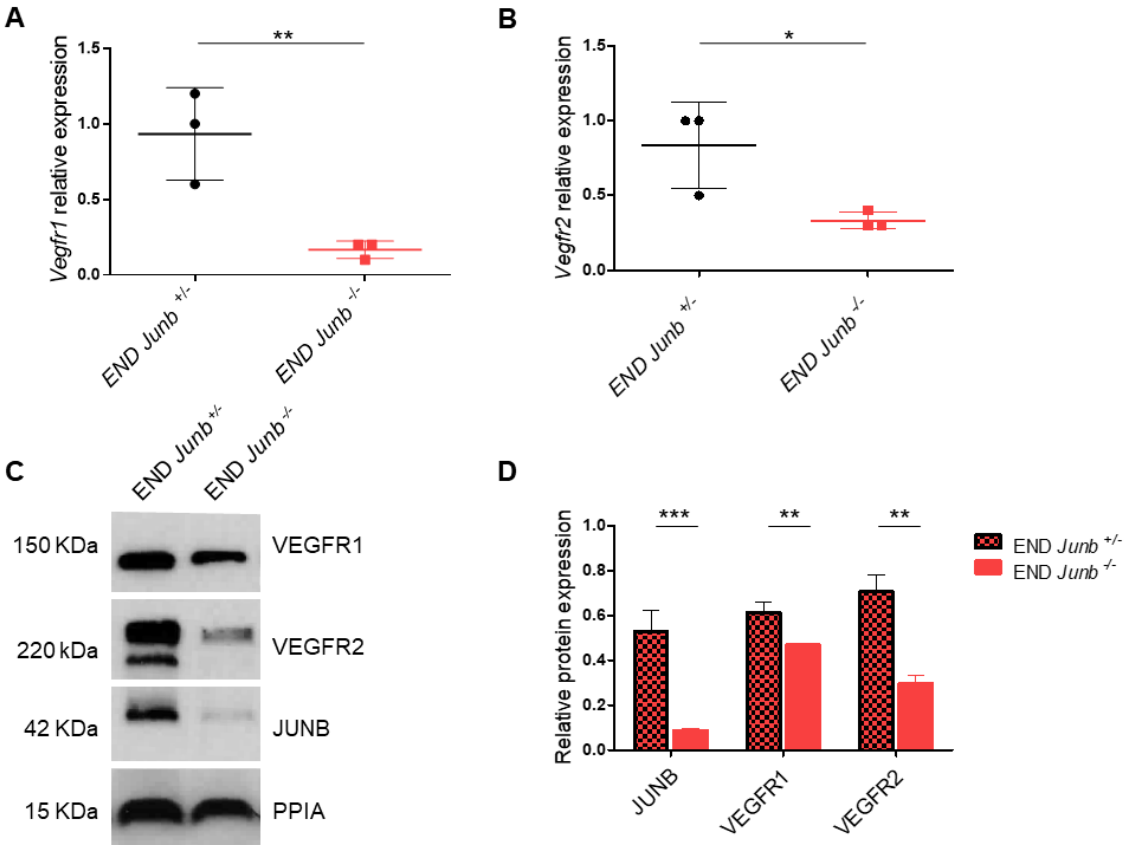

Figure 4-9: Diminished VEGFR1 and VEGFR2 expression in *Junb* $^{-/-}$ endothelioma cells.

A) Relative expression of *Vegfr1* and B) *Vegfr2* transcript levels assessed by qRT-PCR and normalized to *Rplp0*. Fold change is depicted relative to expression levels in murine endothelioma END *Junb*$^{+/-}$ cells which were set to 1. C) Representative western blot for VEGFR1,VEGFR2 and JUNB in endothelioma cells. Cyclophilin A was used as control for equal quality and loading of protein extracts. D) Quantification of protein levels from western blots of biological triplicates N=3. Bars and error lines mark the mean±SD. Asterisks mark statistical significance by unpaired Student t-test. * $p<0.05$, ** $p<0.01$ and *** $p<0.001$. Black dots and black-pattern columns refer to *Junb*$^{+/-}$ cells and red dots and columns refer to *Junb*$^{-/-}$ endothelioma cells.

4.1.5 Surviving *Junb*$^{-/-}$ mESCs form immature LEC-like cells

The small percentage (around 30%) of *Junb*$^{-/-}$ mESCs that survived up to the sixth day of the spontaneous differentiation (SD 6-LIF) was subjected to the final step of the differentiation. In the presence of endothelial growth factors and VEGF-C as stimulus, most of the *Junb*$^{-/-}$ mESCs survived until the LEC endpoint.

In order to investigate whether the surviving cells properly differentiated into mature LECs, gene expression analysis for the key lymphatic markers was performed. Expression of *Prox1, Lyve1* and *Podoplanin* revealed no differences as their transcript levels increased throughout the differentiation process at similar rates in *Junb* $^{-/-}$ and *Junb*$^{+/+}$ mESCs (Figure 4-10).

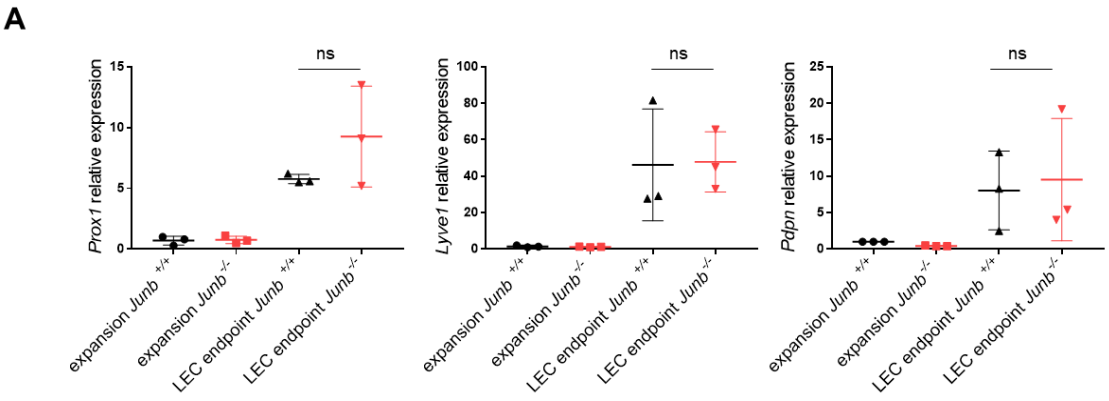

Figure 4-10: *Junb*$^{+/+}$ and *Junb*$^{-/-}$ LEC-like cells express comparable levels of lymphatic markers transcripts.

A) Relative expression of *Prox1, Lyve1 and Podoplanin* transcript levels assessed by qRT-PCR and normalized to *Rplp0*. Fold change of expression at the LEC endpoint relative to the mESCs expansion timepoint which was set to 1 is depicted. Lines and error bars mark the mean±SD among three biological triplicates (N=3). Statistical analysis was performed using unpaired two-tailed t-Student test: ns (not significant). Black dots and red dots refer to *Junb*$^{+/-}$ cells and *Junb*$^{-/-}$ cells respectively.

In addition, the reduced transcript and proteins levels of the vascular receptors *Vegfr1* and *Vegfr2* observed in the *Junb* $^{-/-}$ cells during the spontaneous differentiation (SD 4-LIF), were no longer observed. In fact, the addition of the lymphatic stimuli in *Junb*$^{-/-}$ vascular progenitors restored the expression of these receptors to levels similar to those of the *Junb*$^{+/+}$ cells (Figure 4-11 A-B).

Considering that a significant increment in apoptosis was observed in *Junb*$^{-/-}$ cells at both spontaneous differentiation and LEC endpoint but the decrease on VEGFR1 and VEGFR2 was detected only in the former one; I wondered whether the expression levels of other receptor were impaired. At this later stage of the differentiation, the cells have turned into LEC-like cells and the main signaling is via VEGFR3 activation. Thus, I analyzed the expression of receptor *Vegfr3* and its ligand *Vegf-C*.

It was found out that in the *Junb*$^{-/-}$ cells, *Vegfr3* and *Vegf-c* transcript levels were significantly decreased. This lack of *Vegfr3* in *Junb*$^{-/-}$ cells is in line with the defects on survival pathway observed previously (Figure 4-11 C-D).

Taken together, these data suggest that the minority of the surviving *Junb*$^{-/-}$ cells differentiated into more immature and less-responsive to VEGF-C lymphatic cells

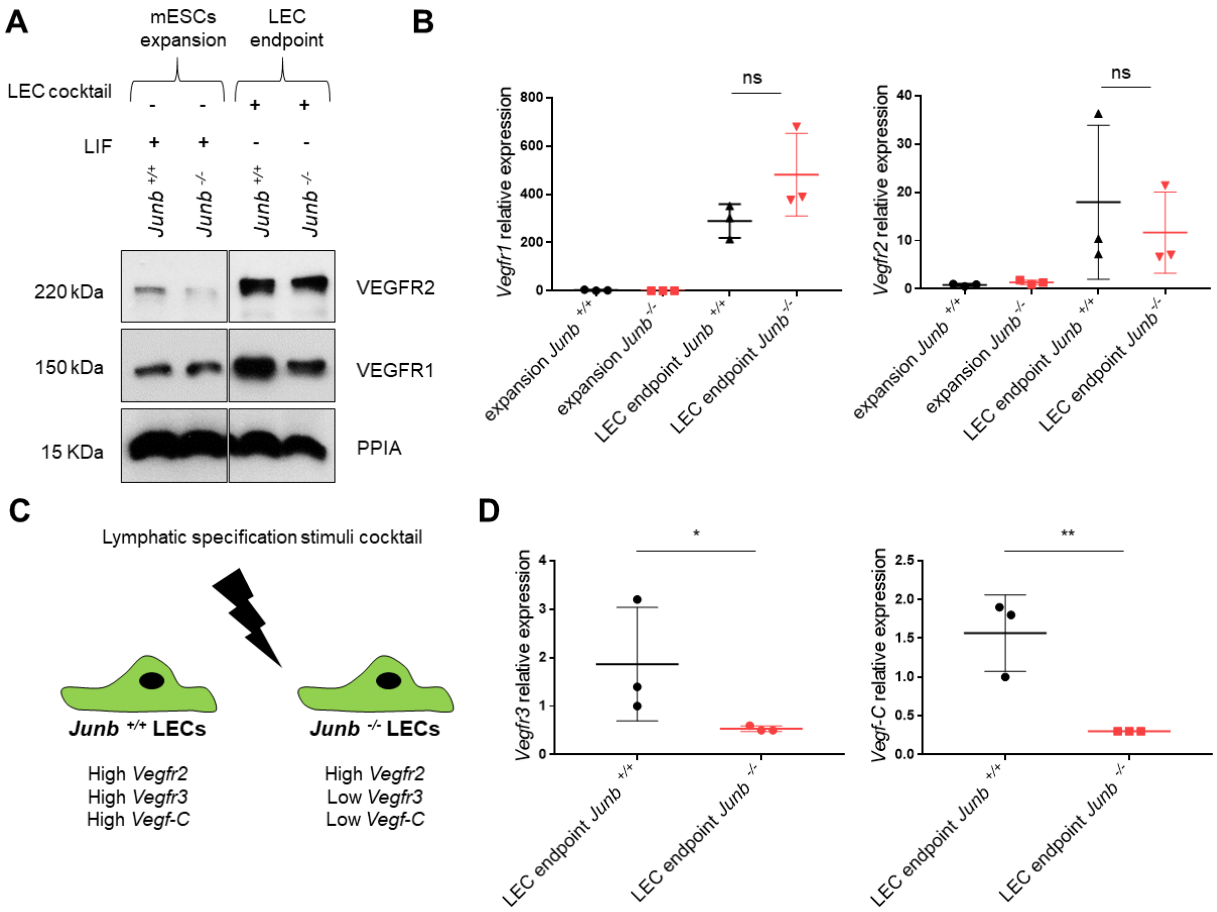

Figure 4-11: Surviving *Junb*$^{-/-}$ cells generate immature LEC-like cells in the presence of endothelial stimuli.

A) Representative western blot of the VEGFR1 and VEGFR2 upregulation throughout the differentiation process (mESC expansion and endpoint) in the presence of endothelial stimuli in *Junb*$^{+/+}$ and *Junb*$^{-/-}$ mESCs. Cyclophilin A was used as control for equal quality and loading of protein extracts. B) Transcript levels of *Vegfr1* and *Vegfr2* were restored upon lymphatic stimulation. mRNA levels were normalized to *Rplp0* levels and depicted as fold change. C) Schematic representation of the obtained LEC-like cells at the endpoint. D) Transcript levels of *Vegfr3* and *Vegfr-C* were significantly reduced in the surviving LEC-like cells. mRNA levels were normalized to *Rplp0* levels and depicted as fold change. Lines refer to mean±SD among biological triplicates (N=3). Asterisks mark statistical significance by unpaired Student t-test. ns (not significant), * $p<0.05$ and ** $p<0.01$.

4.2 Impact of *Junb* in lymphangiogenesis in Zebrafish

Our previous studies in zebrafish embryos with transiently suppressed *junb* (Kiesow et al., 2015) as well as the *in vitro* mESC differentiation data strongly suggested that JUNB is critically implicated in the developmental process of lymphangiogenesis. To further investigate the function of *Junb* in lymphangiogenesis *in vivo* , I used the zebrafish model to i) track the *junb* expression dynamics during embryo development, ii) generate novel loss-of-function mutants and iii) characterize lymphatic vessel development at the embryo stage in the absence of Junb.

4.2.1 *junba* and *junbb* are differently expressed during early zebrafish development.

In zebrafish, a whole-genome duplication took place during the evolution of teleost ancestors (before the divergence of zebrafish, pufferfish and medaka lineages) (Amores et al., 1998; Meyer and Málaga-Trillo, 1999; Meyer and Schartl, 1999). As a result of this, there exist two *Junb* paralogues in zebrafish− the *junba (junb)* and *junbb (junb-like)* genes−(Figure 4-12A).

junba and *junbb* are located on different chromosomes (chromosome 1 and 3, respectively) but they share about 71% identity in their gene sequence. Multiple sequence alignment shows that, besides several other areas, the 5' segment of both genes is especially highly conserved with regard to the murine and human *Junb* gene. At the protein level, they comprise domains similar to mouse and human protein: a JNK-binding domain, a bZIP domain for DNA binding and leucine zipper for dimerization. (Figure 4-12 B-C).

In order to determine which of the two paralogues is relevant for lymphatic development, I aimed to track the expression pattern of these genes during early zebrafish development by qRT-PCR and Whole mount In Situ Hybridization (WISH).

For qRT-PCR analyses, RNA from whole wildtype embryo was isolated at specific time points of development : the 5-somites stage (early timepoint prior to vasculogenesis), 16 hpf (start of LEC specification at the PCV), 24 hpf (formation of first main vessels), 30 hpf (formation of ISVs and lymphatics sprouts), 48 hpf (first rise of PACs) and 72 hpf (completion of PACs) (Padberg et al., 2017).

It was observed that *junba* and *junbb* displayed different expression patterns and kinetics. While *junba* levels were quite low with maximal expression at very early timepoints, the 5-somite stage and the 20 hpf, and then gradually decreased with time. *junbb* levels has their peak at 20hpf (5x fold increase compared to 5-somites time point) and then stayed at a moderate level (2x fold change respect the starting point) until 72 hpf (Figure 4-13A).

A

B

	junba	*junbb*
Location	Chromosome 1	Chromosome 3
Transcript size	1557 bp 873 bp	1405 bp
Protein size	325 aa 245 aa	310 aa
Identity	70.8 %	

C

```
human   ATGTGCACTAAAATGGAACAGCCCTTCTACCACGACGACTCATACACAGCTACGGGATACGGCCGGGCCCCTGGTGGCCTC
mouse   ATGTGCACGAAAATGGAACAGCCTTTCTATCACGACGACTCTTACGCAGCGGCGGGATACGGTCGGAGCCCTGGCAGCCTG
junba   ATGTCAACAAAAATGGAGCAACCGTT---TTATGACGACTCGTTTCTTTCT---------GCTTATGGTCATCCAGACGCT
junbb   ATGAGTACAAAAATGGAGCAGCCGTTTTACCACGACGACTCGTTTCTGTTG---------GGTTACGGTCACAACGACGCG

human   TCTCTACACGACTACAAACTCCTGAAACCGAGCCTGGCGGTCAACCTGGCGGACCCCTACCGGAGTCTCAAAGCGCCTGGG
mouse   TCTCTACACGACTACAAACTCCTGAAACCCACCTTGGCGCTCAACCTGGCGGATCCCTATCGGGGTCTCAAGGGTCCTGGG
junba   GCCCTGCACGACTACAAGCTCCTAAAGCAGAACATGAGCGTGAGCTTCGCCGAACCCTACCGGAACCTCAAGACCCTCC--
junbb   GCTCTACACGACTACAAACTCCAGAAACCGGGCATGAACTTGAACGTGACCGAGCCGCCCT------------ATCGGA--

human   GCTCGCGGACCCGGCCCAGAGGGCGGCGGTGGCGGCAGCTACTTTTCTGGTCAGGGCTCGGACACCGGCGCGTCTCTCAAG
mouse   GCGCGGGGTCCAGGCCCGGAGGGCAGTGGGGCAGGCAGCTACTTTTCGGGTCAGGGATCAGACACAGGCGCATCTCTGAAG
junba   ----------------------------GCTCCGAAATCGACTTCTACACAGCGGCGACCGGAGACGTGGGCTCGCTGAAA
junbb   ----------------------------GCCTCAAATCGGACCTCTATCAGGCGTCCAGCGCCGATGTGGGCTCACTCAAA

human   CTCGCCTCTTCGGAGCTGGAACGCCTGATTGTCCCCAACAGCAACGGCGTGATCACGACGACGCCTACACCCCGGGACAG
mouse   CTAGCCTCCACGGAACTGGAGCGCTTGATCGTCCCCAACAGCAACGGCGTGATCACGACGACGCCCACGCCTCCGGGACAG
junba   CTCGCCTCTCCGGAGCTGGAGAGACTCATCATCCAGAACGGTAACGGCGTCATCACATCACCCACGCC-------------
junbb   CTGGCCTCCCCGGAGCTGGAGAGGCTCATCATCCAGACGGGCAACGGCGTGCTGACGACCCCCACACC-------------

human   TACTTTTACCCCCGCGGGGGTGGCAGCGGTGGAGGTGCAGGGGGCGCAGGGGGCGGCGTCACCGAGGAGCAGGAGGGCTTC
mouse   TACTTTTACCCCCGTGGGGGTGGCAGCGGTGGAGGTACAG---------GGGGCGGCGTCACCGAGGAGCAGGAGGGCTTT
junba   ----------------------------------GGGGCAGTATTTGTACGGTCGGAGCATCACAGAGGAGCAAGAGGGCTTC
junbb   ----------------------------------GGGCCAGTACCTCTACGGTCGGGGGATCACCGACGAGCAGGAGGGCTTC

human   GCCGACGGCTTTGTCAAAGCCCTGGACGATCTGCACAAGATGAACCACGTGACACCCCCCAACGTGTCCCTGGGCGCTACC
mouse   GCGGACGGTTTTGTCAAAGCCCTGGACGACCTGCACAAGATGAACCACGTGACGCCCCCCAACGTGTCCCTGGGCGCCAGC
junba   GCGGACGGATTCGTCAAAGCGCTGGACGAGCTCCACAAAATGAACCAAATGCCCCCGCCGAACGTGTCCATCGGAGCCCCC
junbb   GCGGAGGGCTTCGTCAAGGCTCTGGATGAGCTCCACAAGATGAACCAGATGCCCCCGCCCAACGTGTCGATTGGAGCCGGC

human   GGGGGGCCCCCGGCTGGGCCCGGGGGC---------GTCTACGCCGGCCCGGAGCCACCTCCCGTTTACACCAACCTCAGC
mouse   GGGGGTCCCCAGGCCGGCCCAGGGGGC---------GTCTATGCTGGTCCGGAGCCGCCTCCCGTCTACACCAACCTCAGC
junba   GGGGTGTCGAGTTGTTCGGTGGCGTCGTCAGTCTTCGGCGCCTCCTTACCGCCCGAGACTCCGGTGTACACCACCCTGAAC
junbb   GGCGTGACGACGTGCTCGACAACTGCGTCCGTTTTCGGCTCCTCCCTGCAGTCGGAGCCTCCCATTTACACGACGCTGAAC

human   AGCTACTCCCCAGCCTCTGCGTCCTCGGGAGGCGCCGGGGCTGCCGTCGGGACCGGGAGCTCG-------------TACCC
mouse   AGTTACTCCCCAGCCTCTGCACCCTCTGGAGGCTCCGGGACCGCCGTCGGGACTGGGAGCTCA-------------TACCC
junba   AGCTGCAATCCTAACACTAACCTCACACCTGCAGCCAACTACCCGACAGCCACCATCAGCTACCTGCCTCACCATCACCAC
junbb   GCATACTGCCCAGCACCC------------------AGCCACCGTCCACCCACCATCAGCTACCTGCCGTCCCACATACAG

human   GACGACCACCATCAGCTACCTCCCACACGCGCCGCCCTTCGCCGGTGGCCACCCGGCGCAGCTGGGCTTGGGCCGCGGCGC
mouse   GACGGCCACCATCAGCTACCTCCCACATGCACCACCCTTTGCGGGCGGCCACCCGGCACAGCTGGGCTTGAGTCGCGGCGC
junba   CACCAGCAGTACCACCACCATCA-CCACCAGCCCACGCCGCATCCTCATCACTTCCAGCACTCGCTCCATCCGCAGCGGCT
junbb   CAGAGCCAGCACCCG------GA----------AACC---GCGCACGCGTTCCAGCACCCCGGCGTGCTCCCCCAGCGCTT

human   CTCCACCTTCAAGGAGGAACCGCAGACCGTGCCGGAGGCGCGCAGCCGGGACGCCACGCCGCCGGTGTCCCCCATCAACAT
mouse   TTCCGCCTTTAAAGAGGAACCGCAGACCGTACCGGAGGCACGCAGCCGCGACGCCACGCCGCCTGTGTCCCCCATCAACAT
junba   CGTTACTCTGAAAGAGGAGCCACAGACCGTCCCCGACCTGCAGAGCAGCGATGGTTCTCCTCCCATGTCGCCCATCGACAT
junbb   CTTGCCTTTAAAAGAGGAACCGCAGACTGTTCCCGACATGCATAGCAGCGACGGCTCGCCGCCCATGTCCCCGATCGACAT

human   GGAAGACCAAGAGCGCATCAAAGTGGAGCGCAAGCGGCTGCGGAACCGGCTGGCGGCCACCAAGTGCCGGAAGCGGAAGCT
mouse   GGAAGACCAGGAGCGCATCAAAGTGGAGCGAAAGCGGCTGCGGAACAGGCTGGCGGCCACCAAGTGCCGGAAGCGGAAGCT
junba   GGAGGACCAGGAGCGCATCAAAGCGGAGCGCAAGAGGCTCCGGAACCGACTGGCGGCCACCAAGTGCCGGCGACGGAAGCT
junbb   GGACTCGCAGGAACGCATCAAGGCGGAACGCAAGAGGCTCCGGAACCTACTGGCGGCCACCAAATGCCGAAGGCGCAAACT

human   GGAGCGCATCGCGCGCCTGGAGGACAAGGTGAAGACGCTCAAGGCCGAGAACGCGGGGCTGTCGAGTACCGCCGGCCTCCT
mouse   GGAGCGCATCGCGCGCCTGGAGGACAAGGTGAAGACACTCAAGGCTGAGAACGCGGGGCTGTCGAGTGCTGCCGGTCTCCT
junba   GGAGCGCATCTCCCGGCTGGAGGACAAAGTGAAAGTGCTCAAGTCGGATAACGCCGGACTGTCCAGCACTGCGTCCCTGCT
junbb   AGAACGCATCGCGCGGCTGGAGGAAAAGGTGAAGGTACTGAAGTCCGACAACGCCGGACTGTCCAACACAGCGTCTGTTCT

human   CCGGGAGCAGGTGGCCCAGCTCAAACAGAAGGTCATGACCCACGTCAGCAACGGCTGTCAGCTGCTGCTTGGGGTCAAGGG
mouse   ACGGGAGCAAGTGGCGCAGCTCAAGCAGAAGGTCATGACCCATGTCAGCAACGGCTGCCAGTTGCTGCTAGGGGTCAAGGG
junba   GAGGGAGCAGGTAGCTCAGCTTAAGCAGAAGGTCATGACCCATGTGAGCAGCGGGTGCCAGCTGATGCTGACGCCCAAGAT
junbb   GCGGGAACAGGTGGCGCAACTCAAGCAGAAGGTCCTGAGGCACATGAACAGCGGCTGTCAGCTCATGCTGACCAGTAAGAT

human   ACACGCCTTCTGA
mouse   ACACGCCTTCTGA
junba   CAAGTCGTTTTAG
junbb   GGAGGCGTTTTAA
```

Figure 4-12: *junba* and *junbb* paralogues share sequence homology with their murine and human orthologues.

A) Phylogenetic tree obtained from the alignment and comparison of human, murine and zebrafish *junb* coding sequences. This cladogram is a Neighbour -joining tree without distance corrections. B) Summary table comprising the location and size of the transcripts and proteins of the two *Junb* paralogues in zebrafish. C) Multiple nucleotide sequence alignment of human, murine and zebrafish *junb* sequences revealed high sequence conservation at the 5' area. Red font marks the conserved nucleotides among the four sequences. Yellow shade marks the start and end of the coding sequence.

Furthermore, wildtype zebrafish embryos isolated at the most relevant time points for LEC specification (20 hpf, 24 hpf and 30 hpf) were subjected to WISH using specific probes. Expression of these two genes in eyes, lenses and brain could be observed and was in line with previously described data (Thisse et al., 2004; Kiesow et al., 2015). However, a closer look into the truck area revealed a distinct expression pattern for the two paralogues.

junba is expressed in the ventral part of the embryo around 20 hpf and 24 hpf. At this latter timepoint, it is quite ubiquitously distributed and it is seen in many other tissues as, for example, in the tip of the tail. At 30 hpf and in line with the expression data obtained from the qRT-PCR, nearly no or unspecific signal was detected. *junbb* is also expressed in the ventral part of the trunk around 20hpf. From 20 hpf until 24 hpf a strong signal in the pronephric area that could correspond to the zebrafish blood island was observed (Figure 4-13 B).

These data suggest distinct roles of *junba* and *junbb* during zebrafish development. While *junba* seems to play a role in the earliest steps of embryonic development, *junbb* rather seems to be required for later stages. The fact that both genes are expressed to some extent in the vein and around the time when lymphangiogenesis takes place, prompted me to address the impact of each gene on this process separately.

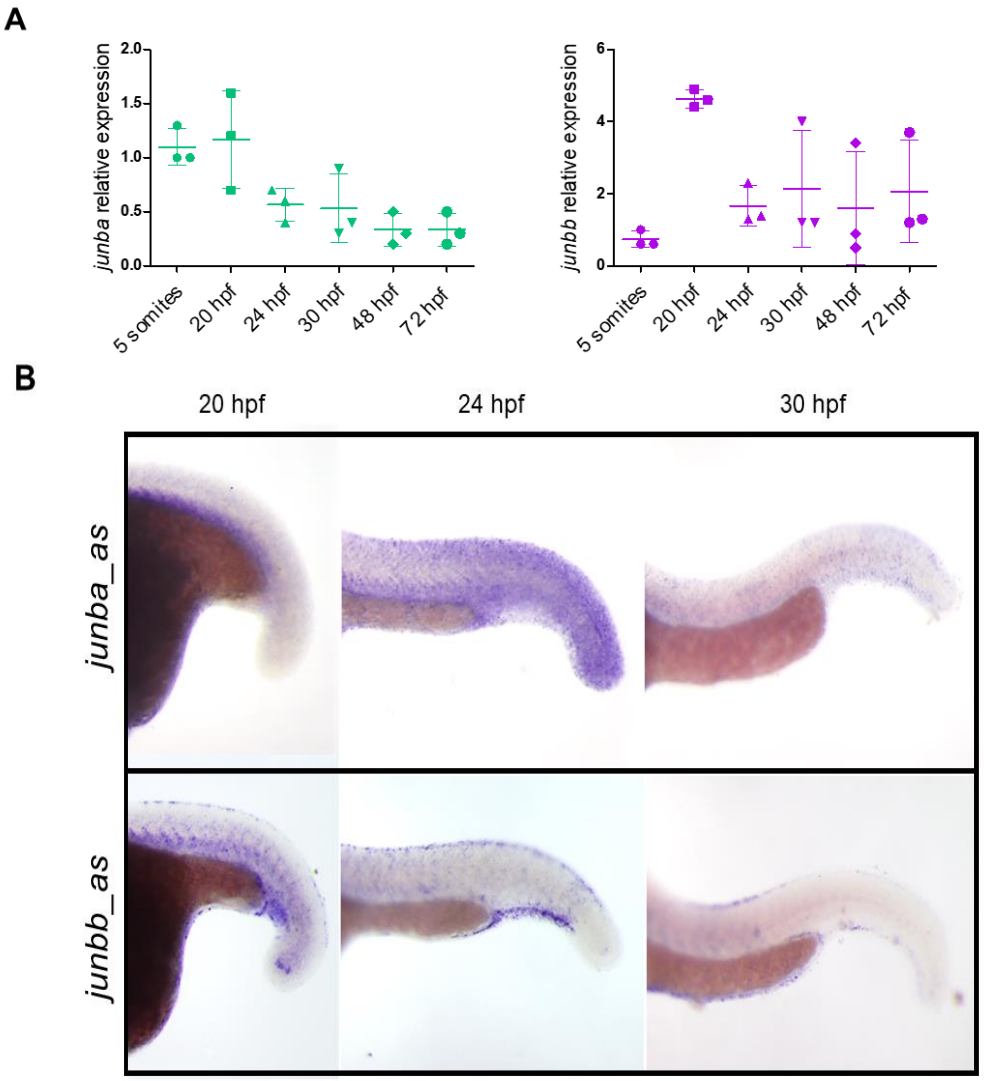

Figure 4-13: Differential expression of *junba* and *junbb* in time and space during zebrafish development.

A) Relative expression of *junba* (left graph, green marks) and *junbb* (right graph, purple marks) during the first three days of development of zebrafish embryo: 5-somites, 20 hpf, 24 hpf, 30 hpf, 48 hpf and 72 hpf. mRNA levels were analyzed by qRT-PCR and normalized to the expression of *beta-actin*. Fold changes were depicted relative to the first time point (5 somites) which was set to 1. Lines and error bars mark mean±SD among biological triplicates. B) Representative brightfield images of wholemount embryos stained with *junba* (top panel) and *junbb* (bottom panel) specific antisense in situ probes at 20 hpf, 24 hpf and 30 hpf.

4.2.2 CRISPR-Cas-mediated generation of *junb* mutants

In order to address the role of *junba* and *junbb* genes in lymphatic development individually, single zebrafish mutants were generated using the CRISPR-Cas9 technology.

Since both *junba* and *junbb* consist only of one exon, CRISPR guideRNAs were *in silico* designed to target the first 200 bp of the exons using two softwares programs: CHOP-CHOP (Labun et al., 2016) and CRISPR-design from the Zhang Lab. Only gRNAs that fulfilled the following criteria were considered: i) PAM location at the start of the exon ii) high mutagenesis potential and iii) low off-target prediction in coding areas. Selected gRNAs were cloned into pT7 plasmid and "*in vitro*" transcribed.

To guarantee the mutagenesis success, two parallel strategies were followed. In the first one, I aimed for a non-homologous end joining repair that will randomly generate insertions or deletions at the targeted area. Moreover, an additional approach aiming a homology directed repair was included so a pre-designed donor DNA could be specifically inserted in the region of interest. Similarly to the described method of Auer et al., (2014), a DNA cassette harboring three stop codons in all possible reading frames was generated so it could be incorporated after Cas9 nuclease activity (Figure 4-14).

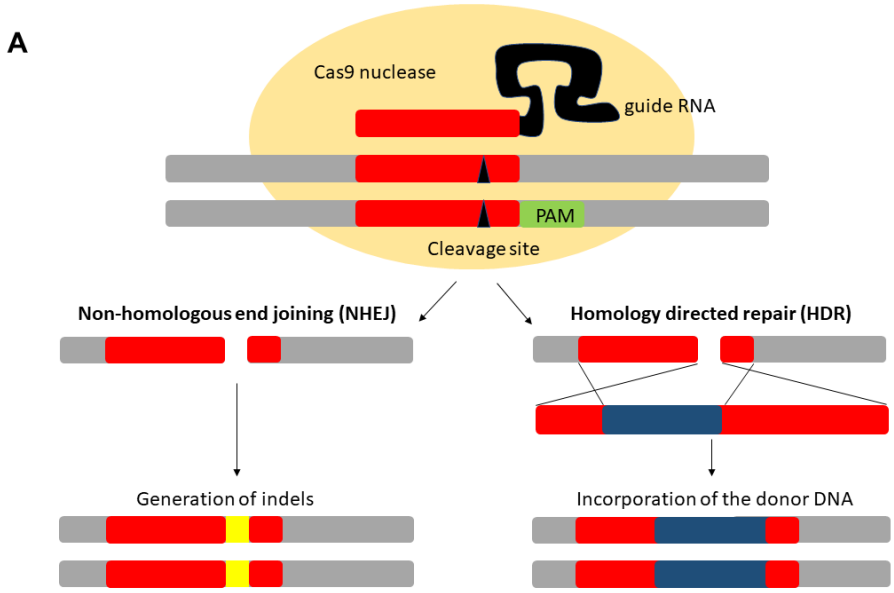

Figure 4-14: Model of the two different approaches followed to generate *junb* mutant fish.

A) Schematic representation of the two types of mutations generated by CRISPR-Cas9 technology in this study. Non-homologous end joining generated random insertion/deletions (indels) at the targeted area and homology directed repair incorporated the donor STOP cassette at a designated area.

Concurrent injection of gRNA, Cas9 protein and STOP cassette oligo were performed into one-cell stage wildtype embryos. In order to check the efficacy of the mutagenesis, DNA from 24 hpf injected embryos was isolated and a PCR reaction was performed using specific primers flanking the targeted region. PCRs were then resolved on a 3% metaphor high resolution agarose gel to detect variations in the amplicon size. gRNAs were only used if indels were noticed as smear on the gels. Providing that the mutagenesis was successful, the injected embryos were grown until adulthood.

In order to address whether the generated mutations were transmitted via the germline, the adults from the previously injected embryos were crossed to wildtype fish in single pairs and their progeny (24 hpf embryos) was studied as described above. A germline transmission of the mutation was assumed when a clear band different from the wildtype amplicon size was observed on the high resolution gel. To characterize the mutation in detail, PCR amplicons were cloned into pGEMT vectors and sequenced. Only fish carrying mutations resulting in premature STOP codons or frameshifts were further propagated.

Table 4-1. Collection of all the mutants sequenced during the study. Grey shaded cells mark the mutants selected for further studies.

	junba	*junbb*
Non-homologous end joining (NHEJ)	5 bp insertion	3 bp deletion
	8 bp deletion	31 bp deletion + 4 mismatch
	5 bp deletion	6 bp deletion
	8 bp deletion + 4 bp mismatch	37 bp insertion + 6 bp mismatch
	5 bp deletion	14 bp deletion
Homology directed repair (HDR)	STOP cassette insertion not found	STOP cassette insertion

For *junba*, a 5bp insertion mutant resulting in a frameshift and premature STOP codon was selected (Figure 4-15A). For *junbb,* a 14bp deletion mutant with a frameshift in the reading frame was identified. Additionally, *junbb* mutants harboring the STOP cassette insertion were considered for further studies (Figure 4-15B).

Founders (F0) that successfully transmitted the mutations to their progeny were further crossed with zebrafish vascular and lymphatic reporter lines and their offspring was raised until adulthood (F1). Fin biopsies of the F1 adult fish were genotyped and only heterozygous animals were kept. Further outcrosses of heterozygous fish with wildtype fish were performed to get rid of possible off target mutations (Figure 4-15C).

In summary, *junba/junbb* zebrafish mutants were successfully generated.

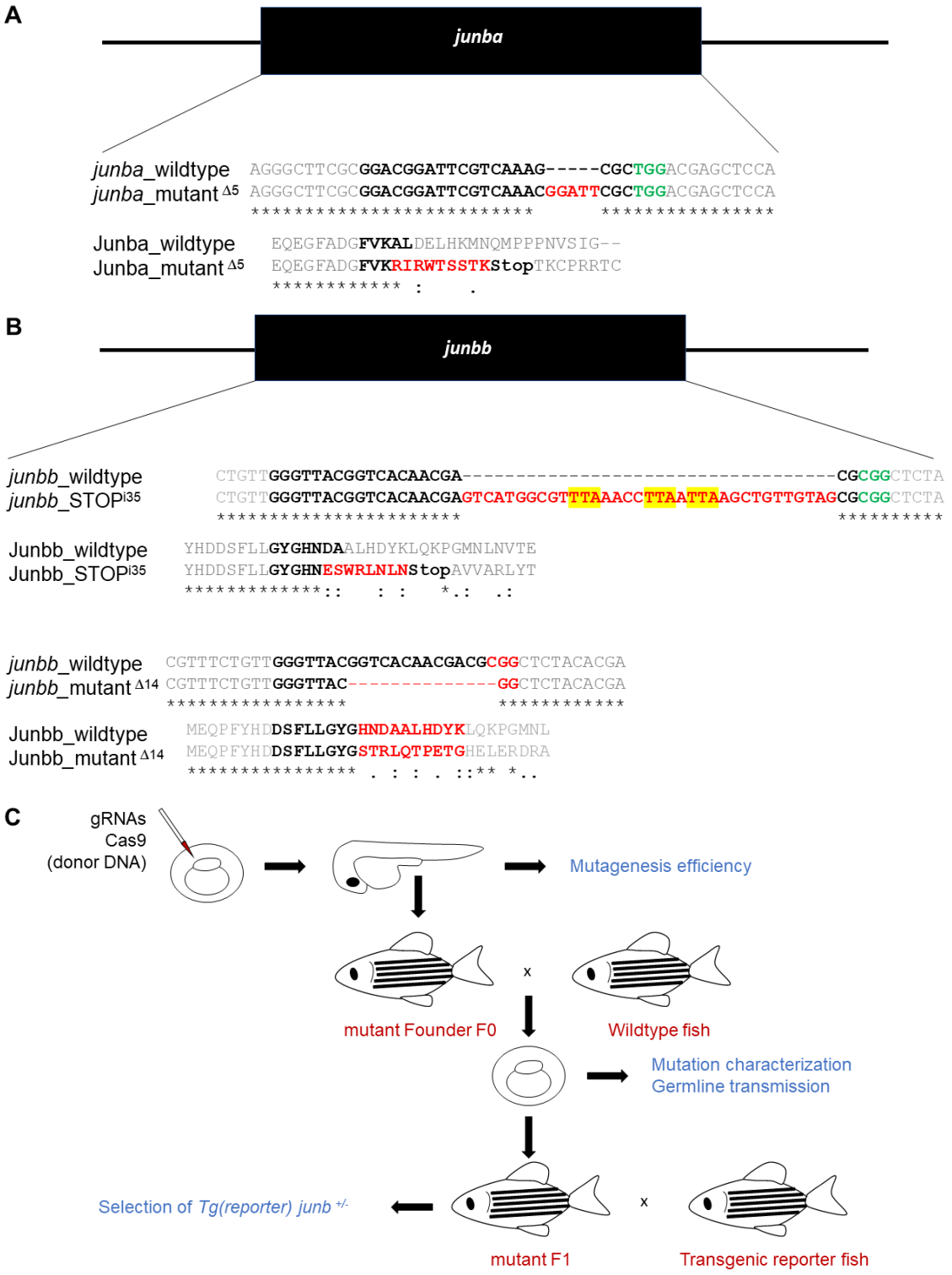

Figure 4-15: Generation of *junb* mutant zebrafish applying the CRISPR-Cas9 technology.

A) Comparison of the DNA and protein sequence of the generated 5bp insertion *junba* mutant and B) STOP cassette insertion and 14 bp deletion *junbb* mutants. Bold letters mark the CRISPR target area, green letters mark the PAM sequence, red letters indicate the mutated base pairs and residues and yellow shade mark the inserted STOP codons. C) Schematic representation of the generation and selection of a new mutant zebrafish line. Each cycle (from embryo to fertile adult fish) lasted 3 months.

4.2.3 *junb* mutants are fertile and reach adulthood.

Next, I aimed to characterize the newly-generated mutants. For that purpose, heterozygous fish were crossed to generate a heterogeneous offspring in which all the possible genotypes were represented. Henceforth *junba*^{5i} and *junbb*^{STOP} mutants are referred as *junba* and *junbb* mutants respectively.

A first global analysis of the genotype distribution among the mutants was done in a blind selection of 24 hpf embryos. Single embryo DNA isolation and subsequent PCR analysis was performed to assess whether the distribution of the mutant alleles followed a Mendelian ratio (Figure 4-16 A-B).

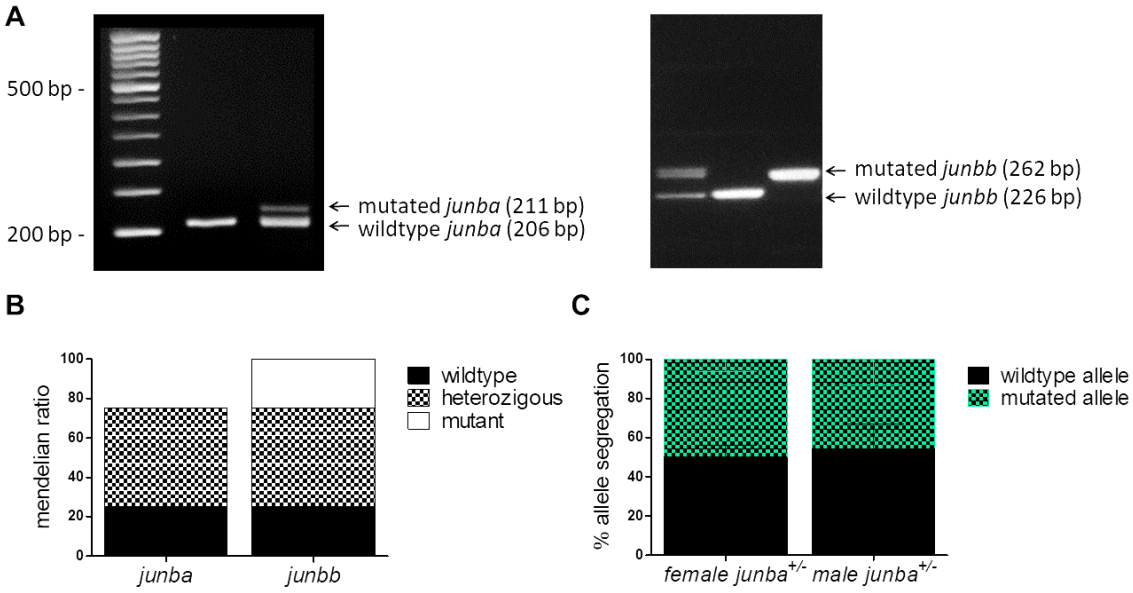

Figure 4-16: Differential Mendelian ratio between *junba* and *junbb* mutants.

A) Genotype of single 24 hpf zebrafish embryos by amplification of the *junba* (left) and *junbb* (right) locus. Mutated and wildtype amplicons are marked with black arrows. B) Mendelian ratio distribution for *junba* (n=98 embryos, N=3) and *junbb* (n=120, N=3) offspring. C) *junba* mutant allele distribution into the germline of *junba* males and females (n=48, N=3).

junbb homozygous and heterozygous mutants were identified by genotyping and were found at the expected Mendelian ratio of 1 wildtype: 2 heterozygous mutants: 1 homozygous mutant. Surprisingly, no *junba* homozygous mutants were identified in the tested 24 hpf samples (~100 embryos). Mendelian ratio of the identified *junba* heterozygous mutant embryos displayed a 2 heterozygous mutants: 1 wildtype ratio distinctive of the recessive lethal genes.(Figure 4-16 C)

In order to rule out the possibility that *junba* Mendelian ratio was due to an impairment of the mutant allele distribution, single *junba*$^{+/-}$ fish were crossed with wildtype fish and their offspring was analyzed. Both *junba*$^{+/-}$ females and males were found to transmit

junba mutated allele equally and *junba* $^{+/-}$ offspring was identified at the expected ratios excluding a problem during *junba* mutant egg and sperm formation. (Figure 4-16D).

Considering that *junba*$^{+/-}$ parents can transmit the allele and that *junba* transcript levels peaked at early time points (Figure 4-13A), I wondered whether *junba*$^{-/-}$ fish may form but die before the 24 hfp.

In order to confirm the importance of *junba* in early zebrafish development, a mutant reporter line following the strategy of the Gal4: Upstream Activator Sequence (UAS) system was generated. Gal4 is a transcriptional activator that binds UAS sequence in trans (Kakidani and Ptashne, 1988; Webster et al., 1988). This system allows the expression of any reporter gene under the control of UAS sequence anywhere where Gal4 is active. Thus, I aimed to generate a construct with *junba* sequence cloned in-frame with *KalT4* sequence, a less toxic variant of Gal4 activator (Figure 4-17A).

This *junba*-Kalt4 construct was co-injected with Cas9 protein and junba gRNAs into one-cell *Tg(UAS:Kaede)* zebrafish embryos. After Cas9 nuclease activity, concurrent cleavage of the genomic locus and the *junba*-Kalt4 plasmid occurred and the *junba-Kalt4* donor plasmid was integrated into the genome by the homology-independent DNA repair machinery (Figure 4-17B).

This generated transgenic zebrafish line drives *Kalt4* expression under the endogenous *junba* promoter so whenever *junba* promoter is active, KALT4 is simultaneously transcribed. KALT4 will then transactivate UAS-driven *Kaede* expression resulting in green fluorescence. *junba*-expressing tissues can then be easily identified by confocal fluorescence microscopy.

The insertion success of this construct was very low (only 5% of the injected embryos exhibited mosaic expression of KAEDE) but this data is in line with the previous reports (Auer et al., 2014). Mosaic fishes that reached adulthood and were fertile were checked for germline transmission and identified as founders.

Microscopic analyses of this line *Tg(UAS:Kaede, junba-Kalt4)* revealed a high expression of *junba* in the vegetal pole of the fertilized egg. At later stages (4 dpf), expression of *junba* was rather low and was restricted mainly to the eyes, the yolk and cardinal vein (Figure 4-17C).

Taken together, the early expression pattern of *junba* suggests an important role for its protein during the first steps of embryo formation.

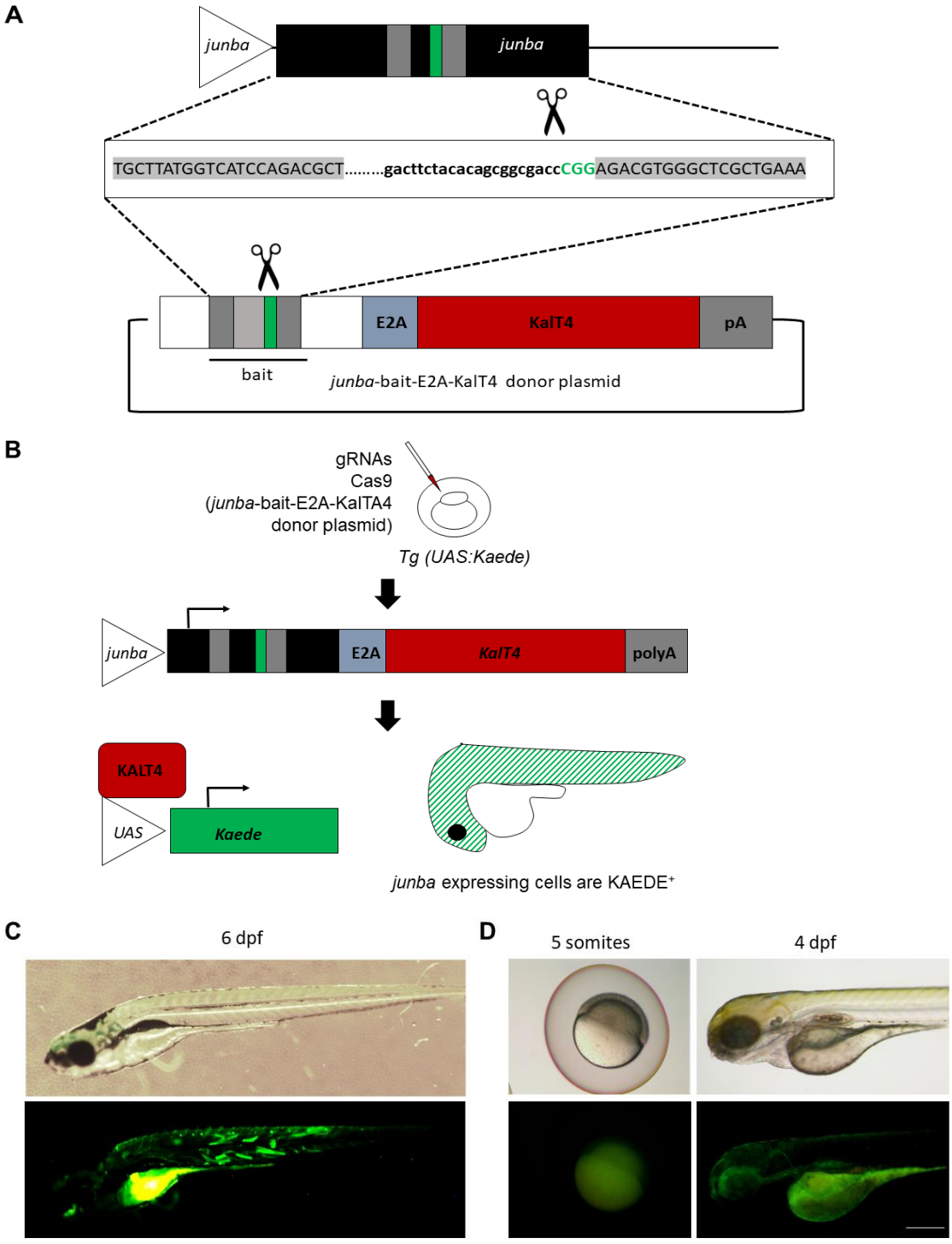

Figure 4-17. Generation of *Tg (UAS:Kaede, junba-Kalt4)* reporter line

A) Schematic representation of the cloning performed to insert a fragment of the *junba* locus (containing the CRISPR targeted area) into a *junba*-E2A-*Kalt4* donor vector. B) Schematic representation of the injection mixture and the CRISPR-mediated recombination. C) Representative brightfield and fluorescence images of an injected 6 dpf mosaic larva. D) Representative brightfield and fluorescence images of 5-somites and 4 dfp *Tg(UAS:kaede, junba-Kalt4)* embryos exhibiting tissue-specific *junba* expression.

4.2.4 *junb* mutants partially phenocopy the morphants

4.2.4.1 *junb* mutants display an allele-dependent loss of PACs

In order to investigate whether *junb* mutants also display defects on the formation of early lymphatic structures similar to the previously published morphants (Kiesow et al., 2015), the formation of PACs was assessed. For that purpose, the mutants were raised in the pan-endothelial *Tg(fli:EGFP)^{y1}* background in which all endothelial cells plus some neuronal cells in the head and in the trunk are labelled with EGFP. Next, crossing of heterozygous fish was performed to obtain a heterogeneous population of embryos with all the possible genotypes and were grown in PTU-containing medium to avoid pigmentation.

A random sample of this population was selected and analyzed by confocal microscopy. The characterization of the lymphatic development was done blindly on a single embryo basis. Each embryo was shortly anaesthetized with 0.25% tricaine solution, quickly oriented and immobilized in 6% methylcellulose prior visualization. After its observation, each embryo was carefully washed, placed back in PTU-containing medium and kept in the incubator until 5dpf for further analyses.

Thus, the presence of PACs throughout on the 7 somites over the yolk extension were quantified. Each hemisegment was analyzed independently and classified as: “complete” when the PACs were present or “absent” when there were no PACs or the PACs sprout from the vein did not reach the horizontal myoseptum.

The analysis of PACs formation in *junba* and *junbb* mutants showed that ,similarly to the morphants, there was a significant allele-dependent loss of PACs.
Solely loss of one *junbb* allele resulted in a significant decrease in the number of PACs formed at 72 hpf (4,389 ± 0,24 versus wildtype siblings 5,433 ± 0,1774). This effect was more evident in the *junbb$^{-/-}$* embryos since at the same time point they only displayed PACs in half of the measured segments in comparison to their wildtype siblings (3,03 ± 0,2153 versus 5,433 ± 0,1774).
Similarly, loss of one *junba* allele also caused a reduction in the formation of the PACs with regard to their respective wildtype siblings (4,105 ± 0,1988 versus 5,88 ± 0,09748).

In order to assess whether loss of both *junba* and *junbb* could lead to a total loss of PACs, *junbb$^{-/-}$ junba$^{+/-}$* mutants were generated and analyzed. Surprisingly, although a significant reduction in the PACs formation was observed, a synergistic effect in the loss of PACs was not observed. Although *junbb$^{-/-}$ junba$^{+/-}$* embryos displayed less PACs that *junba$^{+/-}$* alone (4,105 ± 0,1988 versus 3,542 ± 0,2948), the observed phenotype was not as striking as in the *junbb$^{-/-}$* embryos (3,03 ± 0,2153)(Figure 4-18 A-B).

These data suggest that both *junba* and *junbb* could affect the formation of parachordal cells presumably by participating in the same pathway.

In order to rule out that the defect in the formation of the PACs could be due to a failure during the arterial and venous sprouting, a quantitative analysis of the identity of Intersegmental Vessels (ISVs) was carried out. Primary sprouts derive from the dorsal aorta (DA) and give rise to arteries and secondary sprouts stem from the posterior cardinal vein (PCV) and give rise to the veins. Normal ISVs networks comprises 50%:50% arterial:venous ISVs (Bussmann et al., 2010). Therefore, an imbalance on the A:V ratio suggests a defect in the PCV sprouting.

Thus, the same previously analyzed embryos were carefully examined for the ISVs identity. Calculation of the arterial:venous ratio revealed no significant differences among the analyzed mutants compared to the wildtype siblings (aISVs:vISVs *junbb*$^{+/+}$ 47:53%; *junbb*$^{+/-}$ 47:53%; *junbb*$^{-/-}$ 44:55%; *junba*$^{+/-}$ 48:52% and *junbb*$^{-/-}$ *junba*$^{+/-}$ 49:51%), yet all of them displayed a slight shift towards vISVs (Figure 4-18 C).

In order to exclude a defect in the blood circulation, the embryos were monitored for heart development, heart beat and workflow which were undistinguishable from or similar to wildtype embryos.

These data rule out the possibility of an intrinsic PCV sprouting defect or a cardiovascular secondary effect.

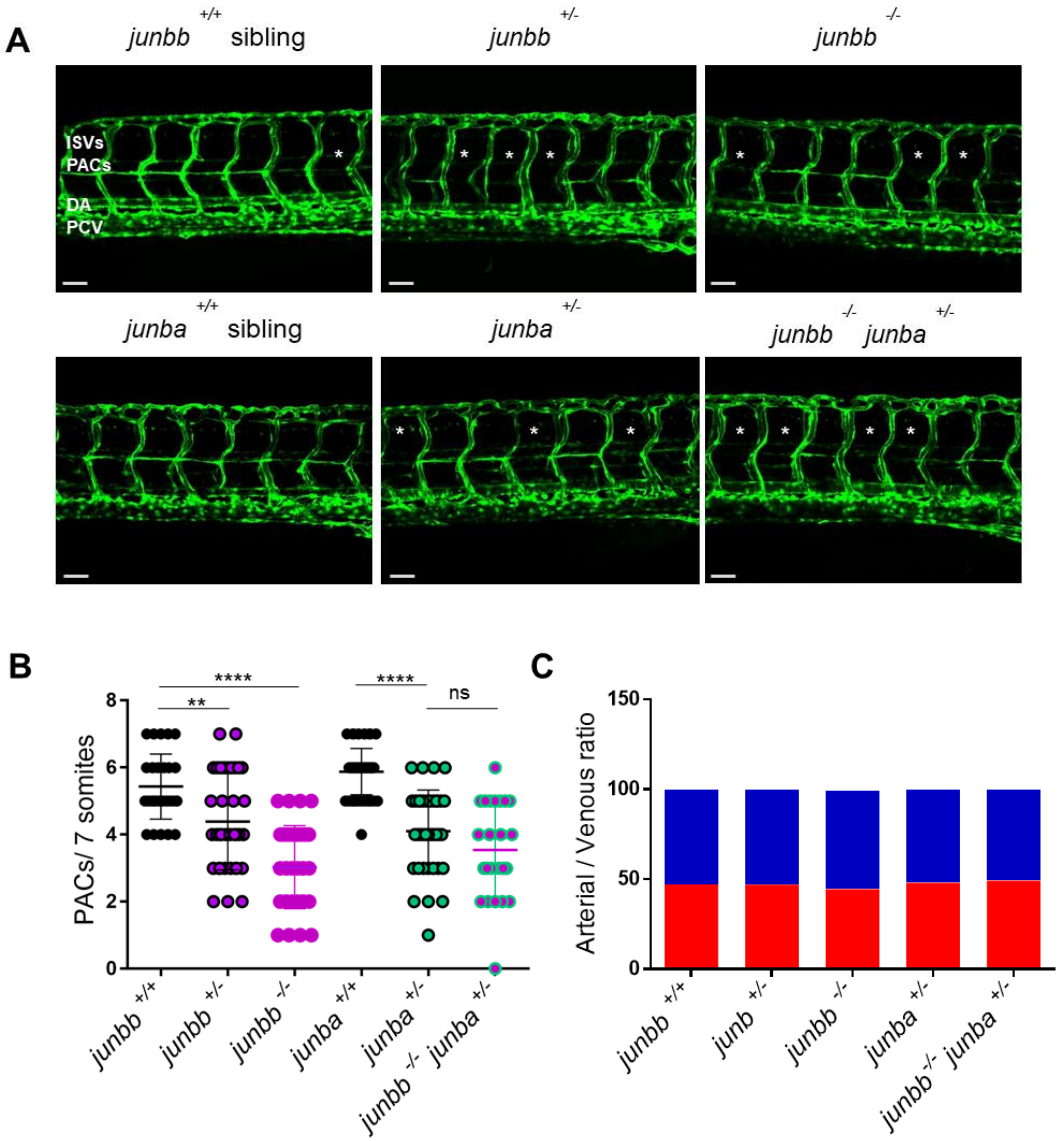

Figure 4-18: *junb* mutants display an allele-dependent decrease in PACs formation at 72 hpf.

A) Representative confocal images of the trunk region of *Tg(fli:EGFP)^{y1} junb* mutant zebrafish embryos in which the PACs from *junba* and *junbb* mutants and their respective wildtype siblings were quantified. Dorsal is up and posterior to the left. White asterisks mark the absence of a hemisegment. ISVs (Intersegmental Vessels), PACs (Parachordal Cells), DA (Dorsal Aorta) and PCV (Posterior Cardinal Vein). Scale bar 30 µm. B) Quantification of the present PACs at 72 hpf (count of 7 hemisegments in n>25, N=3). Each dot marks an independent embryo. The lines and error bars refer to mean ± SD. Statistical analysis was performed using unpaired two-tailed t-Student test. ns (not significant) p>0.05, ** p<0.01 and **** p<0.0001 .C) Quantification of the arterial/venous ratio in *junba* and *junbb* mutants and their respective siblings (count of 7 hemisegments in n>25, N=3).

4.2.4.2 *junb* mutants develop a normal thoracic duct

The parachordal cells are the building blocks of the trunk lymphatics: once formed, they migrate ventrally and dorsally to form the thoracic duct (TD; anatomically located between the DA and the PCV) and the dorsal longitudinal lymphatic vessel (DLLV) and the intersegmental lymphatic vessel (ISLV) respectively (Yaniv et al., 2006; Küchler et al., 2006; Hogan et al., 2009a).

In order to investigate whether the failure in the formation of the PACs also provoked the generation of a defective thoracic duct; 5 dpf embryos were analyzed similarly as described before. Thereafter, each embryo's DNA was isolated and genotyped and PACs and TD counts were associated with each embryo.

The presence of the thoracic duct in the 7 somites over the yolk extension were quantified. Each hemisegment was independently classified as "complete" or "absent".

Solely loss of either 1 or 2 *junbb* alleles did not affect the formation of the thoracic duct and all the analyzed embryos displayed a complete TD (*junbb* $^{-/-}$ 6,389 ± 0,2003 and *junbb*$^{+/-}$ 6,526 ± 0,1404 versus *junbb* wildtype siblings 6,762 ± 0,09524) (Figure 4-19 A/C). The presence of one mutated *junba* allele was not sufficient to affect TD development as most of the analyzed embryos exhibited a complete TD (*junba*$^{+/-}$ 6,838 ± 0,06143 versus *junba* wiltype sibling 6,892 ± 0,05175).
Yet, when one *junba* and *junbb* alleles were lost (*junbb*$^{-/-}$ *junba*$^{+/-}$ mutants) a significant decrease in the TD was observed. Some fragments were discontinuous or were missing in comparison with single *junba*$^{+/-}$ or wiltype sibling (*junbb*$^{-/-}$ *junba*$^{+/-}$ 6,071 ± 0,286 versus *junba*$^{+/-}$ 6,838 ± 0,06143 or *junba* wiltype sibling 6,892 ± 0,05175), yet the majority of the segments displayed a complete TD (Figure 4-19 B/C).

The fact that loss of either junb paralogue exhibited defects on PACs formation and the *junbb*$^{-/-}$ *junba*$^{+/-}$ showed a subtle impairment in TD formation, proposes a role for both *junba* and *junbb* in lymphangiogenesis.

These data suggest that the loss of *junba* and *junbb* is more detrimental for lymphatic vascular development in the early developmental steps while in the later steps the loss might be compensated.

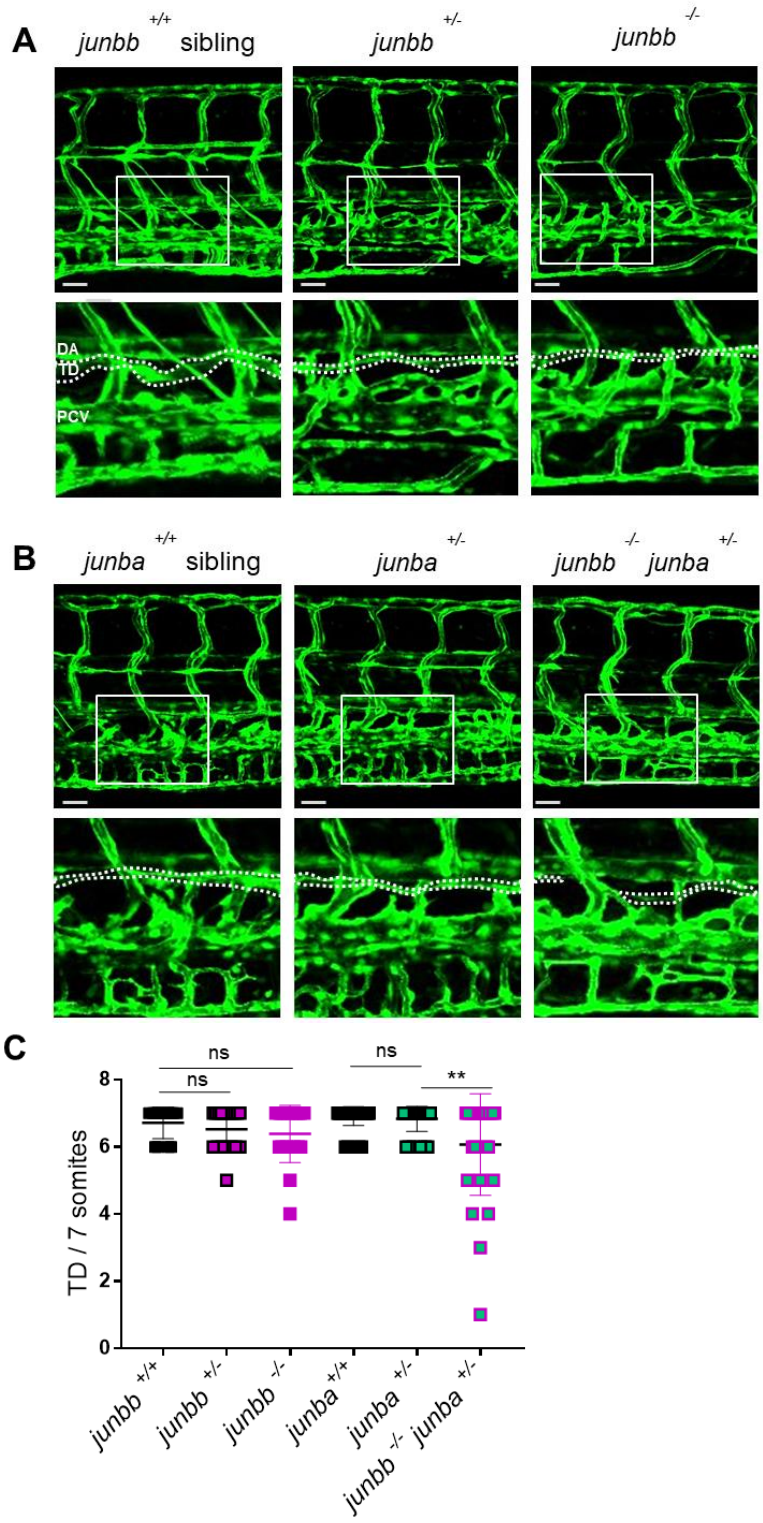

Figure 4-19: *junb* mutants are able to form a complete thoracic duct by 5 dpf.

A) Representative confocal images of the trunk of *Tg(fli:EGFP)^{y1} junbb* and B) *junba* mutant fish. Lower panels are magnifications of the white squared regions of the upper panels.Scale bar 30 µm. The thoracic duct is marked by white dashed lines. Dorsal is up and anterior to the left. C) Quantification of the presence of TD fragments at 5 dpf (count of 7 hemisegments in n>20 embryos, N=3) Each square marks an independent embryo. The lines and error bars refer to mean ± SD. Statistical analysis was performed using unpaired two-tailed t-Student test. ns (not significant) p>0.05, ** p<0.01.

Defects on the formation or malfunction of the lymphatic system are normally associated with the presence of edema, tissue swelling caused by an accumulation of fluid, normally observed in the back of the head, the heart or the yolk of developing embryos.

In order to determine whether the loss of some TD fragments is sufficient to trigger a systematic lymphatic failure, *junb* mutants were grown and 6 dpf larvae were characterized for the presence of edema. Morphological analysis of the growing larvae revealed no edema presence among the mutants. In addition, mutants were found to be undistinguishable with regard to their size and phenotype (Figure 4-20).

The fact that the *junb* mutants are displaying almost a complete and functional TD may explain lack of edema and their ability to reach adulthood.

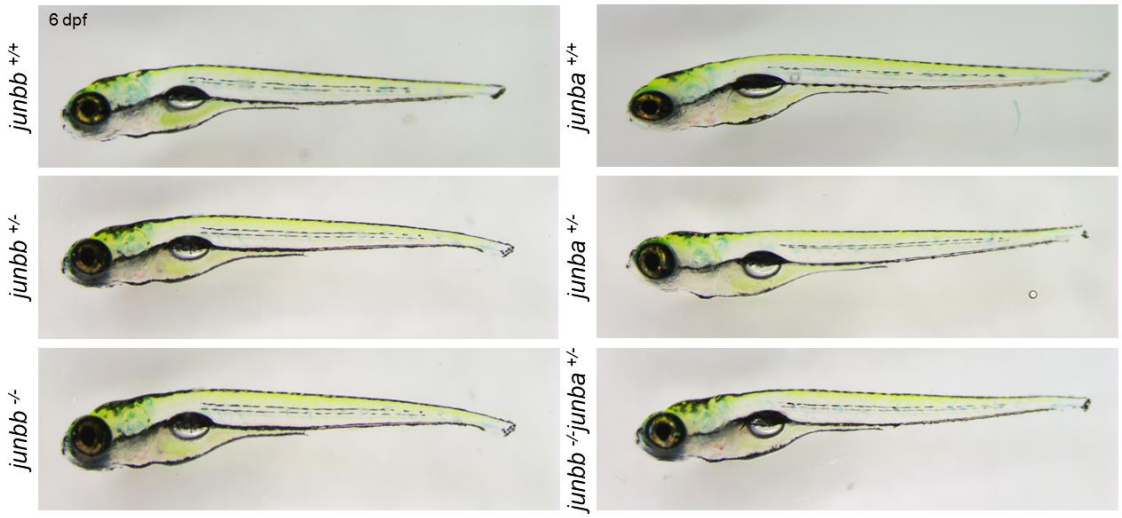

Figure 4-20. *junb* mutants display no signs of edema or lymphatic malfunction at 6 dpf.

Representative brightfield images of 6 dpf *junb* mutant zebrafish larvae exhibiting no features of lymphatic failure or edema in the head or trunk. Dorsal is up and anterior to the left

4.2.5 *junb* mutants generate ectopic sprouts from 3 dfp until 5 dpf.

Aside from the previously described failure in the formation of the PACs at 72 hpf, *junb* mutants exhibited normal development of vascular structures such as: dorsal aorta (DA), posterior cardinal vein (PCV), intersegmental vessels (ISVs) and dorsal longitudinal anastomotic vein (DLAV). Unexpectedly, several *junb* mutants displayed dorsal vascular hyperbranching at the level of the neural tube.

In order to characterize this novel phenotype, *junb* embryos were grown in PTU and analyzed by confocal microscopy as described before.

The presence and the development of the ectopic sprouts on the 7 somites over the yolk extension was analyzed from 72 hpf until 5 dpf.

The analysis of the number of ectopic sprouts revealed a significant difference in the *junbb* mutants at 72 hpf and a significant difference in both *junba* and *junbb* mutants at 5 dpf in comparison to their respective wildtype siblings.

At 72 hpf, solely loss of one *junbb* allele provoked the generation of ectopic sprouts (0,4063 ± 0,098 versus wildtype siblings 0 ± 0). This effect was more evident in the *junbb*$^{-/-}$ embryos since at the same developmental stage they display even more sprouts in comparison to their wildtypes siblings (0.625 ± 0,2069 versus 0 ± 0).
In addition, even though few sprouts were documented in some *junba*$^{+/-}$ mutants, there was no statistical difference between *junba*$^{+/-}$ or *junbb*$^{-/-}$ *junba*$^{+/-}$ mutants and *junba*$^{+/+}$ fishes (Figure 4-21 A-C).

At 5 dpf, a significant increase in the number of ectopic sprouts was observed in *junbb*$^{+/-}$ and *junbb*$^{-/-}$ mutants when compared to *junbb*$^{+/+}$ embryos (0,75 ± 0,168 and 0,5833 ± 0,1797 versus 0 ± 0 respectively). Unexpectedly, the loss of both *junbb* alleles did not aggravated the phenotype.
Also, *junba*$^{+/-}$ mutants exhibited more ectopic sprouts than the wildtype siblings (1,1 ± 0,3317 versus 0,02128 ± 0,02128). *junbb*$^{-/-}$*junba*$^{+/-}$ embryos also developed more branches (0,7917 ± 0,2691 versus 0,02128 ± 0,02128) but there was not significant difference between the loss of one single *junba* or *junbb* allele and the loss of both *junbb* and one *junba* allele (Figure 4-21 A' B' and D).

Taken together, these data uncovered a putative new role of *junb* in controlling proper blood vessel sprouting in zebrafish embryos.

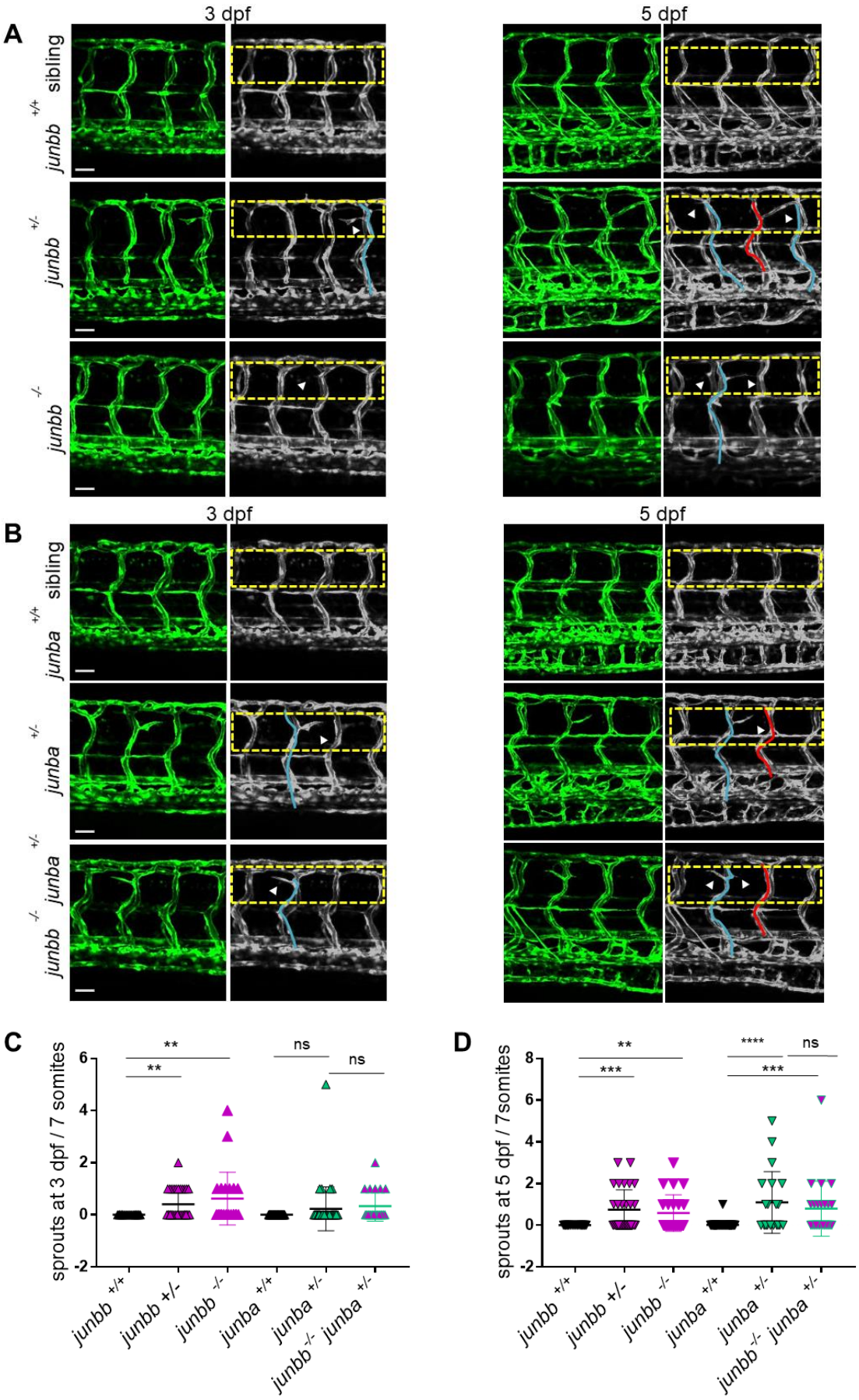
A
3 dpf
5 dpf
sibling
+/+ junbb
+/- junbb
-/- junbb
B
3 dpf
5 dpf
sibling
+/+ junba
+/- junba
+/- junba
-/- junbb
C
sprouts at 3 dpf / 7 somites
**
**
ns
ns
junbb +/+
junbb +/-
junbb -/-
junba +/+
junba +/-
junba +/-
junbb -/- junba
D
sprouts at 5 dpf / 7somites
**
***
****
***
ns
junbb +/+
junbb +/-
junbb -/-
junba +/+
junba +/-
junba +/-
junbb -/- junba

Figure 4-21: *junba* and *junbb* mutants exhibit dorsal vessel branching at 72 hpf until 5 dpf.

A) Representative confocal images of the trunk vasculature of *junbb* mutants at 72hpf and 5 dpf. B) Representative confocal images of the trunk vasculature of *junba* mutants at 72hpf and 5 dpf. Left panels are original images of the mutants in *Tg(fli:EGFP)*^{y1} background and right panels are colored in grey for better visualization of the sprouts. Yellow squares mark the area where the sprouts were found and quantified. White arrowheads mark the ectopic sprouts. Blue and red lines refer to arterial ISVs and venous ISVs respectively.Scale bar 30 µm. C) Quantification of the number of sprouts found along 7 somites of 72hpf embryos and D) 5dpf embryos (n>20 embryos, N=3). Each dot marks an independent embryo. The lines and error bars refer to mean ± SD. Statistical analysis was performed using unpaired two-tailed t-Student test. ns (not significant) p>0.05, ** p<0.01. *** p<0.001, ****p<0.0001

During the recording of the presence of ectopic sprouts, it was observed that their length and presence was dynamic. In order to track the development of the sprouts and analyze their origin and fate, single embryos were subjected to *in vivo* time lapse imaging with confocal microscopy.

For all the analyzed mutants, two behaviors were detected: while some sprouts developed continuously throughout the recording period (~24 hours); some other sprouts stopped growing and retracted until they were no longer visible at 5 dpf (Figure 4-22).

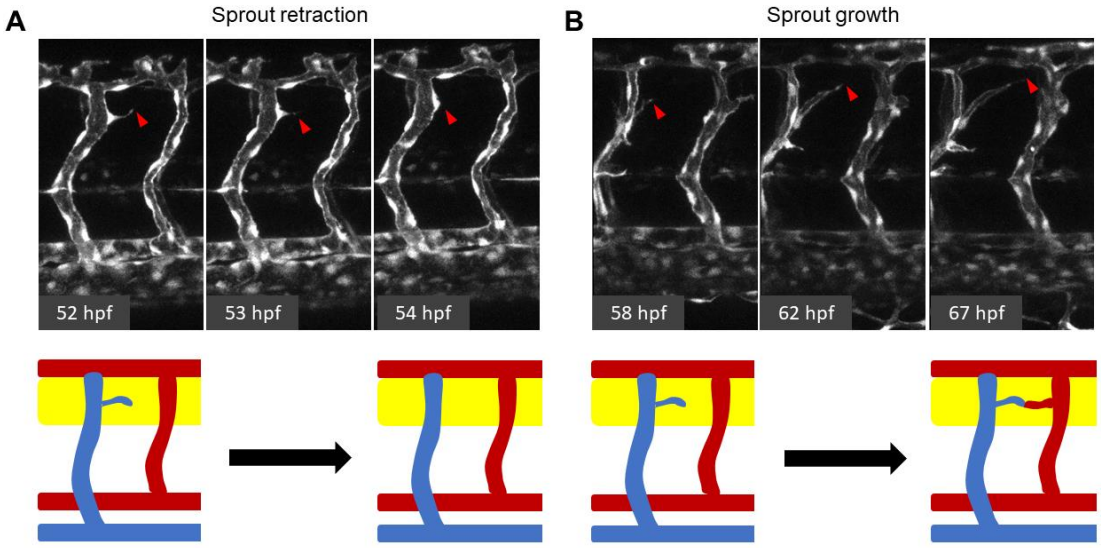

Figure 4-22: Retraction and sprout growth was tracked in the *junb* mutants.

A) Representative selected segments of confocal projections of the time lapse imaging of a spout retracting with time. B) Representative selected segments of confocal projections of the video imaging of a sprout growing with time. Original color was modified to grey for better visualization. Red arrowheads mark the tip of the sprout in each time. Lower panels are schematic representations of the processes observed above.

It was observed that more of half of the documented cases, the sprouts were more prone to grow rather than regress once they were formed (67,86 % in *junbb*$^{+/-}$, 50% in *junbb*$^{-/-}$, 78,26 % *junba*$^{+/-}$ and 79,17 % in *junbb*$^{-/-}$ *junba*$^{+/-}$. The duration of this ectopic sprouting varied from embryo to embryo.

Although most of the sprouts were found to grow, the majority of them never connected with the next ISVs as observed in the 88 %, 78.9 %, 86.2 % and 95.4 % of the *junbb*$^{+/-}$, *junbb*$^{-/-}$, *junba*$^{+/-}$ and *junbb-/-junba*$^{+/-}$ sprouts, respectively (Table 4-2).

Similar phenotypes has been described in the literature: while arterial sprouts have linked liked to the loss of *dll4* (Leslie et al., 2007)and *flt1* (Krueger et al., 2011);sprouts stemming from venous ISVs have been related to a neuronal-specific loss of s*Flt1* (Wild et al., 2017).

To address whether the *junb* mutants were generating ectopic sprouts from arterial or venous ISVs, a careful examination of the origin and fate of the sprouts was performed. It was observed that around 90% of the sprouts were originated from venous ISVs and were migrating toward arterial ISVs (70%). Additional data can be found in Table 4-2.

Table 4-2. Origin and development of the ectopic sprouts at 5 dpf.

Embryo genotype	Number of sprouts	Origin of the sprouts		End of the sprouts		Connection with the ISV	
		Arterial ISV	Venous ISV	Arterial ISVs	Venous ISV	Connected	Not connected
junbb $^{+/-}$	25	12 %	88 %	72 %	28 %	12 %	88 %
junbb $^{-/-}$	20	5,26 %	94,74 %	89,47 %	10,53 %	21,05 %	78,95 %
junba $^{+/-}$	29	3,45 %	96,56 %	72,41 %	27,59 %	13,79 %	86,21 %
junbb $^{-/-}$ ***junba*** $^{+/-}$	22	15 %	85 %	66,67 %	33,33 %	4,55 %	95,45 %

These data was consistent through all the analyzed mutants and are reminiscent of the phenotype observed in zebrafishes with neuronal loss of sFlt1 or Vegfa overexpression (Wild et al., 2017)

4.3 Outlook

4.3.1 *flt1* is a JUNB-direct target

Since both *junba* and *junbb* mutants displayed features previously associated with *flt1* loss and Junba and Junbb protein homology is up to 70%; I wondered, whether both proteins are able to could be transactivate Flt1 expression.

Since the main domains required for transcriptional transactivation are conserved in Junba and Junbb, I evaluated their ability to physically bind to CRE and TRE sequences, well-known JUNB/AP-1 binding sites in the *flt1* promoter as it has been previously observed in our lab for murine and human JUNB (Sator-Schmitt and Schorpp-Kistner, unpublished). Since the zebrafish promoter shared no conserved sequence areas with the mammalian promoters, a large fragment of the promoter region until the first intron (-10000 bp - +3000 bp) of *flt1* was investigated for the presence of AP-1 and CRE putative sites. Although many CREs sites were identified throughout the promoter, not many TREs sites were found to in the proximal promoter region. Yet, a proximal region of the *flt1* promoter of 800 bp was narrowed down as a promising segment since it harbored a cluster of three putative CREs: a consensus CRE site(-196/-188); a putative CRE site (-105/-97) and half CRE site (-72/-67) and one consensus TRE (-42/-35) binding site (Figure 4-23 A).

In order to validate whether *Junba* and *Junbb* can transactivate the zebrafish flt1 promoter, this 800 bp sequence was cloned in front of a luciferase reporter gene (into a pGL3 vector) for further analysis. Since the DNA binding domain is conserved among zebrafish and mammalian JUNB, an *in vitro* system of $Junb^{+/+}$ mouse embryonic fibroblasts was used. These cells were transfected with *flt1* promoter vector for 48 hours prior luciferase measurement. Co-transfection of *renilla* vector was used for the normalization of data.

A statistically significant increase (3x fold) of the luciferase light units compared with the empty pGL3 vector was observed, indicating that *flt1* promoter can be activated in $Junb^{+/+}$ cells (Figure 4-23 B).

Next, I wondered which one of the binding sites was necessary for *flt1* transcription. In order to address this question, site-directed mutagenesis targeting each of the binding sites was performed. At least 3 to 6 nucleotides were modified to assure that the binding activity was lost. Then, vectors containing single mutated versions of the promoter were produced and subjected to the luciferase studies as described above. Comparison of the luciferase/renilla ratio revealed that only the single mutation of the TRE site at position (-42/-35) led to impaired luciferase expression (Figure 4-23C).

Since the signal is reduced by half (2x fold decrease) but still somehow detected, AP-1 is important but not indispensable for *flt1* activation.

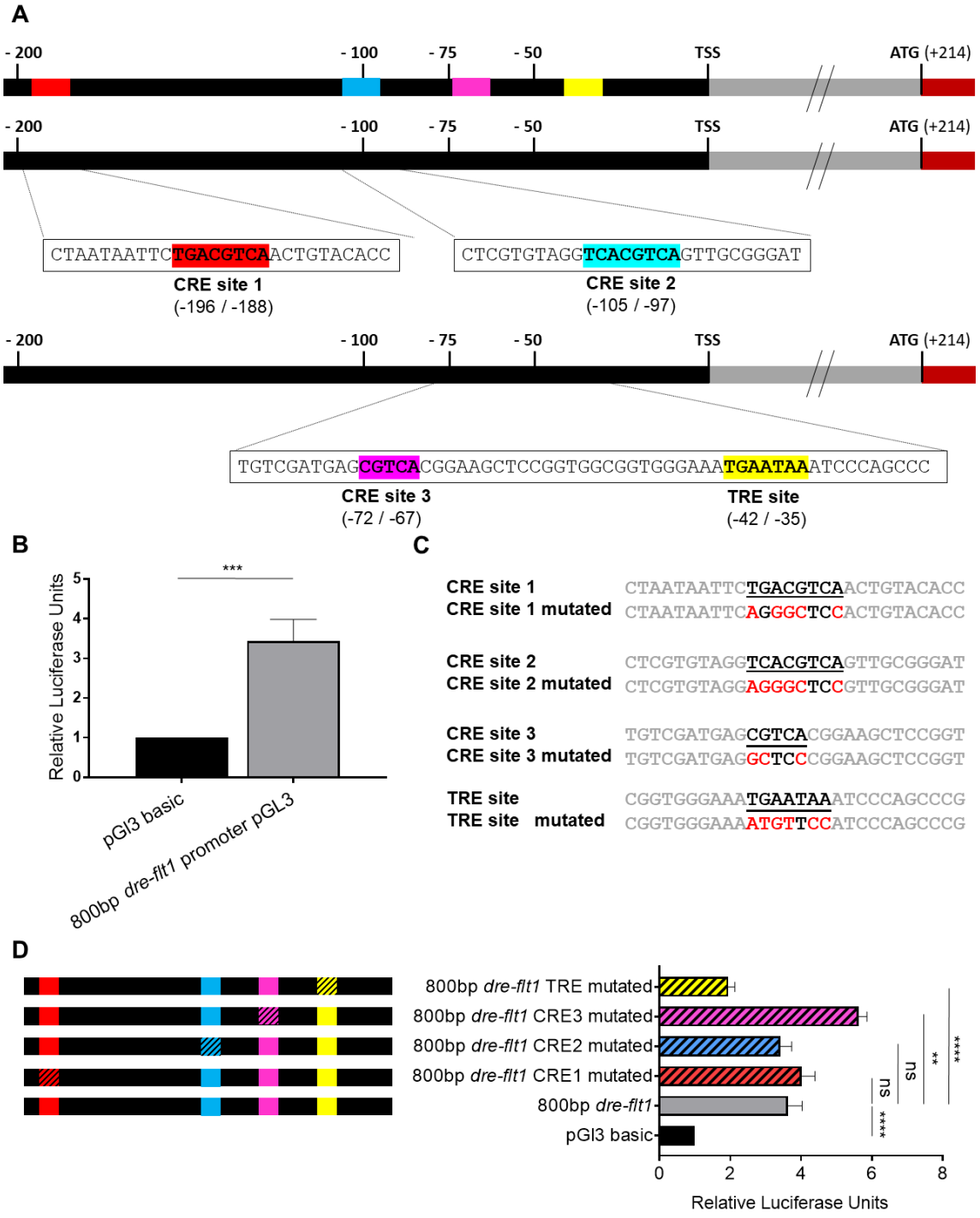

Figure 4-23: *flt1* transactivation is TRE-dependent

A) Illustration of the 800 bp promoter area used in the luciferase assays with the respective putative CRE1, CRE2, CRE3 and TRE sites. B) Luciferase/Renilla ratio graph of the 800bp dre-flt1 promoter vector transactivation study in *Junb* $^{+/+}$ cells. C) Illustration of the site-directed mutagenesis strategy for each of the binding sites. Bold underlined font marks the binding site, red font marks the mutated nucleotides. D) Graph depicting the Luciferase/Renilla ratio of the mutated versions of the zebrafish flt1 promoter in *Junb* $^{+/+}$ cells. Data was normalized to empty pGL3 vector signal which was set to 1. The bars and error lines refer to mean ± SD (N=3). Statistical analysis was performed using unpaired two-tailed t-Student test. ns (not significant) $p>0.05$, ** $p<0.01$ and ****$p<0.0001$.

4.3.2 Generation of a gain of function mutant

In order to demonstrate that the zebrafish ectopic sprouting in the mutants is due to Junb loss, a tissue-specific overexpression construct was generated using the Gateway Multisite Cloning strategy.

For that purpose, a vector with *junba* and *junbb* coding sequence, a 3' UAS promoter vector and a 5' E2A linker and RFP sequence vector were recombined into a destination vector containing flanking Tol2 sites, the UAS:junb-E2A-RFP vector. This Tol2 sites will allow the integration of the vector into the genome by the transposase action.

In order to determine whether this reporter construct could indeed drive the overexpression of *junb*, UAS:junb-E2A-RFP vector was co-transfected with a p16:Gal4 vector into F9 cells, a murine testicular teratoma line devoid of most of the AP1 members.

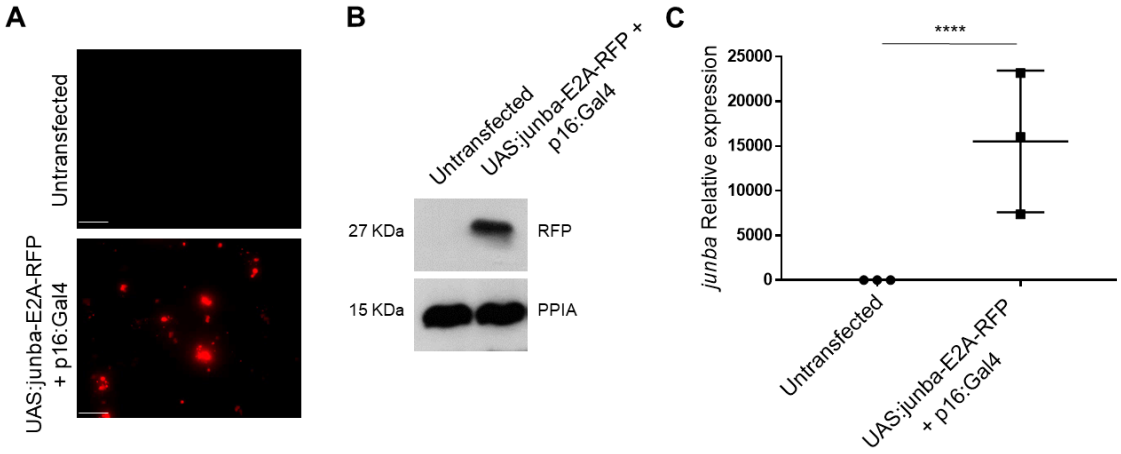

Figure 4-24: Overexpressing vectors drive zebrafish *junb* expression in F9 cells.

A) Representative fluorescence microscopy images of F9 cells untransfected or transfected with overexpressing uas:junb-E2A-RPF vector + p16:Gal4.Scale bar 50 µm B) Representative western blot of RFP signal in transfected cells. Cyclophilin A was used as control for equal quality and loading of protein extracts. C) Relative expression of *junba* in untransfected and transfected cells was analyzed by RT-PCR. mRNA levels were normalized to *Rplp0* levels and depicted as fold change. The lines and error bars refer to mean ± SD of three independent experiments (N=3). Statistical analysis was performed using unpaired two-tailed t-Student test ****p<0.0001.

Due to the lack of antibodies that specifically recognize the zebrafish proteins, RFP expression was initially examined. Fluorescence microscopy and western blot analyses revealed a substantial RFP signal in the transfected cells compared to the untransfected cells indicating that the UAS:junb-E2A-RFP construct was successfully expressed. In addition, total RNA from transfected and untransfected cells was isolated and *junb* expression levels were assessed. Zebrafish *junb* transcript was found to be massively expressed (15000x fold increase) compared with the untransfected cells.

These data are proof of principle that the newly-generated construct is expressed *in vitro* system and could be used for *in vivo* studies (Figure 4-24).

Next, I aimed to generate a new zebrafish line. Thus, the overexpression vector and transposase mRNA were injected into once-cell embryos of the endothelial *Tg(fli:UAS)* or neuronal *Tg(HuC/D:UAS*) background. Since transient overexpression was not enough to assure a successful insertion in the targeted cells, embryos were raised until adulthood. In the future, these new lines will be crossed with the previously described *junba* and *junbb* mutants and the presence and development of ectopic sprouts will be assessed. In these settings, either *junb* mutants with rescued endothelial or neuronal expression are hypothesized to correct the vessel hyperbranching revealing the source of Junb-driven *Flt1* (Figure 4-25).

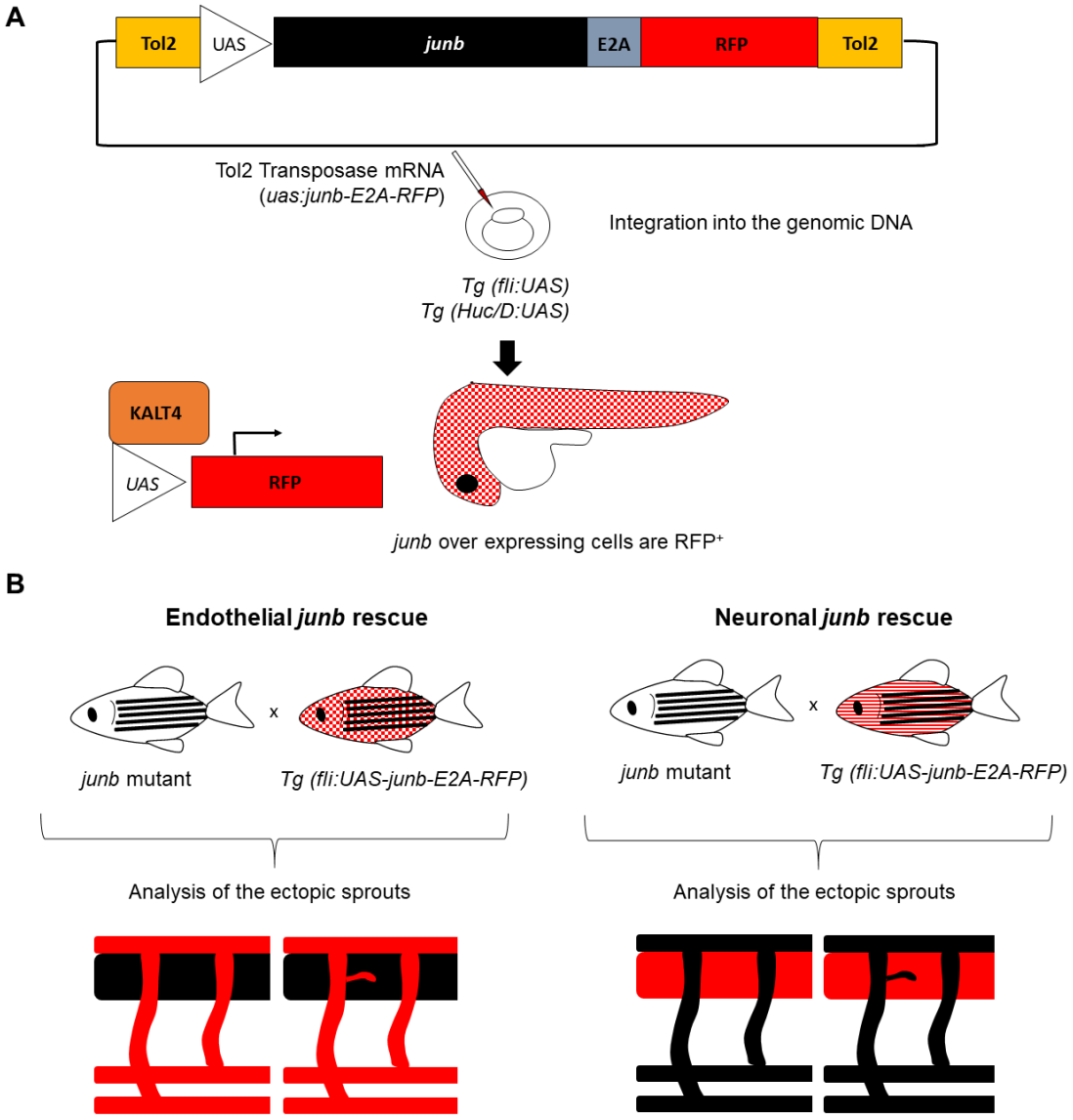

Figure 4-25: Generation of a tissue-specific overexpression *junb* line

A) Schematic illustration of the generated overexpression vector and its integration on the zebrafish genome upon transposase activity. B) Schematic illustration of the zebrafish crossings that need to be performed to obtain embryos with solely expression of *junb* in the endothelial or neuronal tissues. Red marks the tissues where the overexpression construct is active.

5 DISCUSSION AND FUTURE PERSPECTIVES

5.1 JUNB is induced during *in vitro* differentiation of mESCs into LECs

5.2 JUNB-dependent control of VEGFRs during LEC differentiation and its effect on survival and differentiation potential

5.3 *Junb* loss does not affect LEC specification

5.4 *junb* mutants partially phenocopy the morphants

5.4.1 Loss of *junb* provokes a defect on the formation of the lymphatic system

5.4.2 Unlike morphants, *junb* mutants do not display any cardiovascular defects

5.4.3 Development of ectopic sprouts in *junba* and *junbb* mutant zebrafishes

5.4.4 Differences between the murine *Junb*$^{-/-}$ and the zebrafish mutant embryos.

5.1 JUNB is induced during *in vitro* differentiation of mESCs into LECs.

Many studies have demonstrated that JUNB functions as a context-dependent transcription factor of its target genes (Passegué and Wagner, 2000; Andrecht et al., 2002; Bakiri et al., 2000). In general, the transactivating function of JUNB has been mostly related with vascular development and tissue homeostasis control (Schorpp-Kistner et al., 1999; Licht et al., 2006; Schmidt et al., 2007; Licht et al., 2010) and the repressor functions have been associated to the inflammatory response (Florin et al., 2006; Pflegerl et al., 2009).

In addition, as many other AP-1 members, JUNB has been linked to cell differentiation regulating myogenic (Chalaux et al., 1998), erythroid (Jacobs-Helber et al., 2002), osteoclast (Kenner et al., 2004), myeloid (Passegué et al., 2001) as well as Th2 and Th17 cell differentiation (Li et al., 1999; Yamazaki et al., 2017). Importantly, Obier et al., (2016) described the induction of several AP-1 members during *in vitro* differentiation of stem cells towards hemogenic endothelium.

The goal of the present study was to identify whether JUNB was necessary for the lymphatic differentiation process and identify the processes affected by its regulatory functions. Herein, I present a novel role of JUNB in mammalian lymphatic endothelial cell differentiation.

Remarkably, an increase of JUNB at the RNA and protein level was observed throughout the *in vitro* LEC differentiation process. Whereas the prolonged increase of *Junb* mRNA was quite moderate; an enormous increase of JUNB was detected at the fourth day of the spontaneous differentiation (angioblast formation) and was maintained until the end of the LEC differentiation process. These results highlight the activation of the gene regulator JUNB during the reprogramming of cells towards the vascular and specifically lymphatic endothelial fate.

Considering that the differentiation of stem cells into LECs induces a whole new transcriptional program in the cells, it makes sense that if JUNB regulator function is needed, *Junb* is induced.

Interestingly, the transcript levels did not drop even after several days of continuous stimulation. However, at the protein level, both the phosphorylated and non-phosphorylated variants were detected from the fourth day of the spontaneous differentiation until the endpoint of the process. At this latter stage, only the phosphorylated form was observed suggesting that JUNB regulatory function might be more relevant in differentiating cells than in fully differentiated and mature LECs.

Many other factors need to be considered to explain JUNB induction pattern in LEC differentiation such as its transactivation, mRNA half live, translation efficiency and protein degradation dynamics. The amount of mRNAs in the cells does not correlate with the translation rate since many of the mRNAs can remain as untranslated or free messenger ribonucleotides rather than bound to active polysomes (Hershey et al., 2012). Thus, it could be that *Junb* is not only transcriptionally but also post-transcriptionally regulated during LEC differentiation. Schmid et al., (2013) described post-transcriptional and translational control of JUNB in activated human endothelial cells upon thrombin stimulation and uncovered two regulatory mechanisms: i) an increase in the polysome-associated *Junb* mRNA fraction and ii) an association of the 5' cap of the *Junb* mRNA with the eukaryotic initiation factor 4e (eIF4E). The post-transcriptional regulation of JUNB is thought to be stimulus-dependent but the amount of protein detected suggests that JUNB turnover is highly dynamic at the latter step of the differentiation. A post-transcriptional control of the transcripts similar to the one described (Schmid et al., 2013) would indeed facilitate the generation of proteins in a more rapid and precise way during the cell reprogramming.

In addition, post-translational modifications like phosphorylation (Li et al., 1999) and SUMOylation (Garaude et al., 2008) have been reported to regulate the transcriptional activity of JUNB. The high amount of the phosphorylated form during the last parts of the differentiation protocol could be part of the JUNB turnover via accelerated phosphorylation-dependent proteasomal degradation. This turnover has been described in other settings were JUNB breakdown is carefully controlled such as in the cell cycle (Farràs et al., 2008)

Importantly, since JUNB has been described as a TGFβ1 direct target in the JUNB-SMAD signaling (Gervasi et al., 2012), one could not exclude the possibility that the reduced levels of JUNB in the last differentiation step could simply be an effect of the SB431256 inhibition present in the LEC differentiation medium.

In order to investigate the role of JUNB in LEC differentiation, I adapted the most suitable *in vitro* system up to date and included some modifications to optimize the outcome. Yet, the system faced some technical limitations.

Firstly, the conclusions of this study are based on the transdifferentiation of LECs from pre-existing angioblasts so they can only be extrapolated to those cases where a venous structure is previously present. This system aimed to mimic the *in vivo* formation of the first lymphatic structures from the cardinal vein as seen in mammals (Srinivasan et al., 2007a; Yang et al., 2012) and zebrafish (Nicenboim et al., 2015; Koltowska et al., 2015).

Recently, cell tracing experiments have demonstrated that, in mice, some organ-specific lymphatics originate from non-venous structures: the mesenteric lymphatic vessels derive from cKit hemogenic-endothelium cells (Stanczuk et al., 2015); the dermal lymphatics arise *de novo* during a lymphvasculogenesis process in which LECs cluster

together to assemble the lymphatic networks (Martinez-Corral et al., 2015) and a population of heart lymphatics derive from non-venous structures (Klotz et al., 2015).

Due to technical reasons, these alternative origins were not considered during the study although it would be interesting to revisit them in the future.

Secondly, the conclusions were gained from an *in vitro* system and they will need further validation in a *in vivo* mammalian system. The study of organ-specific lymphangiogenesis is also not possible in the *Junb*$^{-/-}$ embryos−which prematurely die at E9.5− because the first lymphatics form at E9.5, mesenteric lymphatics from E12-E14 and skin lymphatics develop over the E12-E18 (Oliver and Srinivasan, 2010). Therefore, future experiments should include the generation of a conditional *Junb* knock out mouse in which ablation of *Junb* is specific for lymphatic endothelial cells. This tissue-specific deletion of *Junb* approach could be achieved by using transgenic mice in which the Cre-recombinase is under the control of specific promoters such us *Sox18, Prox1 or Vegfr3*.

At the time of this study, the characterization of *Prox1*-Cre *Junb*$^{>/>}$ mice was terminated and revealed no morphological or functional abnormalities in adult lymphatic vasculature in comparison with wildtype mice. The inducible system *Prox1*-CreER^{T2} (Srinivasan et al., 2007b) where the Cre-recombinase is active in the lymphatic cells upon tamoxifen treatment was also tested. Both approaches mating either *Prox1*-Cre or *Prox1*-CreER^{T2} to *Junb* $^{>/>}$ mice failed because but Junb was not sufficiently deleted in either adult or embryonic LECs (Sila Appak-Baskoy and Schorpp-Kistner, unpublished).

Alternatively, a combination of *in utero* injections of a lentiviral construct coding for short hairpin *Junb* RNA in tissue-specific Cre transgenic mice, may be used in the future to achieve a cell specific downregulation of *Junb* similarly to the experiments performed in Yoshitomi et al., (2017).

Additionally, now that the JUNB induction pattern has been traced down to the majority of mesodermal cells during the angioblast formation; it would be interesting to investigate lymphangiogenesis in embryoid bodies or 3D-cultures (Fang and Eglen, 2017) so a deeper look into the vessel assembly, orientation and functionality could be performed.

5.2. JUNB-dependent control of VEGFRs during LEC differentiation and its effect in survival and differentiation potential.

Parallel studies in *Junb*$^{+/+}$ and *Junb*$^{-/-}$ mESCs revealed a JUNB-dependent expression of VEGFRs through the LEC differentiation process. After four days of spontaneous differentiation, the mesoderm-derived cells upregulated VEGFR2 to form the vascular precursors as previously described (Hirashima et al., 2003). At this specific step during the angioblast formation, *Junb*$^{-/-}$ cells displayed a small and huge defect on VEGFR1 and VEGFR2 induction respectively.

The loss of these vascular receptors did not affect the cell doubling rates but was linked to an increased apoptotic rate in *Junb*$^{-/-}$ mESCs.

It is known that depending on the cell cycle phase, JUNB can either promote or block the cell cycle by regulating the expression of *p16*^{INK4a} (Passegué and Wagner, 2000), *CyclinD1* (Bakiri et al., 2000) and *CyclinA* (Andrecht et al., 2002). Yet, no difference in the cell doubling rate was detected in the early steps of differentiation (from the expansion of mESCs until the formation of angioblasts in the spontaneous differentiation) between the analyzed *Junb*$^{+/+}$ and *Junb*$^{-/-}$ mESCs. This result was in line with previous reports in *Junb*$^{-/-}$ MEFs (Andrecht et al., 2002) and in *Junb*$^{-/-}$ EC cells (Passegué and Wagner, 2000). A possible explanation is that unlike other cell types, embryonic cells lack D-type cyclins expression, making them unsusceptible to JUNB-dependent p16^{INK4a} variations during the cell cycle (Savatier et al., 1996)

The accumulation of p16^{INK4a} in MEFs was also linked to the presence of premature senescence features in *Junb* expressing MEFs (Passegué and Wagner, 2000). In addition, other AP-1 members have also been associated with apoptosis (Angel and Karin, 1991). In embryonic stem cells, apoptosis is normally initiated after three days of LIF-starvation (Duval et al., 2006). During that period of time, some of the cells promote a transcriptional swift allowing them to adapt and survive.

In the present study, I showed an increase in the apoptotic activity of *Junb*$^{-/-}$ cells during the spontaneous differentiation and LEC endpoint. This increment on the cell death was accompanied with reduced levels of VEGFR1 and VEGFR2 at the angioblast stage and *Vegfr3* at the LEC-like stage suggesting that the cells most likely did not receive survival signals.

On one side, VEGF via its receptors VEGFR1 and VEGFR2 phosphorylation triggers downstream PI3 kinase activity and subsequent AKT activation which leads to survival response (Gerber et al., 1998). On the other side, VEGFR2 and VEGFR3 phosphorylation and PI3K -mediated survival signaling have also been described for angioblasts and LECs. In addition, phosphorylation of the human 1175-PY of VEGFR2 and the VEGFR2-PLCγ axis is essential for the specification of VEGFR2^{+} angioblasts (Sase et al., 2009).

Taken together, my *in vitro* data strongly suggest that *Junb*$^{-/-}$ mESCs died during LEC differentiation due to i) a defect on the formation of VEGFR2^{+} angioblasts and ii) an impaired survival signaling of the angioblasts via VEGFR1/VEGFR2 signaling.

Furthermore, surviving *Junb*$^{-/-}$ LEC-like cells were found to express lymphatics markers such as *Prox1, Lyve1* and *Podoplanin* at comparable levels as *Junb*$^{+/+}$ LEC-like cells. Importantly, *Vegfr3* and *Vegf-C* expression in *Junb*$^{-/-}$ LEC-like cells was quite diminished when compared with the wildtype cells suggesting that surviving *Junb*$^{-/-}$ angioblasts formed more immature structures.

Considering the increased levels of apoptotic cells and the low expression levels of both *Vegf-C* and *Vegfr3* in *Junb*$^{-/-}$ LEC-like cells, one might argue about the viability of these cells at later stages. Since VEGF-C-induced VEGFR3 activation controls LEC proliferation, survival and migration (Oliver and Srinivasan, 2010) and that PROX1-VEGFR3 positive feedback loop together with VEGF-C are essential for the maintenance of LEC identity in LEC progenitors and mature LECs (Srinivasan et al., 2014); survival of *Junb*$^{-/-}$ LEC-like cells is highly impaired if these signals are not properly compensated.

In the present study, I showed a JUNB-dependent decrease of VEGFR2 levels during the angioblast formation step. However, this decrease of VEGFR2 expression in the *Junb*$^{-/-}$ cells was no longer detectable if the surviving *Junb*$^{-/-}$ cells were subjected to LEC-directed differentiation.The reduced number of *Junb*$^{-/-}$ LEC-like cells that survived during the differentiation process expressed comparable levels of VEGFR2 at the RNA and protein level suggesting that compensation of VEGFR2 levels was necessary for survival.

Unlike VEGFR1, VEGFR2 signaling is still very relevant for LECs signaling. Since VEGFR2 is the main transducer of VEGF-A, the observed increased of the receptor in the last step of the differentiation could be explained by the ectopic addition of VEGF-A and other growth factors in the media. In fact, it has been described that the binding of VEGF-A to VEGFR2 initiates the uptake of VEGFR2 and stimulates the trafficking of newly synthetized VEGFR2 from the Golgi to the plasmatic membrane (Koch and Claesson-Welsh, 2012).

However, VEGFR3 expression is detrimental for LEC development and functionality and VEGFR2 upregulation alone could never maintain the VEGF-C-driven signaling. The upregulation of VEGFR2 levels and downstream signaling as a result of the loss of VEGFR3 has only been observed in blood endothelial cells (Heinolainen et al., 2017). In fact, LECs submitted to VEGFR3 deletion displayed unaltered VEGFR2 levels (Zhang et al., 2018). In addition, although VEGF-C also binds VEGFR2, VEGF-C-derived VEGFR2 signaling in lymphangiogenesis has only been described to promote vessel enlargement and very limited sprouting (Wirzenius et al., 2007). Therefore, LEC-like cells expressing low levels of *Vegfr3* would be severely impaired to function as proper lymphatic endothelial cell.

My data suggests that JUNB regulates the expression of *Vegfr1, Vegfr2* and *Vegfr3* at different steps of the differentiation potential. However, whether JUNB is directly controlling the transactivation of these genes or indirectly controlling specific regulators remains unclear.

As it has been described that *Junb* physically binds to *Vegf* promoter (Schmidt et al., 2007); one may speculate that *Vegfr1, Vegfr2* and *Vegfr3* are direct JUNB targets. Unpublished data from our lab (Sator-Schmitt and Schorpp-Kistner, unpublished) identified several JUNB binding areas within the murine *Vegfr1* promoter using Electrophoretic Mobility Shift Assay (EMSA) and luciferase transactivation assays. In addition, *in silico* analysis of the human *Vegfr2* and *Vegfr3* promoters also identified several putative AP-1 binding sites. Hence, it would be interesting to perform similar promoter studies to investigate whether *Vegfr2* and *Vegfr3* are also JUNB direct targets

In conclusion, these results underscore the importance of JUNB regulating key vascular receptors during the *in vitro* differentiation of mESCs into LECs.

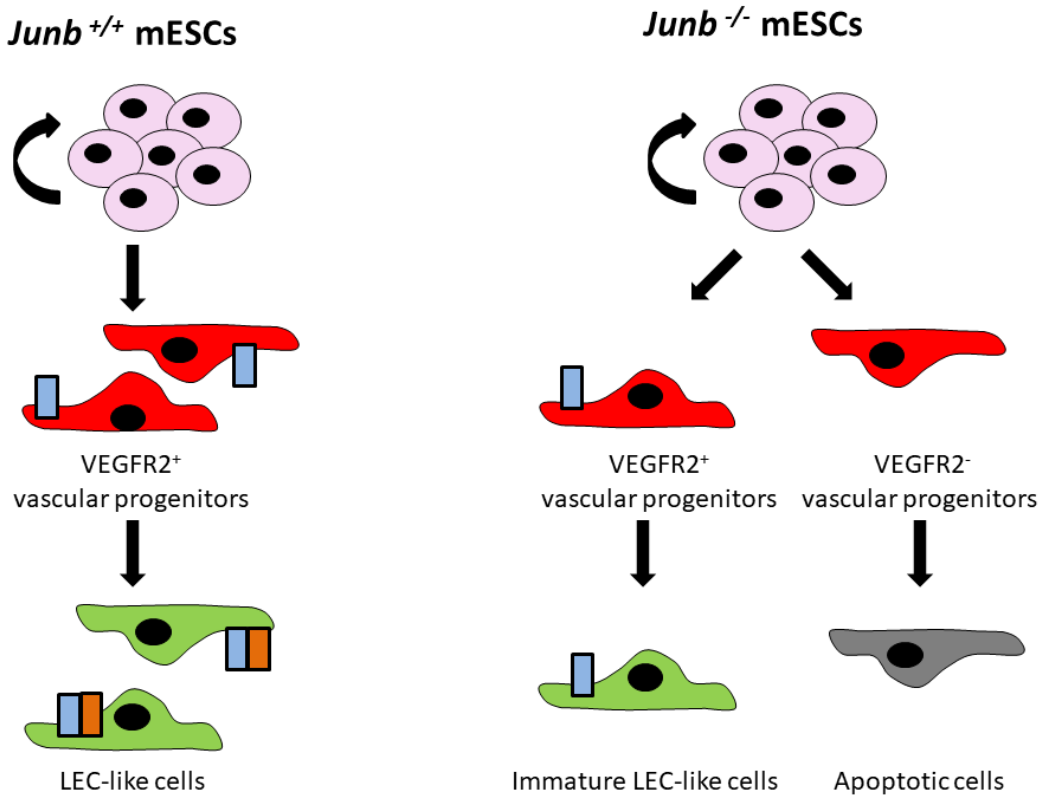

Figure 5-1. Schematic model of the *in vitro* LEC differentiation

Left panel: Model of LEC differentiation in *Junb*$^{+/+}$ mESCs in which mesodermal VEGFR2^{+} vascular progenitors were formed prior differentiation into VEGFR2^{+} VEGFR3^{+} LEC-like cells. Right panel: Loss of *Junb* in mESCs lead to a mixed population during the spontaneous differentiation. The vast majority of the cells (VEGFR2^{-})failed to expressed VEGFR2^{-} and as a result of this, they initiated the apoptotic cascade and die. The remaining VEGFR2^{+} cells survived to the later LEC-like stage although lacking VEGFR3 expression.

5.3 *Junb* loss does not affect LEC specification

It is proven that blocking or eliminating regulators of early steps of lymphangiogenesis −LEC competence and LEC specification− will lead to the total absence of LECs. However, defects on regulators of later steps of the process such as LEC determination would not affect the formation of LECs itself rather than provoke other defects in LEC vasculature like valve malformation, aberrant patterning or reduced number of vessels.

PROX1 is sufficient and necessary to trigger the LEC fate *in vivo* an *in vitro* (Hong et al., 2002; Petrova et al., 2002; Wigle and Oliver, 1999; Wigle et al., 2002). This transcription factor was detected and monitored throughout the LEC differentiation and although a difference in the protein formation and stabilization was indeed observed at the very early stages; this variation was not perceptible at the later stage where both $Junb^{+/+}$ and $Junb^{-/-}$ LEC-like cells expressed similar RNA and protein levels.

It is conceivable that in a setting where cells are lacking $Junb^{-/-}$ expression, *Vegf-C* and *Vegfr3* receptor expression are reduced. A failure in the expression of the ligand and receptor is linked to defects on the formation of the first lymphatic structures, the lymph sacs and further lymphovenous separation as well as reduced LEC maturation and LEC sprouting.

The data presented in this study revealed an essential role of JUNB in angioblast formation. These results are in line with previous studies in mice (Schorpp-Kistner et al., 1999) in which *Junb*-deficient embryos displayed strong defects in vasculogenesis. Additionally, a previous investigation revealed that $VEGFR2^{+}$ embryonic cells subjected to complete AP-1 inhibition, reduced the transcript levels of a cluster of genes related to angiogenesis, vessel development and morphogenesis (Obier et al., 2016).

Taking all the data together, this study provides robust evidence for JUNB control of angioblast formation via regulation of *Vegfr1* and *Vegfr2*. Furthermore, JUNB does not seem to act as a lymphatic cell fate factor itself but rather modulate fate cell decision in later steps for the maintenance of the fate in a quiescent state.

5.4 *junb* mutants partially phenocopy the morphants

5.4.1 Loss of *junb* provokes a defect on the formation of the lymphatic system.

Previous studies of *junba* and *junbb* were performed using morpholinos, oligos of analogue DNA that bind to the complementary sequence of the target gene blocking translation (Kiesow et al., 2015). In the present study, I generated novel mutants for ablated *junba* and *junbb* using CRISPR-Cas9 technology. One mutant for each gene harboring mutations that caused a premature end of the frameshift were selected and raised in the pan-endothelial *Tg(fli:EGFP)*^{y1} background to fine trace the development of the vasculature.

Kiesow et al., (2015) showed that silencing of either *junba* or *junbb* or of a combination of both by injection of antisense morpholinos led to a defect in the formation of the parachordal cells and subsequent thoracic duct formation. Like the morphants, the mutants also displayed a reduced number of complete PACs by 3 dpf. In the morphants, both downregulation of *junba* or *junbb* provoked a defect on PACs formation displaying only 60% of their total PACs at 72 hpf. This feature was shared with the *junba* and *junb* heterozygous mutants since they also displayed similar values of formed PACs at 72hpf. *junbb*$^{-/-}$ mutants displayed even less formed PACs since only half of the hemisegments were completed by 72 hpf. Contrary to the morphants, the analysis of the *junbb*$^{-/-}$ *junba*$^{+/-}$ mutants did not reveal any synergistic effect.

In contrast to the morphants, the failure of the TD formation was not observed in the mutants. Whilst only 20% of the TD was formed upon simultaneous *junba* and *junbb* downregulation or CRISPR-gRNAs injection; single mutation of *junba* or *junbb* or combined loss of *junba* and *junbb* showed very little or no effect on TD formation. In fact, most of the analyzed mutants displayed a complete thoracic duct. Only some of the *junbb*$^{-/-}$*junba*$^{+/-}$ mutants exhibited a very mild defect on the TD with some missing fragments throughout the trunk at 5 dpf. Once again, the concomitant loss of both *junba* and *junbb* did not evoke a stronger lymphatic malformation. This lack of synergistic phenotype in comparison with single gene manipulation has also been observed for other lymphatic regulators like *Prox1a* and *Prox1b* whose simultaneous downregulation did not generate a stronger lymphatic defect in either morphants (Giacco et al., 2010) or mutants (van Impel et al., 2014).

The presented data differ from those from Kiesow et al., (2015) who described the maintenance of the morphant phenotype in injected embryos with CRISPR-gRNAs. However, the characterization of the lymphatic vasculature was performed in a batch of mosaic injected embryos rather than in a clean mutant line with a characterized mutation. The analysis of mosaic embryos, in which only a cluster of cells may be

mutated and not sufficient to trigger a compensatory mechanism, could explain the similarity to the morphant phenotype.

In addition, in both morphants and mutants, a general sprouting defect from the PCV could be discarded since in both cases the arterial: venous ratio aISVs:vISVs was quite similar. Yet, in both cases a shift towards the venous compartment formation was detected (Kiesow et al., 2015). The presence of arterial ISVs is required for the proper lymphatic patterning (Bussmann et al., 2010). The lymphatic cells located at the horizontal myoseptum migrate dorsally and ventrally to form the lymphatic vessels (TD, ISLVs and DLLV) and they migrate exclusively along the arterial ISVs. Thus, a reduced number of arteries is linked to defective LEC migration and explains the failure in the formation of the TD , ISLV and DLLV in the trunk.

The reason why the loss of PACs is not accompanied by the loss of TD remains unclear. Parallel control of wildtype siblings and analysis of the formation of other anatomical structures ruled out the possibility of a developmental delay in the mutants at 72 hpf. A possible explanation is that even though there are only few PACs at 72 hpf, they are sufficient to migrate ventrally and form part of the TD. Another possibility is that the effect of *junba* and *junbb* loss is only important at the early stages of PACs formation but no later.

In any case, the results in this study are reminiscent of the discordance in the phenotypes between gene knockdowns and gene mutations in zebrafish (Rossi et al., 2015). These discrepant phenotypes have been described for many genes (Kok et al., 2015) and for most of the key lymphatic regulators in zebrafish (Semo et al., 2016) as is summarized in Table 5-1.

The inactivation of a gene induces a compensation program that regulates a whole new set of genes at the transcriptomic and proteomic level. However, these modifications cannot be observed in transient down-regulation approaches.

The presence of damaged DNA and mutant mRNA among others are considered to be the main triggers of the transcriptional response (El-Brolosy and Stainier, 2017). During gene manipulation of *junba* and *junbb* using the CRISPR-Cas9 system, a double break in the DNA was generated and the DNA repair machinery was activated. As a result of these processes, a lot of DNA damage was created. DNA damage is normally accompanied by a chromatin reorganization which may affect the neighboring and compensating genes. In addition, the mutants generate mutant RNA which is degraded by the RNA surveillance pathways like the nonsense mediated-decay (NMD) pathway (Lykke-Andersen and Jensen, 2015). In contrast to translation-blocking morpholino injection, where the morpholino binds and stabilize the transcript, the presence of fragmentated or degraded RNA was linked to milder phenotypes due to its ability to trigger genetic compensation (Schuermann et al., 2015).

New developments and tools are constantly appearing for the study of vascular biology in zebrafish. In the future, it would be interesting to generate *junba* and *junbb* tissue-specific mutants (Wild et al., 2017) or heat-inducible mutants (Shoji and Sato-Maeda, 2008) in order to address the role of these transcription factors in specific cell types or at specific time points.

Table 5-1 Comparison of morphants and mutants phenotypes of lymphatic regulators

Gene	Morphant phenotype	Knock Out phenotype
prox1	Loss of PACs and TD and edema (Yaniv et al., 2006)	Reduced number of PACs and TD segments and edema around the eyes and gut in prox1a^{i278} mutant(van Impel et al., 2014); Loss of PACs and TD in maternal zygotic mutants MZprox1a^{i278} (Koltowska et al., 2015)
prox1b	Loss of TD and cardiac edema (Giacco et al., 2010)No phenotype (Tao et al., 2011)	No phenotype in prox1b^{hu3510} mutant (Tao et al., 2011); No phenotype in prox1b^{SA0035} mutant (van Impel et al., 2014)
sox 18	Loss of PACs and TD (Cermenati et al., 2013)	No phenotype in sox18^{hu10320} mutant (van Impel et al., 2014)
coupTFII (Nr2f2)	Loss of PACs and TD (Aranguren et al., 2011)	No phenotype in coup-TFII^{hu10330} mutant (van Impel et al., 2014)
vegfr3	Loss of TD (Hogan et al., 2009b); Defect on lymphatic branchial arches and Ventral Aorta lymphangioblast (Okuda et al., 2012)	Loss of TD in *expando* Flt4^{hu4602} (Hogan et al., 2009b) Loss of PACs and TD in Flt4^{hu4602} (Le Guen et al., 2014)
lyve 1	No phenotype (Flores et al., 2010)	
ccbe1	Loss of PACs (Le Guen et al., 2014) Loss of Facial lymphatic sprout and Ventral Aorta Lymphangioblast (Okuda et al., 2012)	Loss of PACs and TD ccbe1^{hu3613} mutants (Le Guen et al., 2014)
vefg-c	Loss of PACs (Cermenati et al., 2013)	Loss of TD in vegfc^{hu5055} (Le Guen et al., 2014)
junba/ junbb	Loss of PACs and TD (Kiesow et al., 2015)	Loss of PACs but present TD (Gutierrez-Miranda et al, Unpublished)

In zebrafish, the duplication of genes caused the partition and generation of new functions as well as regulating their activation (Conant and Wolfe, 2008; Hahn, 2009). Since individual loss of *junba* or *junbb* provoked similar lymphatic defects; one may suggest that these two genes share some of their targets. In line with that, it is conceivable that the single mutant phenotype may be compensated.

An exhaustive research on *junba* and *junbb* regulation is still needed since very little is known. In the present study I show that in wildtypes, these two genes showed two different pattern and expression kinetics during the early zebrafish development. This differential expression in development could be due to i) different inducers ii) different temporal induction pattern or iii) differential epigenetic control. It is known that promoter methylation blocks downstream expression in mammals and plants (Weber et al., 2007; Zemach et al., 2010). In zebrafish, it has been described that for many duplicated genes, whilst the promoter of one gene is methylated and inactive, the other duplicated gene promoter is hypomethylated and active at the same time (Zhong et al., 2016). Therefore, further studies should be performed to understand *junba* and *junbb* chromatin dynamics in gene regulation.

Despite the fact that the role of *junba* and *junbb* in PACs formation was addressed, the role of these genes in zebrafish angioblast formation remains uncertain. Time lapse imaging of the mutants at early time points was performed to observe the development of the first venous and lymphatics sprouts from the PVC. However, technical difficulties and the limited movie footage did not allow to draw a clear conclusion. One could claim that there should not be a big difference in the angioblast population since the formation of lymphatic structures is not completely impaired. However, since the *in vitro* data obtained in this study showed a dramatic decrease of the angioblast population, further experiments should be performed. It would be important to repeat the time-lapse experiments in mutants raised in another zebrafish background like the transgenic *Tg(flt1_9a_cFos:GFP)*, a line generated and used by Nicenboim et al.,(2015) because apart from the arterial expression of Flt1, it could label the angioblast population within the PCV. The quantification of the ventral angioblasts in the PCV and the quantification of the committed Prox1^{+} dorsal cells in the PCV (Koltowska et al., 2015) may help to clarify whether *junba* and *junbb* play a role in the early steps of zebrafish lymphangiogenesis.

In addition, the mutants could also be crossed into a *Tg(fli1:gal4^{ubs3};UAS:Kaede^{rk8})* line (Herwig et al., 2011) to perform photo-switching of the ventral PCV similarly to the experiments performed by Nicenboim et al., (2015). KAEDE is a green fluorescent protein that will shift to a red fluorescent protein upon UV exposure. Thus, applying UV light to the ventral side of the PCV, would turn the expression of Kaede from green to red fluorescence allowing a fine tracing of the angioblast differentiation through time.

Besides, phosphorylation of Junb proteins has been described as key events of wound healing and fin regeneration of larval and adult zebrafishes (Ishida et al., 2010). Whether *junba* and *junbb* are necessary for vascular regeneration are important questions that should be addressed in the future.

5.4.2 Unlike morphants, mutants do not display any cardiovascular defects

In addition to the lymphatic phenotype, two other vascular-related phenotypes were observed in the *junb* morphants and were absent in the mutants.

In Meder et al., (2010), the reduction of *junba* an *junbb* levels by morpholino-mediated knockdown resulted in cardiac edema and abnormal blood circulation at 3 dpf. These features were caused by aberrations in the Z-disc structure of the myofilaments affecting the heart and skeletal muscle development. In (Kiesow et al., 2015), this cardiac defect was not present in individual *junba* and *junbb* morphants as well as double *junba/junbb* morphants which displayed normal heart development and continuous blood flow. Intriguingly, some *junbb* morphants developed hemorrhages in the aortic branch and the carotid artery branches at 48hpf and 72 hpf.

The difference between these studies relies on the design of the targeted morpholinos and their doses. While (Meder et al., 2010) used 4 ng of *junba* morpholino that could not completely target the *junbb* sequence; (Kiesow et al., 2015) used two different sets of morpholinos per gene and their doses were finely adapted to 2 ng. With this approach, a detectable downregulation of the transcripts was achievable without jeopardizing normal embryonal development.

The *junba* and *junbb* mutants presented on this study were devoid of any cardiovascular defects. Although (Meder et al., 2010) described hypo-contractile and dilated ventricles in the morphants, *junb* mutants developed normal heart cavities and their heart beat was similar to their wildtype siblings. In addition, all the mutants lacked any sign of internal bleeding in the heart and in the trunk area.

As previously mentioned, a combination of the off-target effects or the toxicity of the down-regulation and the dosage compensation might explain the differences between these morphants and the mutant's phenotypes.

5.4.3 Development of ectopic sprouts in *junba* and *junbb* mutant zebrafishes

Both *junba* and *junbb* mutants exhibited normal blood circulation and the formation of the main blood vessels such as PCV, DA and DLAV remained unaltered. However, small ectopic sprouts in the dorsal part of the ISVs were detected in the trunk of embryos from the 3 dpf until 5 dpf. Most of these sprouts were generally sprouting from a venous ISVs towards aortic ISVs and appeared to be mostly disconnected to their neighboring vessels.

Sprouting angiogenesis is important for the formation of the vascular network and requires the specification of endothelial cells into tip or stalk cells. The tip cells are located at the edge and generate filopodia to migrate towards a gradient of cues. The stalk cells on the other side, follow the tip cells. Some of the receptors involved in this cell differentiation are the vascular endothelial Growth Factor Receptors (VEGFR1, VEGFR2 and VEGFR3) and the Notch-Delta like 4 (Dll4) (Phng and Gerhardt, 2009; Roca and Adams, 2007).

The development of hyperbranching in the dorsal areas has been associated with the loss of two tip cell markers: VEGFR1 (Krueger et al., 2011) and DLL4 (Leslie et al., 2007).

In mammals and in zebrafish, VEGFR1 (also known as Flt1) encodes for a membrane-bound receptor and smaller soluble form that contains the VEGF binding domain (Sela et al., 2008; Krueger et al., 2011). While membrane-bound VEGFR1 binds its ligands and controls downstream signaling via its tyrosine kinase domain; the soluble VEGFR1 binds VEGF-A controlling its availability in the surrounding tissues (Ambati et al., 2006; Gerhardt et al., 2003). In mice, *Vegfr1* expression is observed in the blood islands and extra-embryonic tissues (Fong et al., 1995) and *Vegfr1*$^{-/-}$ embryos die prematurely (E8.5) due to aberrant vascular formation. In zebrafish, *vegfr1* expression is mostly found in endothelial cells of arterial origin such as dorsal aorta and arterial intersegmental vessels and in some spinal cord neurons. Studies with *vegfr1* morpholino knockdown revealed that Vegfr1 regulates arterial branching and tip cell formation in zebrafish embryos (Krueger et al., 2011).

DLL4 is a key player of the Notch signaling and is linked to the proliferation and branching control in endothelial cells. In zebrafish, it is also expressed in the endothelial cells of the dorsal aorta and in the intersegmental vessels and in a small cluster of neural cells. Morpholino-mediated knock-down also revealed the formation of aberrant sprouts at the neural tube level (Leslie et al., 2007).

In these both reports, the loss of these tip cell markers ended in the formation of aortic ectopic sprouts that generated connections with adjacent vessels.

Recently, neuronal sVEGFR1 has been proposed to be the main regulator of neural tube vascularization in both mice (Himmels et al., 2017) and zebrafish (Wild et al., 2017). In this later study, *vegfr1* mutants also exhibited ectopic sprouts in the dorsal area of the ISVs at the neural tube level. They proposed that the neural tissue controls vascularization by expressing the pro-angiogenic molecule Vegfaa and scavenger, sVegfr1. Thus, an increase of the angiogenic molecule or a decrease of the anti-angiogenic receptor results in a similar outcome: an increased availability of Vegfaa in the tissue. This Vegfaa increase is detected by the responsive endothelial cells triggering the hyperbranching of the vein endothelial cells (Wild et al., 2017)

Remarkably, the *junba* and *junbb* mutants displayed venous sprouts at the neural tube level similarly to the phenotype described in (Wild et al., 2017). However, the number of sprouts present in the *junb* mutants was much lower in comparison with the description of the *vegfr1* mutant.

There is very little information about the function of JUNB in the neurovascular plexus. A recent report described JUNB as a regulator of neurovascular alignment in mouse embryos (Yoshitomi et al., 2017). In zebrafish, the immunolabeling of motorneurons in *junba* and *junbb* morphants revealed no differences in the development of the neural tube (Kiesow et al., 2015), although the differences in the expression within the neural tissue were not addressed. The collected data suggest that the loss of *junba* and *junbb* might affect to some extent the expression of sVegfr1 in the neuronal tube. Thus, it would be interesting to cross the generated mutants to other reporter lines indicative for the neural tube such as *Tg(Xla.Tubb:DsRed)*^{zf148} (Wild et al., 2017) to analyze whether i) the neural tube develops normally and ii) isolated cells from the *junba* and *junbb* mutants express lower levels of *vegfr1* in comparison with wildtype neural tube cells.

For these purposes, the mutants should be crossed to a transgenic neuronal reporter line and subjected to cell sorting prior to transcriptomic analysis. The generation of the mutants in the double transgenic background is quite time-consuming, as zebrafishes have the generation time of four months. Thus, due to the lack of appropriate experimental tools , I unfortunately was not able to measure *vegfr1* levels in the neural tube of the presently analyzed Junb mutant embryos.

In light of the previous *in vitro* data regarding JUNB-dependent VEGFR1 expression and the similarity of the phenotypes of *junb* and *vegfr1* mutants, a closer look into the *Vegfr1* promoter was undertaken.

In the human *Vegfr1* promoter, the cAMP response element binding protein/ Activating Transcription Factor (CREB/ATF) and the ets motifs were identified to be essential for *Vegfr1* transcription (Morishita et al., 1995; Wakiya et al., 1996).

In addition, the unpublished data on the murine *Vegfr1* promoter revealed JUNB-dependent transcription via direct binding to TRE and CRE sites (Sator-Schmitt and Schorpp-Kistner, unpublished). As the AP-1 transcription Factor JUNB has been described to bind TRE as well as CRE binding sites within the promoter of many target genes; a study on the zebrafish promoter was initiated.

The zebrafish promoter shares very little conserved regions with the human and murine *Vegfr1* promoter as well as with other vertebrates. Hence, the zebrafish promoter was investigated to identify areas enriched on the TRE and CRE binding sites. An 800 bp region of the promoter was selected and cloned and directed mutations were performed to individually destroy each of the putative binding sites. Subsequently, the wildtype zebrafish promoter and the respective mutated versions were transfected in a murine cell type and subjected to luciferase reporter assays. The transactivation studies revealed that the luciferase activity decreased in half when the TRE (-42/-35) site was mutated suggesting that this specific TRE site may be actively involved in *vegfr1* transcription. Contrary to TRE site,the manipulation of the CRE putative binding sites had no effect on *vegfr1* transactivation.

This last *in vitro* experiment had some limitations due to the murine nature of the cells. Although there are some commercially available zebrafish cell lines, almost none of them are used in the community. In a first approach, I used the teratocarcinoma cell line F9 because of its low levels of AP-1 members and tried to overexpress both the zebrafish *vegfr1* promoter construct and either *junba* or *junbb* or a combination of both. However, neither of the zebrafish proteins could be successfully expressed in this system. At least two constructs with different promoters were used for the construction of the vectors containing the zebrafish variants with similar results. In addition, there are not commercially available antibodies to detect specifically the zebrafish Junba and Junbb proteins so I could never validate whether the zebrafish proteins were properly formed in the murine cells. Therefore, since I could not assess the individual effect of the zebrafish genes, I decided to analyze whether murine JUNB (which shares most of the carboxyl terminal part with the zebrafish proteins including the DNA binding domain) could recognize and bind any of the TRE and CRE candidate sites. Thus, I used wildtype MEFs to perform the transactivation studies with the wildtype promoter and the mutant variants. The results obtained from the luciferase reporter assay suggested that similarly to the human and murine promoter, the zebrafish *vegfr1* transactivation is TRE-dependent.

Still, these results should be taken with caution since I cannot rule out the possibility that in the murine cells, the transactivation of the *dre-vegfr1* promoter is performed by a combination of transcription factors that might not be necessarily present in the zebrafish cells. In order to prove the direct binding of Junba or Junbb to the zebrafish, CHIP-seq experiments should be performed in isolated neurons.

Nevertheless, the data collected from the characterization of the mutants and the luciferase reporter together with the mESC differentiation data and the unpublished reporter studies clearly point to *Vegfr1* as a putative JUNB-direct target.

If true, *Vegfr1* would be another example of conserved JUNB targets. *Cbfb*, for example, was also proven to be directly regulated in mouse (Licht et al., 2006) and downstream of Junb in zebrafish (Meder et al., 2010).

5.4.4 Differences between the murine *Junb*$^{-/-}$ and the zebrafish mutant embryos.

Over all, the zebrafish mutants exhibited a less severe phenotype than the described *Junb*$^{-/-}$ mouse embryos which is lethal at E9.5 (Schorpp-Kistner et al., 1999). *junbb* mutants are viable until adulthood and although *junba* seems to be recessive embryonic lethal similar as murine Junb, the specific stage of development in which they are lost could not be identified during the duration of this study. In a first approach, a time-point among the first four hours of development was considered since only during this period of time embryo lethality was observed. However, due to the low number of cells at those stages and the rapid DNA degradation, no clear *junba*$^{-/-}$ embryos could be identified. Therefore, until the presence of *junba*$^{-/-}$ embryos can be detected at specific developmental stages, one cannot exclude that they might still be formed in a very reduced ratio.

Still, there are many differences between the phenotypes in the two species: On one hand, the phenotype observed in the mouse was a result of impaired vasculogenesis. The embryos displayed defects in the vascularization of the embryo and extra-embryonic tissues. As a result of this improper feto-maternal circulation of oxygen and nutrients, the murine *Junb*$^{-/-}$ embryos were grossly retarded in development and were much smaller compared to the wiltype mice. Except for *junba*, the *junbb* phenotype observed in the zebrafish was not as dramatic as there was not effect on vasculogenesis. In fact, the vascular defects comprised the formation of PACs and ectopic sprouts towards the neural tube. In addition, the *junba* and *junbb* mutants as well as *junbb*$^{-/-}$ *junba*$^{+/-}$ developed normally and were indistinguishable from the wildtype embryos at least until the larval stage.

These differences might be explained by the i) *ex utero* fertilization of zebrafish embryos and the ii) passive transport of oxygen. The zebrafish embryo development takes place externally following fertilization and lacks the placentation step for which JUNB has been described to be absolutely essential in mammals (Schorpp-Kistner et al., 1999). Also, the zebrafish profits from passively diffused oxygen even in the absence of a proper cardiovascular system for the first days of development (Stainier et al., 1996). JUNB has also been described to regulate *Vegf-a* and *Hmox-1* upon hypoxia induction in mice

(Schmidt et al., 2007; Textor et al., 2006; Hock et al., 2007). The fact that the oxygen supply is guaranteed during the first steps of development in zebrafish might also explain the differential relevance of JUNB regulatory functions in the development of their vascular systems.

In both cases, the vascular phenotype has been linked to the loss of *Vegfr1*. On one hand, the mouse *Junb*$^{-/-}$ embryos displayed an allele-dependent reduction in the expression of *Vegfr1* in the yolk sac. On the other hand, the zebrafish mutants displayed a phenotype similar to the one described for the loss of soluble *vegfr1* in the neural tube and a JUNB-dependent activation of the zebrafish promoter was detected.

Final conclusions

In summary, the present thesis unraveled evidence of JUNB regulating different steps of lymphangiogenesis in murine cells and zebrafish.

For the first time, JUNB induction was detected and traced during lymphatic endothelial cell differentiation in a mammalian cell system. The data disclosed in this study provide robust evidence on the JUNB induction and JUNB-dependent regulation of vascular endothelial growth factors receptors during the *in vitro* angioblast formation and differentiation process. JUNB-dependent VEGFR2 expression was essential for the activation of the survival cascade in angioblasts and LEC like cells. In addition, the data suggest that JUNB is not directly controlling the lymphatic fate regulators but it is needed at later stages of the differentiation for proper lymphatic cell maturation.

In addition, novel zebrafish mutants were generated using CRISPR-Cas9 technology. Morphological characterization of the development of the lymphatic system validated previous results highlighting the importance of *junba* and *junbb* in the formation of the first lymphatic structures in zebrafish, the parachordal cells. Additionally, novel transgenic lines were generated to investigate crucial steps of vascular development that were not possible before due to the embryonic lethality of the *Junb*-deficient mice.

Moreover, the characterization of the mutants revealed the presence of ectopic sprouts around the neural tube opening new questions about the role of Junb in neurovascularization. Due to the similarity of a previous report relating the presence of ectopic sprouts with the loss of soluble Vegfr1, the zebrafish *vegfr1* promoter was further investigated.

Taken together, this study pinpoints JUNB as one of the key regulators in vascular biology. Further studies on the transcriptomic variations upon *Junb* loss together with chromatin immunoprecipitation studies would provide a deeper understanding of the downstream effectors of JUNB signaling in vascular development.

The establishment of the LEC differentiation protocol as well as the generation of novel Junb zebrafish mutants generated during this study are important tools that may used to address the remaining questions such us the validation of *vegfr1* and *vegfr2* as direct Junb targets and the role of Junb in adult and tissue-specific lymphangiogenesis.

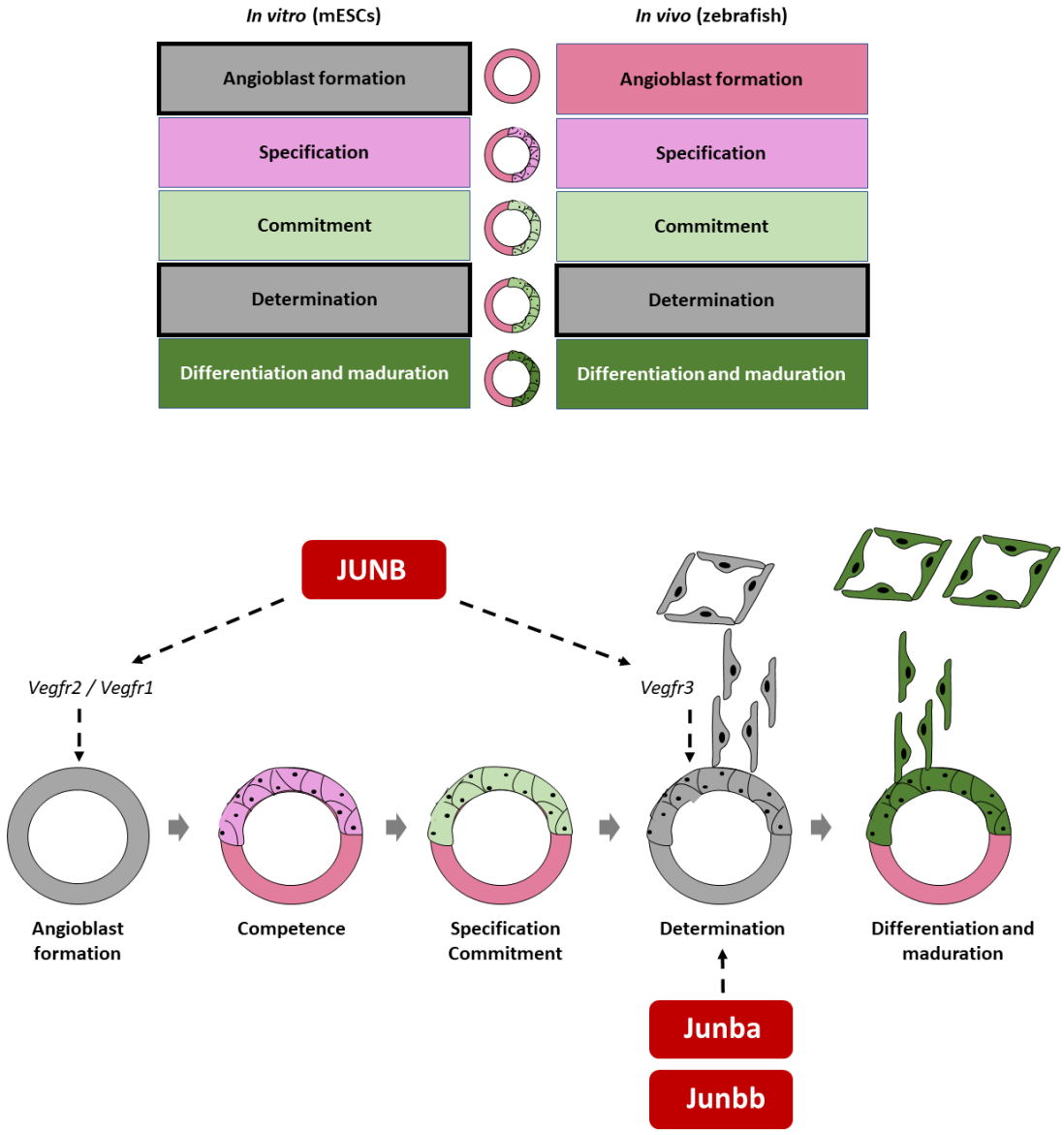

Figure 5-2. Schematic model of the lymphangiogenesis steps that are affected upon *Junb* loss.

Upper panel. Schematic illustration of the lymphangiogenesis steps affected upon *Junb* loss during *in vitro* LEC differentiation and in zebrafish embryos. Lower panel: Detailed description of the putative JUNB targets and processes altered upon *Junb* loss. mESC *in vitro* differentiation studies revealed a big defect on the angioblast formation and survival due to a big defect in *Vegfr2* expression and subtle defect in *Vegfr1* expression. In addition, *Junb*$^{-/-}$ cells displayed reduced levels of *Vegfr3* during the determination step. *In vivo* studies of the zebrafish mutants did not reveal any defect on angioblast formation but a defect on the formation of the parachordal cells which are the primitive lymphatic structures similar to the lymph sacs in mammals.

6 REFERENCES

Achen, M.G., McColl, B.K., and Stacker, S.A. (2005). Focus on lymphangiogenesis in tumor metastasis. Cancer Cell *7*, 121–127.

Alitalo, K., and Carmeliet, P. (2002). Molecular mechanisms of lymphangiogenesis in health and disease. Cancer Cell *1*, 219–227.

Alitalo, K., Tammela, T., and Petrova, T.V. (2005). Lymphangiogenesis in development and human disease. Nature *438*, 946–953.

Ambati, B.K., Nozaki, M., Singh, N., Takeda, A., Jani, P.D., Suthar, T., Albuquerque, R.J.C., Richter, E., Sakurai, E., Newcomb, M.T., et al. (2006). Corneal avascularity is due to soluble VEGF receptor-1. Nature *443*, 993–997.

Amores, A., Force, A., Yan, Y.L., Joly, L., Amemiya, C., Fritz, A., Ho, R.K., Langeland, J., Prince, V., Wang, Y.L., et al. (1998). Zebrafish hox clusters and vertebrate genome evolution. Science *282*, 1711–1714.

Andrecht, S., Kolbus, A., Hartenstein, B., Angel, P., and Schorpp-Kistner, M. (2002). Cell cycle promoting activity of JunB through cyclin A activation. J. Biol. Chem. *277*, 35961–35968.

Angel, P., and Karin, M. (1991). The role of Jun, Fos and the AP-1 complex in cell-proliferation and transformation. Biochim. Biophys. Acta *1072*, 129–157.

Aranguren, X.L., Beerens, M., Vandevelde, W., Dewerchin, M., Carmeliet, P., and Luttun, A. (2011). Transcription factor COUP-TFII is indispensable for venous and lymphatic development in zebrafish and Xenopus laevis. Biochem. Biophys. Res. Commun. *410*, 121–126.

Auer, T.O., Duroure, K., De Cian, A., Concordet, J.-P., and Del Bene, F. (2014). Highly efficient CRISPR/Cas9-mediated knock-in in zebrafish by homology-independent DNA repair. Genome Res. *24*, 142–153.

Avilion, A.A., Nicolis, S.K., Pevny, L.H., Perez, L., Vivian, N., and Lovell-Badge, R. (2003). Multipotent cell lineages in early mouse development depend on SOX2 function. Genes Dev. *17*, 126–140.

Avraham, T., Daluvoy, S., Zampell, J., Yan, A., Haviv, Y.S., Rockson, S.G., and Mehrara, B.J. (2010). Blockade of transforming growth factor-beta1 accelerates lymphatic regeneration during wound repair. Am. J. Pathol. *177*, 3202–3214.

Avraham-Davidi, I., Ely, Y., Pham, V.N., Castranova, D., Grunspan, M., Malkinson, G., Gibbs-Bar, L., Mayseless, O., Allmog, G., Lo, B., et al. (2012). ApoB-containing lipoproteins regulate angiogenesis by modulating expression of VEGF receptor 1. Nat. Med. *18*, 967–973.

Bakiri, L., Lallemand, D., Bossy-Wetzel, E., and Yaniv, M. (2000). Cell cycle-dependent variations in c-Jun and JunB phosphorylation: a role in the control of cyclin D1 expression. EMBO J. *19*, 2056–2068.

Banerji, S., Ni, J., Wang, S.X., Clasper, S., Su, J., Tammi, R., Jones, M., and Jackson, D.G. (1999). LYVE-1, a new homologue of the CD44 glycoprotein, is a lymph-specific receptor for hyaluronan. J. Cell Biol. *144*, 789–801.

Blancas, A.A., Lauer, N.E., and McCloskey, K.E. (2008). Endothelial differentiation of embryonic stem cells. Curr. Protoc. Stem Cell Biol. *Chapter 1*, Unit 1F.5.

Boeuf, H., Merienne, K., Jacquot, S., Duval, D., Zeniou, M., Hauss, C., Reinhardt, B., Huss-Garcia, Y., Dierich, A., Frank, D.A., et al. (2001). The Ribosomal S6 Kinases, cAMP-responsive Element-binding, and STAT3 Proteins Are Regulated by Different Leukemia Inhibitory Factor Signaling Pathways in Mouse Embryonic Stem Cells. J. Biol. Chem. *276*, 46204–46211.

Boussif, O., Lezoualc'h, F., Zanta, M.A., Mergny, M.D., Scherman, D., Demeneix, B., and Behr, J.P. (1995). A versatile vector for gene and oligonucleotide transfer into cells in culture and in vivo: polyethylenimine. Proc. Natl. Acad. Sci. U. S. A. *92*, 7297–7301.

Bradford, M.M. (1976). A rapid and sensitive method for the quantitation of microgram quantities of protein utilizing the principle of protein-dye binding. Anal. Biochem. *72*, 248–254.

Breiteneder-Geleff, S., Soleiman, A., Kowalski, H., Horvat, R., Amann, G., Kriehuber, E., Diem, K., Weninger, W., Tschachler, E., Alitalo, K., et al. (1999). Angiosarcomas express mixed endothelial phenotypes of blood and lymphatic capillaries: podoplanin as a specific marker for lymphatic endothelium. Am. J. Pathol. *154*, 385–394.

Bussmann, J., Bos, F.L., Urasaki, A., Kawakami, K., Duckers, H.J., and Schulte-Merker, S. (2010). Arteries provide essential guidance cues for lymphatic endothelial cells in the zebrafish trunk. Dev. Camb. Engl. *137*, 2653–2657.

Cermenati, S., Moleri, S., Neyt, C., Bresciani, E., Carra, S., Grassini, D.R., Omini, A., Goi, M., Cotelli, F., François, M., et al. (2013). Sox18 genetically interacts with VegfC to regulate lymphangiogenesis in zebrafish. Arterioscler. Thromb. Vasc. Biol. *33*, 1238–1247.

Chalaux, E., López-Rovira, T., Rosa, J.L., Bartrons, R., and Ventura, F. (1998). JunB is involved in the inhibition of myogenic differentiation by bone morphogenetic protein-2. J. Biol. Chem. *273*, 537–543.

Chambers, I., Colby, D., Robertson, M., Nichols, J., Lee, S., Tweedie, S., and Smith, A. (2003). Functional expression cloning of Nanog, a pluripotency sustaining factor in embryonic stem cells. Cell *113*, 643–655.

Choi, K., Kennedy, M., Kazarov, A., Papadimitriou, J.C., and Keller, G. (1998). A common precursor for hematopoietic and endothelial cells. Dev. Camb. Engl. *125*, 725–732.

Chomczynski, P., and Sacchi, N. (1987). Single-step method of RNA isolation by acid guanidinium thiocyanate-phenol-chloroform extraction. Anal. Biochem. *162*, 156–159.

Clavin, N.W., Avraham, T., Fernandez, J., Daluvoy, S.V., Soares, M.A., Chaudhry, A., and Mehrara, B.J. (2008). TGF-beta1 is a negative regulator of lymphatic regeneration during wound repair. Am. J. Physiol. Heart Circ. Physiol. *295*, H2113-2127.

Conant, G.C., and Wolfe, K.H. (2008). Turning a hobby into a job: how duplicated genes find new functions. Nat. Rev. Genet. *9*, 938–950.

Costa, M., Sourris, K., Lim, S.M., Yu, Q.C., Hirst, C.E., Parkington, H.C., Jokubaitis, V.J., Dear, A.E., Liu, H.B., Micallef, S.J., et al. (2013). Derivation of endothelial cells from human embryonic stem cells in fully defined medium enables identification of lysophosphatidic acid and platelet activating factor as regulators of eNOS localization. Stem Cell Res. *10*, 103–117.

Cueni, L.N., and Detmar, M. (2008). The lymphatic system in health and disease. Lymphat. Res. Biol. *6*, 109–122.

Durchdewald, M., Guinea-Viniegra, J., Haag, D., Riehl, A., Lichter, P., Hahn, M., Wagner, E.F., Angel, P., and Hess, J. (2008). Podoplanin is a novel fos target gene in skin carcinogenesis. Cancer Res. *68*, 6877–6883.

Duval, D., Trouillas, M., Thibault, C., Dembelé, D., Diemunsch, F., Reinhardt, B., Mertz, A.L., Dierich, A., and Boeuf, H. (2006). Apoptosis and differentiation commitment: novel insights revealed by gene profiling studies in mouse embryonic stem cells. Cell Death Differ. *13*, 564–575.

El-Brolosy, M.A., and Stainier, D.Y.R. (2017). Genetic compensation: A phenomenon in search of mechanisms. PLOS Genet. *13*, e1006780.

Ellertsdóttir, E., Lenard, A., Blum, Y., Krudewig, A., Herwig, L., Affolter, M., and Belting, H.-G. (2010). Vascular morphogenesis in the zebrafish embryo. Dev. Biol. *341*, 56–65.

Ema, H., Morita, Y., Yamazaki, S., Matsubara, A., Seita, J., Tadokoro, Y., Kondo, H., Takano, H., and Nakauchi, H. (2006). Adult mouse hematopoietic stem cells: purification and single-cell assays. Nat. Protoc. *1*, 2979–2987.

Fang, Y., and Eglen, R.M. (2017). Three-Dimensional Cell Cultures in Drug Discovery and Development. SLAS Discov. Adv. Life Sci. RD *22*, 456–472.

Farràs, R., Baldin, V., Gallach, S., Acquaviva, C., Bossis, G., Jariel-Encontre, I., and Piechaczyk, M. (2008). JunB breakdown in mid-/late G2 is required for down-regulation of cyclin A2 levels and proper mitosis. Mol. Cell. Biol. *28*, 4173–4187.

Faucherre, A., and López-Schier, H. (2011). Delaying Gal4-Driven Gene Expression in the Zebrafish with Morpholinos and Gal80. PLoS ONE *6*, e16587.

Flores, M.V., Hall, C.J., Crosier, K.E., and Crosier, P.S. (2010). Visualization of embryonic lymphangiogenesis advances the use of the zebrafish model for research in cancer and lymphatic pathologies. Dev. Dyn. Off. Publ. Am. Assoc. Anat. *239*, 2128–2135.

Florin, L., Knebel, J., Zigrino, P., Vonderstrass, B., Mauch, C., Schorpp-Kistner, M., Szabowski, A., and Angel, P. (2006). Delayed wound healing and epidermal hyperproliferation in mice lacking JunB in the skin. J. Invest. Dermatol. *126*, 902–911.

Fong, G.H., Rossant, J., Gertsenstein, M., and Breitman, M.L. (1995). Role of the Flt-1 receptor tyrosine kinase in regulating the assembly of vascular endothelium. Nature *376*, 66–70.

François, M., Caprini, A., Hosking, B., Orsenigo, F., Wilhelm, D., Browne, C., Paavonen, K., Karnezis, T., Shayan, R., Downes, M., et al. (2008). Sox18 induces development of the lymphatic vasculature in mice. Nature *456*, 643–647.

Garaude, J., Farrás, R., Bossis, G., Charni, S., Piechaczyk, M., Hipskind, R.A., and Villalba, M. (2008). SUMOylation Regulates the Transcriptional Activity of JunB in T Lymphocytes. J. Immunol. *180*, 5983–5990.

Gerber, H.P., McMurtrey, A., Kowalski, J., Yan, M., Keyt, B.A., Dixit, V., and Ferrara, N. (1998). Vascular endothelial growth factor regulates endothelial cell survival through the phosphatidylinositol 3'-kinase/Akt signal transduction pathway. Requirement for Flk-1/KDR activation. J. Biol. Chem. *273*, 30336–30343.

Gerhardt, H., Golding, M., Fruttiger, M., Ruhrberg, C., Lundkvist, A., Abramsson, A., Jeltsch, M., Mitchell, C., Alitalo, K., Shima, D., et al. (2003). VEGF guides angiogenic sprouting utilizing endothelial tip cell filopodia. J. Cell Biol. *161*, 1163–1177.

Gervasi, M., Bianchi-Smiraglia, A., Cummings, M., Zheng, Q., Wang, D., Liu, S., and Bakin, A.V. (2012). JunB contributes to Id2 repression and the epithelial-mesenchymal transition in response to transforming growth factor-β. J. Cell Biol. *196*, 589–603.

Giacco, L.D., Pistocchi, A., and Ghilardi, A. (2010). prox1b Activity Is Essential in Zebrafish Lymphangiogenesis. PLoS ONE *5*, e13170.

Green, M.R., Sambrook, J., and Sambrook, J. (2012). Molecular cloning: a laboratory manual (Cold Spring Harbor, N.Y: Cold Spring Harbor Laboratory Press).

Hahn, M.W. (2009). Distinguishing among evolutionary models for the maintenance of gene duplicates. J. Hered. *100*, 605–617.

Hamada, K., Oike, Y., Takakura, N., Ito, Y., Jussila, L., Dumont, D.J., Alitalo, K., and Suda, T. (2000). VEGF-C signaling pathways through VEGFR-2 and VEGFR-3 in vasculoangiogenesis and hematopoiesis. Blood *96*, 3793–3800.

Hartenstein, B., Teurich, S., Hess, J., Schenkel, J., Schorpp-Kistner, M., and Angel, P. (2002). Th2 cell-specific cytokine expression and allergen-induced airway inflammation depend on JunB. EMBO J. *21*, 6321–6329.

Harvey, N.L., Srinivasan, R.S., Dillard, M.E., Johnson, N.C., Witte, M.H., Boyd, K., Sleeman, M.W., and Oliver, G. (2005). Lymphatic vascular defects promoted by Prox1 haploinsufficiency cause adult-onset obesity. Nat. Genet. *37*, 1072–1081.

Heinolainen, K., Karaman, S., D'Amico, G., Tammela, T., Sormunen, R., Eklund, L., Alitalo, K., and Zarkada, G. (2017). VEGFR3 Modulates Vascular Permeability by Controlling VEGF/VEGFR2 Signaling. Circ. Res. *120*, 1414–1425.

Herbert, S.P., Huisken, J., Kim, T.N., Feldman, M.E., Houseman, B.T., Wang, R.A., Shokat, K.M., and Stainier, D.Y.R. (2009). Arterial-venous segregation by selective cell sprouting: an alternative mode of blood vessel formation. Science *326*, 294–298.

Hershey, J.W.B., Sonenberg, N., and Mathews, M.B. (2012). Principles of Translational Control: An Overview. Cold Spring Harb. Perspect. Biol. *4*, a011528–a011528.

Herwig, L., Blum, Y., Krudewig, A., Ellertsdottir, E., Lenard, A., Belting, H.-G., and Affolter, M. (2011). Distinct cellular mechanisms of blood vessel fusion in the zebrafish embryo. Curr. Biol. CB *21*, 1942–1948.

Hess, J., Hartenstein, B., Teurich, S., Schmidt, D., Schorpp-Kistner, M., and Angel, P. (2003). Defective endochondral ossification in mice with strongly compromised expression of JunB. J. Cell Sci. *116*, 4587–4596.

Hess, J., Angel, P., and Schorpp-Kistner, M. (2004). AP-1 subunits: quarrel and harmony among siblings. J. Cell Sci. *117*, 5965–5973.

Himmels, P., Paredes, I., Adler, H., Karakatsani, A., Luck, R., Marti, H.H., Ermakova, O., Rempel, E., Stoeckli, E.T., and Ruiz de Almodóvar, C. (2017). Motor neurons control blood vessel patterning in the developing spinal cord. Nat. Commun. *8*, 14583.

Hirashima, M., Ogawa, M., Nishikawa, S., Matsumura, K., Kawasaki, K., Shibuya, M., and Nishikawa, S.-I. (2003). A chemically defined culture of VEGFR2+ cells derived from embryonic stem cells reveals the role of VEGFR1 in tuning the threshold for VEGF in developing endothelial cells. Blood *101*, 2261–2267.

Hock, T.D., Liby, K., Wright, M.M., McConnell, S., Schorpp-Kistner, M., Ryan, T.M., and Agarwal, A. (2007). JunB and JunD regulate human heme oxygenase-1 gene expression in renal epithelial cells. J. Biol. Chem. *282*, 6875–6886.

Hogan, B.M., Bos, F.L., Bussmann, J., Witte, M., Chi, N.C., Duckers, H.J., and Schulte-Merker, S. (2009a). Ccbe1 is required for embryonic lymphangiogenesis and venous sprouting. Nat. Genet. *41*, 396–398.

Hogan, B.M., Herpers, R., Witte, M., Heloterä, H., Alitalo, K., Duckers, H.J., and Schulte-Merker, S. (2009b). Vegfc/Flt4 signalling is suppressed by Dll4 in developing zebrafish intersegmental arteries. Dev. Camb. Engl. *136*, 4001–4009.

Hong, Y.-K., Harvey, N., Noh, Y.-H., Schacht, V., Hirakawa, S., Detmar, M., and Oliver, G. (2002). Prox1 is a master control gene in the program specifying lymphatic endothelial cell fate. Dev. Dyn. Off. Publ. Am. Assoc. Anat. *225*, 351–357.

Hsu, P.D., Scott, D.A., Weinstein, J.A., Ran, F.A., Konermann, S., Agarwala, V., Li, Y., Fine, E.J., Wu, X., Shalem, O., et al. (2013). DNA targeting specificity of RNA-guided Cas9 nucleases. Nat. Biotechnol. *31*, 827–832.

Huntington, G.S., and McClure, C.F.W. (1910). The anatomy and development of the jugular lymph sacs in the domestic cat (Felis domestica). Am. J. Anat. *10*, 177–312.

van Impel, A., Zhao, Z., Hermkens, D.M.A., Roukens, M.G., Fischer, J.C., Peterson-Maduro, J., Duckers, H., Ober, E.A., Ingham, P.W., and Schulte-Merker, S. (2014). Divergence of zebrafish and mouse lymphatic cell fate specification pathways. Dev. Camb. Engl. *141*, 1228–1238.

Ishida, T., Nakajima, T., Kudo, A., and Kawakami, A. (2010). Phosphorylation of Junb family proteins by the Jun N-terminal kinase supports tissue regeneration in zebrafish. Dev. Biol. *340*, 468–479.

Isogai, S., Horiguchi, M., and Weinstein, B.M. (2001). The vascular anatomy of the developing zebrafish: an atlas of embryonic and early larval development. Dev. Biol. *230*, 278–301.

Isogai, S., Lawson, N.D., Torrealday, S., Horiguchi, M., and Weinstein, B.M. (2003). Angiogenic network formation in the developing vertebrate trunk. Dev. Camb. Engl. *130*, 5281–5290.

Jacobs-Helber, S.M., Abutin, R.M., Tian, C., Bondurant, M., Wickrema, A., and Sawyer, S.T. (2002). Role of JunB in Erythroid Differentiation. J. Biol. Chem. *277*, 4859–4866.

Jao, L.-E., Wente, S.R., and Chen, W. (2013). Efficient multiplex biallelic zebrafish genome editing using a CRISPR nuclease system. Proc. Natl. Acad. Sci. U. S. A. *110*, 13904–13909.

Kaipainen, A., Korhonen, J., Mustonen, T., van Hinsbergh, V.W., Fang, G.H., Dumont, D., Breitman, M., and Alitalo, K. (1995). Expression of the fms-like tyrosine kinase 4 gene becomes restricted to lymphatic endothelium during development. Proc. Natl. Acad. Sci. U. S. A. *92*, 3566–3570.

Kakidani, H., and Ptashne, M. (1988). GAL4 activates gene expression in mammalian cells. Cell *52*, 161–167.

Kampmeier, O.F. (1928). The genetic history of the valves in the lymphatic system of man. Am. J. Anat. *40*, 413–457.

Karkkainen, M.J., Haiko, P., Sainio, K., Partanen, J., Taipale, J., Petrova, T.V., Jeltsch, M., Jackson, D.G., Talikka, M., Rauvala, H., et al. (2004). Vascular endothelial growth factor C is required for sprouting of the first lymphatic vessels from embryonic veins. Nat. Immunol. *5*, 74–80.

Kenner, L., Hoebertz, A., Beil, F.T., Beil, T., Keon, N., Karreth, F., Eferl, R., Scheuch, H., Szremska, A., Amling, M., et al. (2004). Mice lacking JunB are osteopenic due to cell-autonomous osteoblast and osteoclast defects. J. Cell Biol. *164*, 613–623.

Kent, W.J., Sugnet, C.W., Furey, T.S., Roskin, K.M., Pringle, T.H., Zahler, A.M., and Haussler, a. D. (2002). The Human Genome Browser at UCSC. Genome Res. *12*, 996–1006.

Kiesow, K., Bennewitz, K., Miranda, L.G., Stoll, S.J., Hartenstein, B., Angel, P., Kroll, J., and Schorpp-Kistner, M. (2015). Junb controls lymphatic vascular development in zebrafish via miR-182. Sci. Rep. *5*, 15007.

Kimmel, C.B., Ballard, W.W., Kimmel, S.R., Ullmann, B., and Schilling, T.F. (1995). Stages of embryonic development of the zebrafish. Dev. Dyn. Off. Publ. Am. Assoc. Anat. *203*, 253–310.

Klotz, L., Norman, S., Vieira, J.M., Masters, M., Rohling, M., Dubé, K.N., Bollini, S., Matsuzaki, F., Carr, C.A., and Riley, P.R. (2015). Cardiac lymphatics are heterogeneous in origin and respond to injury. Nature *522*, 62–67.

Koch, S., and Claesson-Welsh, L. (2012). Signal Transduction by Vascular Endothelial Growth Factor Receptors. Cold Spring Harb. Perspect. Med. *2*, a006502–a006502.

Kok, F.O., Shin, M., Ni, C.-W., Gupta, A., Grosse, A.S., van Impel, A., Kirchmaier, B.C., Peterson-Maduro, J., Kourkoulis, G., Male, I., et al. (2015). Reverse genetic screening reveals poor correlation between morpholino-induced and mutant phenotypes in zebrafish. Dev. Cell *32*, 97–108.

Koltowska, K., Lagendijk, A.K., Pichol-Thievend, C., Fischer, J.C., Francois, M., Ober, E.A., Yap, A.S., and Hogan, B.M. (2015). Vegfc Regulates Bipotential Precursor Division and Prox1 Expression to Promote Lymphatic Identity in Zebrafish. Cell Rep. *13*, 1828–1841.

Kreuger, J., Nilsson, I., Kerjaschki, D., Petrova, T., Alitalo, K., and Claesson-Welsh, L. (2006). Early lymph vessel development from embryonic stem cells. Arterioscler. Thromb. Vasc. Biol. *26*, 1073–1078.

Krueger, J., Liu, D., Scholz, K., Zimmer, A., Shi, Y., Klein, C., Siekmann, A., Schulte-Merker, S., Cudmore, M., Ahmed, A., et al. (2011). Flt1 acts as a negative regulator of tip cell formation and branching morphogenesis in the zebrafish embryo. Dev. Camb. Engl. *138*, 2111–2120.

Küchler, A.M., Gjini, E., Peterson-Maduro, J., Cancilla, B., Wolburg, H., and Schulte-Merker, S. (2006). Development of the zebrafish lymphatic system requires VEGFC signaling. Curr. Biol. CB *16*, 1244–1248.

Kusuma, S., Shen, Y.-I., Hanjaya-Putra, D., Mali, P., Cheng, L., and Gerecht, S. (2013). Self-organized vascular networks from human pluripotent stem cells in a synthetic matrix. Proc. Natl. Acad. Sci. *110*, 12601–12606.

Labun, K., Montague, T.G., Gagnon, J.A., Thyme, S.B., and Valen, E. (2016). CHOPCHOP v2: a web tool for the next generation of CRISPR genome engineering. Nucleic Acids Res. *44*, W272–W276.

Laemmli, U.K. (1970). Cleavage of structural proteins during the assembly of the head of bacteriophage T4. Nature *227*, 680–685.

Lawson, N.D., and Weinstein, B.M. (2002). In vivo imaging of embryonic vascular development using transgenic zebrafish. Dev. Biol. *248*, 307–318.

Le Guen, L., Karpanen, T., Schulte, D., Harris, N.C., Koltowska, K., Roukens, G., Bower, N.I., van Impel, A., Stacker, S.A., Achen, M.G., et al. (2014). Ccbe1 regulates Vegfc-mediated induction of Vegfr3 signaling during embryonic lymphangiogenesis. Dev. Camb. Engl. *141*, 1239–1249.

Leak, L.V., and Burke, J.F. (1966). Fine structure of the lymphatic capillary and the adjoining connective tissue area. Am. J. Anat. *118*, 785–809.

Leak, L.V., and Burke, J.F. (1968). Ultrastructural studies on the lymphatic anchoring filaments. J. Cell Biol. *36*, 129–149.

Leslie, J.D., Ariza-McNaughton, L., Bermange, A.L., McAdow, R., Johnson, S.L., and Lewis, J. (2007). Endothelial signalling by the Notch ligand Delta-like 4 restricts angiogenesis. Dev. Camb. Engl. *134*, 839–844.

Li, B., Tournier, C., Davis, R.J., and Flavell, R.A. (1999). Regulation of IL-4 expression by the transcription factor JunB during T helper cell differentiation. EMBO J. *18*, 420–432.

Licht, A.H., Pein, O.T., Florin, L., Hartenstein, B., Reuter, H., Arnold, B., Lichter, P., Angel, P., and Schorpp-Kistner, M. (2006). JunB is required for endothelial cell morphogenesis by regulating core-binding factor beta. J. Cell Biol. *175*, 981–991.

Licht, A.H., Nübel, T., Feldner, A., Jurisch-Yaksi, N., Marcello, M., Demicheva, E., Hu, J.-H., Hartenstein, B., Augustin, H.G., Hecker, M., et al. (2010). Junb regulates arterial contraction capacity, cellular contractility, and motility via its target Myl9 in mice. J. Clin. Invest. *120*, 2307–2318.

Liersch, R., Nay, F., Lu, L., and Detmar, M. (2006). Induction of lymphatic endothelial cell differentiation in embryoid bodies. Blood *107*, 1214–1216.

Lykke-Andersen, S., and Jensen, T.H. (2015). Nonsense-mediated mRNA decay: an intricate machinery that shapes transcriptomes. Nat. Rev. Mol. Cell Biol. *16*, 665–677.

Makinen, T. (2001). Isolated lymphatic endothelial cells transduce growth, survival and migratory signals via the VEGF-C/D receptor VEGFR-3. EMBO J. *20*, 4762–4773.

Martinez-Corral, I., Ulvmar, M.H., Stanczuk, L., Tatin, F., Kizhatil, K., John, S.W.M., Alitalo, K., Ortega, S., and Makinen, T. (2015). Nonvenous origin of dermal lymphatic vasculature. Circ. Res. *116*, 1649–1654.

Masui, S., Nakatake, Y., Toyooka, Y., Shimosato, D., Yagi, R., Takahashi, K., Okochi, H., Okuda, A., Matoba, R., Sharov, A.A., et al. (2007). Pluripotency governed by Sox2 via regulation of Oct3/4 expression in mouse embryonic stem cells. Nat. Cell Biol. *9*, 625–635.

Meder, B., Just, S., Vogel, B., Rudloff, J., Gartner, L., Dahme, T., Huttner, I., Zankl, A., Katus, H.A., and Rottbauer, W. (2010). JunB-CBF signaling is essential to maintain sarcomeric Z-disc structure and when defective leads to heart failure. J. Cell Sci. *123*, 2613–2620.

Meyer, A., and Málaga-Trillo, E. (1999). Vertebrate genomics: More fishy tales about Hox genes. Curr. Biol. CB *9*, R210-213.

Meyer, A., and Schartl, M. (1999). Gene and genome duplications in vertebrates: the one-to-four (-to-eight in fish) rule and the evolution of novel gene functions. Curr. Opin. Cell Biol. *11*, 699–704.

Mitsui, K., Tokuzawa, Y., Itoh, H., Segawa, K., Murakami, M., Takahashi, K., Maruyama, M., Maeda, M., and Yamanaka, S. (2003). The homeoprotein Nanog is required for maintenance of pluripotency in mouse epiblast and ES cells. Cell *113*, 631–642.

Morishita, K., Johnson, D.E., and Williams, L.T. (1995). A Novel Promoter for Vascular Endothelial Growth Factor Receptor (*flt* -1) That Confers Endothelial-specific Gene Expression. J. Biol. Chem. *270*, 27948–27953.

Murry, C.E., and Keller, G. (2008). Differentiation of embryonic stem cells to clinically relevant populations: lessons from embryonic development. Cell *132*, 661–680.

Nguyen, M.T.X., Okina, E., Chai, X., Tan, K.H., Hovatta, O., Ghosh, S., and Tryggvason, K. (2016). Differentiation of Human Embryonic Stem Cells to Endothelial Progenitor Cells on Laminins in Defined and Xeno-free Systems. Stem Cell Rep. *7*, 802–816.

Nicenboim, J., Malkinson, G., Lupo, T., Asaf, L., Sela, Y., Mayseless, O., Gibbs-Bar, L., Senderovich, N., Hashimshony, T., Shin, M., et al. (2015). Lymphatic vessels arise from specialized angioblasts within a venous niche. Nature *522*, 56–61.

Nichols, J., Zevnik, B., Anastassiadis, K., Niwa, H., Klewe-Nebenius, D., Chambers, I., Schöler, H., and Smith, A. (1998). Formation of pluripotent stem cells in the mammalian embryo depends on the POU transcription factor Oct4. Cell *95*, 379–391.

Niwa, H., Burdon, T., Chambers, I., and Smith, A. (1998). Self-renewal of pluripotent embryonic stem cells is mediated via activation of STAT3. Genes Dev. *12*, 2048–2060.

Niwa, H., Miyazaki, J., and Smith, A.G. (2000). Quantitative expression of Oct-3/4 defines differentiation, dedifferentiation or self-renewal of ES cells. Nat. Genet. *24*, 372–376.

Obier, N., Cauchy, P., Assi, S.A., Gilmour, J., Lie-A-Ling, M., Lichtinger, M., Hoogenkamp, M., Noailles, L., Cockerill, P.N., Lacaud, G., et al. (2016). Cooperative binding of AP-1 and TEAD4 modulates the balance between vascular smooth muscle and hemogenic cell fate. Dev. Camb. Engl. *143*, 4324–4340.

Oka, M., Iwata, C., Suzuki, H.I., Kiyono, K., Morishita, Y., Watabe, T., Komuro, A., Kano, M.R., and Miyazono, K. (2008). Inhibition of endogenous TGF-beta signaling enhances lymphangiogenesis. Blood *111*, 4571–4579.

Okuda, K.S., Astin, J.W., Misa, J.P., Flores, M.V., Crosier, K.E., and Crosier, P.S. (2012). lyve1 expression reveals novel lymphatic vessels and new mechanisms for lymphatic vessel development in zebrafish. Development *139*, 2381–2391.

Oliver, G., and Srinivasan, R.S. (2010). Endothelial cell plasticity: how to become and remain a lymphatic endothelial cell. Dev. Camb. Engl. *137*, 363–372.

Padberg, Y., Schulte-Merker, S., and van Impel, A. (2017). The lymphatic vasculature revisited-new developments in the zebrafish. Methods Cell Biol. *138*, 221–238.

Passegué, E., and Wagner, E.F. (2000). JunB suppresses cell proliferation by transcriptional activation of p16(INK4a) expression. EMBO J. *19*, 2969–2979.

Passegué, E., Jochum, W., Schorpp-Kistner, M., Möhle-Steinlein, U., and Wagner, E.F. (2001). Chronic myeloid leukemia with increased granulocyte progenitors in mice lacking junB expression in the myeloid lineage. Cell *104*, 21–32.

Passegué, E., Wagner, E.F., and Weissman, I.L. (2004). JunB deficiency leads to a myeloproliferative disorder arising from hematopoietic stem cells. Cell *119*, 431–443.

Petrova, T.V., Mäkinen, T., Mäkelä, T.P., Saarela, J., Virtanen, I., Ferrell, R.E., Finegold, D.N., Kerjaschki, D., Ylä-Herttuala, S., and Alitalo, K. (2002). Lymphatic endothelial reprogramming of vascular endothelial cells by the Prox-1 homeobox transcription factor. EMBO J. *21*, 4593–4599.

Pfaffl, M.W. (2001). A new mathematical model for relative quantification in real-time RT-PCR. Nucleic Acids Res. *29*, e45.

Pflegerl, P., Vesely, P., Hantusch, B., Schlederer, M., Zenz, R., Janig, E., Steiner, G., Meixner, A., Petzelbauer, P., Wolf, P., et al. (2009). Epidermal loss of JunB leads to a SLE phenotype due to hyper IL-6 signaling. Proc. Natl. Acad. Sci. U. S. A. *106*, 20423–20428.

Phng, L.-K., and Gerhardt, H. (2009). Angiogenesis: a team effort coordinated by notch. Dev. Cell *16*, 196–208.

Piechaczyk, M., and Farràs, R. (2008). Regulation and function of JunB in cell proliferation. Biochem. Soc. Trans. *36*, 864–867.

Roca, C., and Adams, R.H. (2007). Regulation of vascular morphogenesis by Notch signaling. Genes Dev. *21*, 2511–2524.

Rossi, A., Kontarakis, Z., Gerri, C., Nolte, H., Hölper, S., Krüger, M., and Stainier, D.Y.R. (2015). Genetic compensation induced by deleterious mutations but not gene knockdowns. Nature *524*, 230–233.

Sabin, F.R. (1902). On the origin of the lymphatic system from the veins and the development of the lymph hearts and thoracic duct in the pig. Am. J. Anat. *1*, 367–389.

Sabin, F.R. (1904). On the development of the superficial lymphatics in the skin of the pig. Am. J. Anat. *3*, 183–195.

Sanger, F., Nicklen, S., and Coulson, A.R. (1977). DNA sequencing with chain-terminating inhibitors. Proc. Natl. Acad. Sci. U. S. A. *74*, 5463–5467.

Santaguida, M., Schepers, K., King, B., Sabnis, A.J., Forsberg, E.C., Attema, J.L., Braun, B.S., and Passegué, E. (2009). JunB protects against myeloid malignancies by limiting hematopoietic stem cell proliferation and differentiation without affecting self-renewal. Cancer Cell *15*, 341–352.

Sase, H., Watabe, T., Kawasaki, K., Miyazono, K., and Miyazawa, K. (2009). VEGFR2-PLC 1 axis is essential for endothelial specification of VEGFR2+ vascular progenitor cells. J. Cell Sci. *122*, 3303–3311.

Savatier, P., Lapillonne, H., van Grunsven, L.A., Rudkin, B.B., and Samarut, J. (1996). Withdrawal of differentiation inhibitory activity/leukemia inhibitory factor up-regulates D-type cyclins and cyclin-dependent kinase inhibitors in mouse embryonic stem cells. Oncogene *12*, 309–322.

Schmid, D.I., Schwertz, H., Jiang, H., Campbell, R.A., Weyrich, A.S., McIntyre, T.M., Zimmerman, G.A., and Kraiss, L.W. (2013). Translational control of JunB, an AP-1 transcription factor, in activated human endothelial cells. J. Cell. Biochem. *114*, 1519–1528.

Schmidt, D., Textor, B., Pein, O.T., Licht, A.H., Andrecht, S., Sator-Schmitt, M., Fusenig, N.E., Angel, P., and Schorpp-Kistner, M. (2007). Critical role for NF-kappaB-induced JunB in VEGF regulation and tumor angiogenesis. EMBO J. *26*, 710–719.

Schorpp-Kistner, M., Wang, Z.Q., Angel, P., and Wagner, E.F. (1999). JunB is essential for mammalian placentation. EMBO J. *18*, 934–948.

Schuermann, A., Helker, C.S.M., and Herzog, W. (2015). Metallothionein 2 regulates endothelial cell migration through transcriptional regulation of vegfc expression. Angiogenesis *18*, 463–475.

Sela, S., Itin, A., Natanson-Yaron, S., Greenfield, C., Goldman-Wohl, D., Yagel, S., and Keshet, E. (2008). A novel human-specific soluble vascular endothelial growth factor receptor 1: cell-type-specific splicing and implications to vascular endothelial growth factor homeostasis and preeclampsia. Circ. Res. *102*, 1566–1574.

Semo, J., Nicenboim, J., and Yaniv, K. (2016). Development of the lymphatic system: new questions and paradigms. Dev. Camb. Engl. *143*, 924–935.

Shibuya, M. (2011). Vascular Endothelial Growth Factor (VEGF) and Its Receptor (VEGFR) Signaling in Angiogenesis: A Crucial Target for Anti- and Pro-Angiogenic Therapies. Genes Cancer *2*, 1097–1105.

Shoji, W., and Sato-Maeda, M. (2008). Application of heat shock promoter in transgenic zebrafish. Dev. Growth Differ. *50*, 401–406.

Sievers, F., Wilm, A., Dineen, D., Gibson, T.J., Karplus, K., Li, W., Lopez, R., McWilliam, H., Remmert, M., Söding, J., et al. (2011). Fast, scalable generation of high-quality protein multiple sequence alignments using Clustal Omega. Mol. Syst. Biol. *7*, 539.

Smith, R.O. (1949). Lymphatic contractility; a possible intrinsic mechanism of lymphatic vessels for the transport of lymph. J. Exp. Med. *90*, 497–509.

Smith, A.G., Heath, J.K., Donaldson, D.D., Wong, G.G., Moreau, J., Stahl, M., and Rogers, D. (1988). Inhibition of pluripotential embryonic stem cell differentiation by purified polypeptides. Nature *336*, 688–690.

Srinivasan, R.S., and Oliver, G. (2011). Prox1 dosage controls the number of lymphatic endothelial cell progenitors and the formation of the lymphovenous valves. Genes Dev. *25*, 2187–2197.

Srinivasan, R.S., Dillard, M.E., Lagutin, O.V., Lin, F.-J., Tsai, S., Tsai, M.-J., Samokhvalov, I.M., and Oliver, G. (2007a). Lineage tracing demonstrates the venous origin of the mammalian lymphatic vasculature. Genes Amp Dev. *21*, 2422–2432.

Srinivasan, R.S., Dillard, M.E., Lagutin, O.V., Lin, F.-J., Tsai, S., Tsai, M.-J., Samokhvalov, I.M., and Oliver, G. (2007b). Lineage tracing demonstrates the venous origin of the mammalian lymphatic vasculature. Genes Dev. *21*, 2422–2432.

Srinivasan, R.S., Geng, X., Yang, Y., Wang, Y., Mukatira, S., Studer, M., Porto, M.P.R., Lagutin, O., and Oliver, G. (2010). The nuclear hormone receptor Coup-TFII is required for the initiation and early maintenance of Prox1 expression in lymphatic endothelial cells. Genes Dev. *24*, 696–707.

Srinivasan, R.S., Escobedo, N., Yang, Y., Interiano, A., Dillard, M.E., Finkelstein, D., Mukatira, S., Gil, H.J., Nurmi, H., Alitalo, K., et al. (2014). The Prox1–Vegfr3 feedback loop maintains the identity and the number of lymphatic endothelial cell progenitors. Genes Dev. *28*, 2175–2187.

Stacker, S.A., Baldwin, M.E., and Achen, M.G. (2002). The role of tumor lymphangiogenesis in metastatic spread. FASEB J. Off. Publ. Fed. Am. Soc. Exp. Biol. *16*, 922–934.

Stainier, D.Y., Fouquet, B., Chen, J.N., Warren, K.S., Weinstein, B.M., Meiler, S.E., Mohideen, M.A., Neuhauss, S.C., Solnica-Krezel, L., Schier, A.F., et al. (1996). Mutations affecting the formation and function of the cardiovascular system in the zebrafish embryo. Dev. Camb. Engl. *123*, 285–292.

Stanczuk, L., Martinez-Corral, I., Ulvmar, M.H., Zhang, Y., Laviña, B., Fruttiger, M., Adams, R.H., Saur, D., Betsholtz, C., Ortega, S., et al. (2015). cKit Lineage Hemogenic Endothelium-Derived Cells Contribute to Mesenteric Lymphatic Vessels. Cell Rep.

Swift, M.R., and Weinstein, B.M. (2009). Arterial-venous specification during development. Circ. Res. *104*, 576–588.

Szuba, A., and Rockson, S.G. (1998). Lymphedema: classification, diagnosis and therapy. Vasc. Med. *3*, 145–156.

Takahashi, K., and Yamanaka, S. (2006). Induction of pluripotent stem cells from mouse embryonic and adult fibroblast cultures by defined factors. Cell *126*, 663–676.

Tamm, C., Pijuan Galitó, S., and Annerén, C. (2013). A Comparative Study of Protocols for Mouse Embryonic Stem Cell Culturing. PLoS ONE *8*, e81156.

Tammela, T., Enholm, B., Alitalo, K., and Paavonen, K. (2005). The biology of vascular endothelial growth factors. Cardiovasc. Res. *65*, 550–563.

Tao, S., Witte, M., Bryson-Richardson, R.J., Currie, P.D., Hogan, B.M., and Schulte-Merker, S. (2011). Zebrafish prox1b mutants develop a lymphatic vasculature, and prox1b does not specifically mark lymphatic endothelial cells. PloS One *6*, e28934.

Textor, B., Sator-Schmitt, M., Richter, K.H., Angel, P., and Schorpp-Kistner, M. (2006). c-Jun and JunB are essential for hypoglycemia-mediated VEGF induction. Ann. N. Y. Acad. Sci. *1091*, 310–318.

Textor, B., Licht, A.H., Tuckermann, J.P., Jessberger, R., Razin, E., Angel, P., Schorpp-Kistner, M., and Hartenstein, B. (2007). JunB is required for IgE-mediated degranulation and cytokine release of mast cells. J. Immunol. Baltim. Md 1950 *179*, 6873–6880.

Thisse, B., Heyer, V., Lux, A., Alunni, V., Degrave, A., Seiliez, I., Kirchner, J., Parkhill, J.-P., and Thisse, C. (2004). Spatial and temporal expression of the zebrafish genome by large-scale in situ hybridization screening. Methods Cell Biol. *77*, 505–519.

Tobler, N.E., and Detmar, M. (2006). Tumor and lymph node lymphangiogenesis--impact on cancer metastasis. J. Leukoc. Biol. *80*, 691–696.

Towbin, H., Staehelin, T., and Gordon, J. (1979). Electrophoretic transfer of proteins from polyacrylamide gels to nitrocellulose sheets: procedure and some applications. Proc. Natl. Acad. Sci. U. S. A. *76*, 4350–4354.

Truett, G.E., Heeger, P., Mynatt, R.L., Truett, A.A., Walker, J.A., and Warman, M.L. (2000). Preparation of PCR-quality mouse genomic DNA with hot sodium hydroxide and tris (HotSHOT). BioTechniques *29*, 52, 54.

Tso, P., and Balint, J.A. (1986). Formation and transport of chylomicrons by enterocytes to the lymphatics. Am. J. Physiol. *250*, G715-726.

Vittet, D., Merdzhanova, G., Prandini, M.-H., Feige, J.-J., and Bailly, S. (2012). TGFβ1 inhibits lymphatic endothelial cell differentiation from mouse embryonic stem cells. J. Cell. Physiol. *227*, 3593–3602.

Wakiya, K., Begue, A., Stehelin, D., and Shibuya, M. (1996). A cAMP Response Element and an Ets Motif Are Involved in the Transcriptional Regulation of *flt* -1 Tyrosine Kinase (Vascular Endothelial Growth Factor Receptor 1) Gene. J. Biol. Chem. *271*, 30823–30828.

Weber, M., Hellmann, I., Stadler, M.B., Ramos, L., Pääbo, S., Rebhan, M., and Schübeler, D. (2007). Distribution, silencing potential and evolutionary impact of promoter DNA methylation in the human genome. Nat. Genet. *39*, 457–466.

Webster, N., Jin, J.R., Green, S., Hollis, M., and Chambon, P. (1988). The yeast UASG is a transcriptional enhancer in human hela cells in the presence of the GAL4 trans-activator. Cell *52*, 169–178.

Wigle, J.T., and Oliver, G. (1999). Prox1 function is required for the development of the murine lymphatic system. Cell *98*, 769–778.

Wigle, J.T., Harvey, N., Detmar, M., Lagutina, I., Grosveld, G., Gunn, M.D., Jackson, D.G., and Oliver, G. (2002). An essential role for Prox1 in the induction of the lymphatic endothelial cell phenotype. EMBO J. *21*, 1505–1513.

Wild, R., Klems, A., Takamiya, M., Hayashi, Y., Strähle, U., Ando, K., Mochizuki, N., van Impel, A., Schulte-Merker, S., Krueger, J., et al. (2017). Neuronal sFlt1 and Vegfaa determine venous sprouting and spinal cord vascularization. Nat. Commun. *8*, 13991.

Williams, R.L., Hilton, D.J., Pease, S., Willson, T.A., Stewart, C.L., Gearing, D.P., Wagner, E.F., Metcalf, D., Nicola, N.A., and Gough, N.M. (1988). Myeloid leukaemia inhibitory factor maintains the developmental potential of embryonic stem cells. Nature *336*, 684–687.

Wirzenius, M., Tammela, T., Uutela, M., He, Y., Odorisio, T., Zambruno, G., Nagy, J.A., Dvorak, H.F., Ylä-Herttuala, S., Shibuya, M., et al. (2007). Distinct vascular endothelial growth factor signals for lymphatic vessel enlargement and sprouting. J. Exp. Med. *204*, 1431–1440.

Yamazaki, S., Tanaka, Y., Araki, H., Kohda, A., Sanematsu, F., Arasaki, T., Duan, X., Miura, F., Katagiri, T., Shindo, R., et al. (2017). The AP-1 transcription factor JunB is required for Th17 cell differentiation. Sci. Rep. *7*.

Yang, Y., Garcia-Verdugo, J.M., Soriano-Navarro, M., Srinivasan, R.S., Scallan, J.P., Singh, M.K., Epstein, J.A., and Oliver, G. (2012). Lymphatic endothelial progenitors bud from the cardinal vein and intersomitic vessels in mammalian embryos. Blood *120*, 2340–2348.

Yaniv, K., Isogai, S., Castranova, D., Dye, L., Hitomi, J., and Weinstein, B.M. (2006). Live imaging of lymphatic development in the zebrafish. Nat. Med. *12*, 711–716.

Ye, J., Coulouris, G., Zaretskaya, I., Cutcutache, I., Rozen, S., and Madden, T.L. (2012). Primer-BLAST: a tool to design target-specific primers for polymerase chain reaction. BMC Bioinformatics *13*, 134.

Yoshitomi, Y., Ikeda, T., Saito, H., Yoshitake, Y., Ishigaki, Y., Hatta, T., Kato, N., and Yonekura, H. (2017). JunB regulates angiogenesis and neurovascular parallel alignment in mouse embryonic skin. J. Cell Sci. *130*, 916–926.

You, L.-R., Lin, F.-J., Lee, C.T., DeMayo, F.J., Tsai, M.-J., and Tsai, S.Y. (2005). Suppression of Notch signalling by the COUP-TFII transcription factor regulates vein identity. Nature *435*, 98–104.

Young, R.A. (2011). Control of the embryonic stem cell state. Cell *144*, 940–954.

Zemach, A., McDaniel, I.E., Silva, P., and Zilberman, D. (2010). Genome-wide evolutionary analysis of eukaryotic DNA methylation. Science *328*, 916–919.

Zhang, X., Jin, J.Y., Wu, J., Qin, X., Streilein, R., Hall, R.P., and Zhang, J.Y. (2015). RNA-Seq and ChIP-Seq reveal SQSTM1/p62 as a key mediator of JunB suppression of NF-κB-dependent inflammation. J. Invest. Dermatol. *135*, 1016–1024.

Zhang, Y., Ulvmar, M.H., Stanczuk, L., Martinez-Corral, I., Frye, M., Alitalo, K., and Mäkinen, T. (2018). Heterogeneity in VEGFR3 levels drives lymphatic vessel hyperplasia through cell-autonomous and non-cell-autonomous mechanisms. Nat. Commun. *9*.

Zhong, Z., Du, K., Yu, Q., Zhang, Y.E., and He, S. (2016). Divergent DNA Methylation Provides Insights into the Evolution of Duplicate Genes in Zebrafish. G3amp58 GenesGenomesGenetics.

Declaration of Authorship

I hereby declare that the content of the thesis entitled

“JUNB regulatory functions in lymphangiogenesis: from mESCs to zebrafish”

is original and based on my own investigations, except where otherwise stated.

Furthermore, I verify that this thesis has not been submitted as part of another examination process neither in identical or similar form.

Heidelberg, October 2018

Laura Adriana Gutiérrez Miranda